THE EFFECTS OF QUANTUM DOT NANOPARTICLES ON THE POLYJET DIRECT 3D PRINTING PROCESS

Amelia McDow Elliott

Dissertation submitted to the faculty of the Virginia Polytechnic Institute and State University in partial fulfillment of the requirements for the degree of

Doctor of Philosophy
In
Mechanical Engineering

Christopher B. Williams, Chair
Jan Helge Bøhn
Thomas A. Campbell
Mary E. F. Kasarda
Timothy E. Long

February 17th, 2014
Blacksburg, VA

Keywords: Additive Manufacturing, PolyJet, Inkjet, Physical Unclonable Functions, Quantum Dot, Photopolymer

ADDITIVELY MANUFACTURED PHYSICAL UNCLONABLE FUNCTIONS: THE EFFECTS OF QUANTUM DOT NANOPARTICLES ON POLYJET DIRECT 3D PRINTING PROCESS

Amelia M. Elliott

ABSTRACT

Additive Manufacturing (AM) is a unique method of fabrication that, in contrast to traditional manufacturing methods, builds objects layer by layer. The ability of AM (when partnered with 3D scanning) to "clone" physical objects has raised concerns in the area of intellectual property (IP). To address this issue, the goal of this dissertation is to characterize and model a method to incorporate unique security features within AM builds. By adding optically detectable nanoparticles into transparent AM media, Physical Unclonable Function (PUFs) can be embedded into AM builds and serve as an anti-counterfeiting measure. The nanoparticle selected for this work is a Quantum Dot (QD), which absorbs UV light and emits light in the visible spectrum. This unique interaction with light makes the QDs ideal for a security system since the "challenge" (UV light) is a different signal from the "response" (the visible light emitted by the QDs).

PolyJet, the AM process selected for this work, utilizes inkjet to deposit a photopolymer into layers, which are then cured with a UV light. An investigation into the visibility of the QDs within the printed PolyJet media revealed that the QDs produce PUF patterns visible via fluorescent microscopy. Furthermore, rheological data shows that the ink-jetting properties of the printing media are not significantly affected by QDs in sufficient concentrations to produce PUFs.

The final objective of this study is to characterize the effects of the QDs on photocuring. The mathematical model to predict the critical exposure of the QD-doped photopolymer utilizes light scattering theory, QD characterization results, and photopolymer-curing characterization results. This mathematical representation will contribute toward the body of knowledge in the area of Additive Manufacturing of nanomaterials in photopolymers.

Overall, this work embodies the first investigations of the effects of QDs on rheological characteristics of ink-jetted media, the effects of QDs on curing of AM photopolymer media, visibility of nanoparticles within printed AM media, and the first attempt to incorporate security features within AM builds. Finally, the major scientific contribution of this work is the theoretical model developed to predict the effects of QDs on the curing properties of AM photopolymers.

“Research is what I'm doing when I don't know what I'm doing.”

-Wernher Von Braun

To my best friends: my husband and my twin sister.

ACKNOWLEDGEMENTS

I would like to thank Don Leber, Phil Lambert, and Earl Campaigne for their help in performing the curing and index of refraction experiments. Also, I would like to thank Nancy Zhang for her help in characterizing the photopolymer.

I would like to thank my twin sister Lori Beth for always being willing to share in all the ups and downs I experienced in graduate school. The many hours I spent on the road between school and my husband's home several hundred miles away were filled with many lovely conversations with her. She has always been there to offer a sympathetic ear as well as rejoice in all the small victories. She was my biggest cheerleader, and I would have never had the confidence to march onward without her support.

I would like to thank my colleague Olga Ivanova, who was a tremendous pillar of support in this research project. Not only is she a talented chemist, but she is a diligent scientist, amazing mentor, and cherished friend. I hope we can continue our collaborations together in developing new and exciting technology.

I would like to thank my loving husband Sam, who has had the burden of dealing with a long distance marriage during my time in graduate school. Even though we only were able to see each other on the weekends, we managed to make our time together meaningful and fun enough to last through the week. Thanks for being an understanding, loving, and selfless supporter for the past 4 years.

I would like to thank our co-PI, Dr. Tom Campbell, for providing lab space and guidance on this project.

Finally, I would like to thank my advisor, Dr. Chris Williams, for being the caring, insightful, polite, intelligent, and awesome human being that he is. I have never met anyone that comes close to his level of competency, humility, personality, and work ethic. It was Dr. Williams who encouraged me to pursue the PhD and guided me through every step of the way. He was not only a mentor and advisor, but he also served the role of therapist and friend. I will be forever grateful for the opportunities I now have because of his avid support and care.

TABLE OF CONTENTS

LIST OF FIGURES

Figure

LIST OF TABLES

Table

List of Abbreviations

AM – Additive Manufacturing

PUF – Physical Uncloneable Function

QDs – Quantum Dots

3D – Three Dimensional

SL – Stereolithography

IP – Intellectual Property

IC – Integrated Circuit

UV – Ultra Violet

CHAPTER 1 INTRODUCTION AND MOTIVATION

1.1 Introduction to Additive Manufacturing (AM)

Traditional manufacturing methods include machining, injection molding, casting, stamping, and welding. These processes utilize mechanical removal of material, shaping of material with a mold, and fusing pre-made geometries together, respectively. Additive Manufacturing (AM), also referred to as Rapid Prototyping or 3D Printing, is unique among manufacturing processes in that objects are created by building them up layer-by-layer. Many methods exist for creating objects in a layer-wise fashion, mostly commonly known methods include hot-plastic extrusion (technically called “Fused Filament Fabrication”), laser sintering in a powder bed (known as Powder Bed Fusion), laser curing in a photopolymer vat (Stereolithography or SL), and others. In each AM method, energy and/or material is sequentially patterned into two dimensional layers, with each layer constituting one planar cross-section of the 3D geometry to be manufactured.

When compared to traditional manufacturing methods, AM offers much freedom to the mechanical designer in terms of complex geometries, integrated assemblies, and manufacturing turnaround time on custom parts. First, creating an object one layer at a time permits complete control to the inner geometries of the part, allowing geometries to be created that would be impossible to create via machining, injection molding, casting, or other traditional manufacturing processes. Second, the control over each layer allows moving joints and assemblies to be created, the designer must simply allow the proper clearances within the joints. Also, since the machine operator has access to every layer

of the artifact, embedding objects such as memory wire, motors, or even nanoparticles becomes possible [1]. Finally, since AM builds do not require special tooling or setup and can be run relatively unattended, parts can be created with the push of a button overnight or over a weekend, massively reducing labor costs and lead times for special parts.

1.2 Motivation for Security Features in AM

A critical issue that has arisen due to the decrease in cost and size of AM is increased access to the technology - and that access, unfortunately, may be misused. Just as the digital formatting of music files opened the doors for illegal transfer of music, AM has now made possible the physical manifestation of digital, three-dimensional (3D) designs without the explicit permission of original designer or intellectual property (IP) or copyright owner. Also, since sharing and creating digital 3D models for use in AM machines is relatively simple and already popular amongst AM users [2-3], the potential for counterfeiting products created via AM is inevitable [4]. Counterfeiting becomes a major issue when considering product liability, and as AM moves into customized, low-volume manufacturing, marking objects with security features can mitigate illegal warranty claims or lawsuits held for product failure.

As a final argument for the need for security features in AM builds, the recent attempts to develop an additively-manufactured assault rifle, also known as a “wiki weapon,” have raised concerns about the implications of AM technology on government-regulated products [5]. Alone, adding the capability of incorporating security features within AM builds will not deter a lawbreaker from illegally producing a firearm. The wiki weapon itself is a demonstration of the lack of security behind AM technology.

However, future generations of AM equipment could be regulated such that security features are automatically embedded, read, and cataloged in a database which associates the security feature's code with a particular AM machine. Thus, any government-regulated geometries created via AM could be traced to the specific AM machine of origin, and the registered owner of the machine can be held responsible.

The work proposed in this dissertation is not an attempt to develop a complete system to create, embed, and encode security features within AM builds. On the contrary, this work constitutes the first steps toward developing a process for incorporating security features within AM builds. In the remainder of this chapter, the selection of the type of security feature, the type of AM process, and the materials with which to create the security feature will be described. The overall project goals will be detailed, which involve studying the effects of incorporating security features within an existing AM process. Finally, the outline of this dissertation will be provided in the form of a roadmap at the end of this chapter.

1.2.1 Physical Unclonable Functions (PUFs)

An effective method to combat counterfeiting is to fully embed security features within additively manufactured parts, just as RFID (Radio Frequency Identification) tags are embedded within security badges for ID recognition. Ideally, this security feature would be non-repeatable, even with the use of a 3D scanner or skilled CAD technician. The majority of security features are based on challenge-response authentication, which is a type of security protocol in which a question or "challenge" must be answered with the correct response to gain access to the secured object or information. In proper terms, the "challenge" is presented by a "probe" to the "system," which must produce

the correct “output” to achieve authentication. An issue that arises in challenge-response authentication is the mapping and cloning of the system or the output, thus undermining the authentication protocol. To circumvent this issue, a new type of security feature was imagined in which neither the system nor the output could be replicated. This type of security feature is known as a Physical Unclonable Function (PUF) [6].

A PUF is a type of security feature that takes advantage of randomness in the arrangement of matter or in manufacturing processes to produce a security key which is virtually impossible to replicate. PUFS, originally called “physical one-way functions (POWFs),” evolved from the idea that the optimal security feature would be comprised of numerous, binary-state, quantum particles of which the quantum state theoretically cannot be controlled. The security of quantum particles is derived from a fundamental theory called the “Quantum No-Clone Theory” that states that quantum states cannot be cloned with certainty. Although the use of quantum states is theoretically very secure, the practical use of quantum states would fail due to the inevitable altering of the quantum states by the environment. However, from this original idea of using quantum states of particles, the new idea of using random, uncontrollable systems as security tokens emerged. The basic characteristic of such a system would be uniqueness, tamper resistance, and unforgeability [7-8].

A method originally used to create PUFs was the random dispersing of bubbles within an epoxy. A laser in combination with a light sensor was used to scan the artifact and map the pattern of the bubbles. This is known as an Optical PUF. Figure 1-1 is an image of an optical PUF. Since then, PUFs have advanced to the world of integrated

circuits (IC's), where the variation in the manufacturing of the IC chips becomes the unclonable aspect of the PUF [9]. Forms of IC PUFs include silicon PUFs and coating PUFs. Coating PUFs are IC's which receive a coating of di-electric particles, and a challenge to the circuit detects the random effects in the presence of the particles. A silicon PUF is also an IC but the variation in the conductive tracks and individual components of the IC are detected.

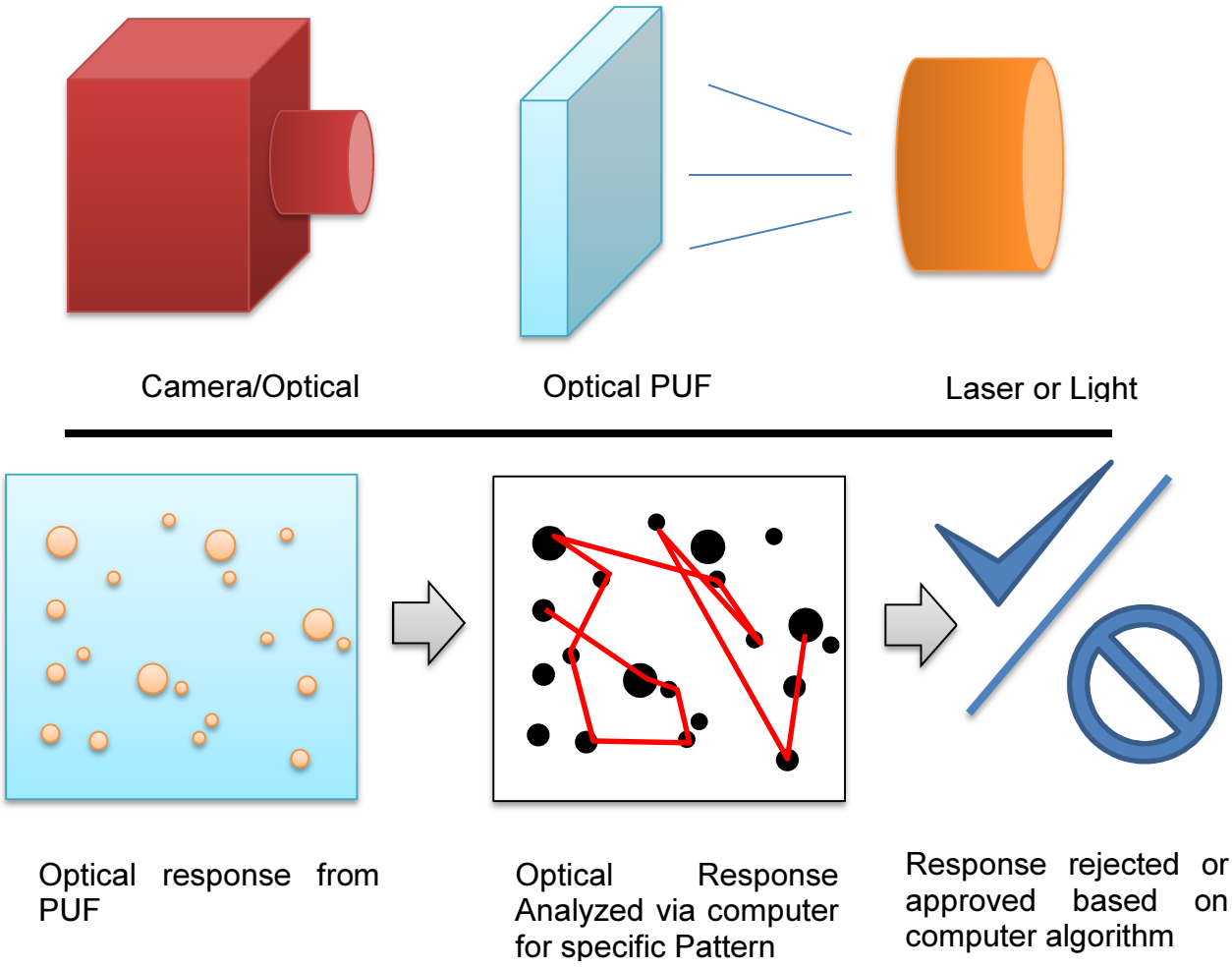

Figure 1-1: Schematic representation of an optical PUF. A laser or light source illuminates the pattern of the particles within the transparent media. A camera detects the response, and the pattern of the particles is analyzed.

AM Process Selection

Of the many methods that exist for additively manufacturing artifacts, some methods are more suited for PUFs than others. Since the PUF is to be selectively placed within the AM build by an existing AM process, it is preferred that the AM process selected is able to process multiple materials. Furthermore, incorporating PUFs into AM builds requires the ability to build with transparent materials. Stereolithography (SL), PolyJet, and Fused Filament Fabrication (FFF) are the three types of AM processes that currently utilize transparent media.

Of these three processes that utilize clear material, SL and FFF are the least suited for the creating PUFs. SL is considered a high-resolution process which consists of a build platform, a vat of photopolymer, and a UV laser that selectively cures the photopolymer. The build platform is first lowered into the vat just below the surface of the photopolymer. The UV laser cures the photopolymer in the desired layer shape, the build platform is lower further into the resin, and the process repeats until the build is complete. Due to the nature of this process, only one material is able to be easily processed for each build. Methods exist for incorporating multiple materials into SL builds, but these systems are custom-made and not commercially available. In contrast, FFF and PolyJet are able to incorporate multiple materials in a single build by using multiple nozzles. For FFF, a thermo-plastic filament is forced through a hot nozzle, and the molten plastic is deposited into the desired layer shape. After each layer is completed, either the nozzle raises or the build platform lowers to create room for the next layer. Although FFF can process multiple materials, the clarity of the so-called “transparent” FFF parts is compromised by the low-resolutions of the printing process

itself, which inherently leaves visible traces of the build layers and tool paths. Therefore, due to the lack of multiple material handling and a lack of clarity, respectively, neither SL nor FFF is well-suited for optical PUFs. This leaves PolyJet as the best candidate for incorporating the creation of PUFs within AM builds, and the PolyJet process will be described in more detail next.

1.2.2 PolyJet

The Stratasys PolyJet Direct 3D Printing process (Stratasys; Tel Aviv, Israel) is most suited for creating PUFs due to its multiple material capabilities, fluid feed material, and clear resin. An example of the clarity that can be achieved in PolyJet builds is shown in Figure 2 below:

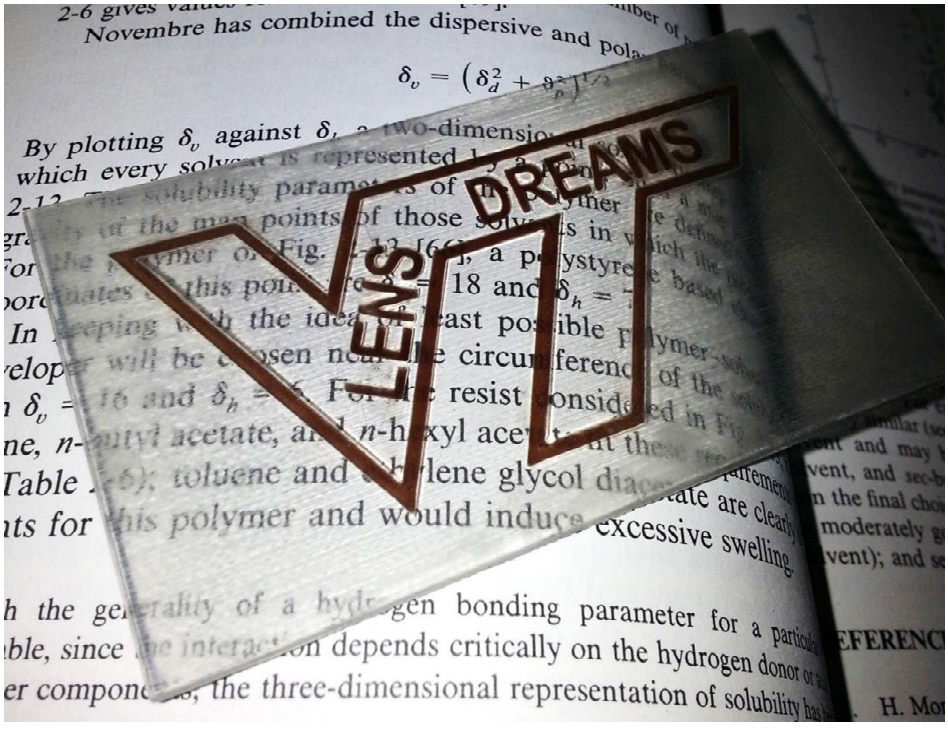

Figure 1-2: Stratasys PolyJet VeroClear Build

The PolyJet process utilizes inkjet printing (IJP) technology in the deposition of photopolymer into layers. First, the IJP block traverses over the build platform,

depositing a layer of liquid photopolymer. After the liquid layer is formed, a roller on the print block smoothes the layer flat. Finally, the ultra violet (UV) lamps on the print block shine onto the layer, curing the liquid photopolymer into a solid layer. The cycle repeats until all layers of the object are created. A hydrophobic, gel-like support material is deposited within the voids of the build and around the perimeter of each layer to serve as a barrier to movement of the build material when it is in liquid form. Figure 2 below depicts the print block and the overall printing process.

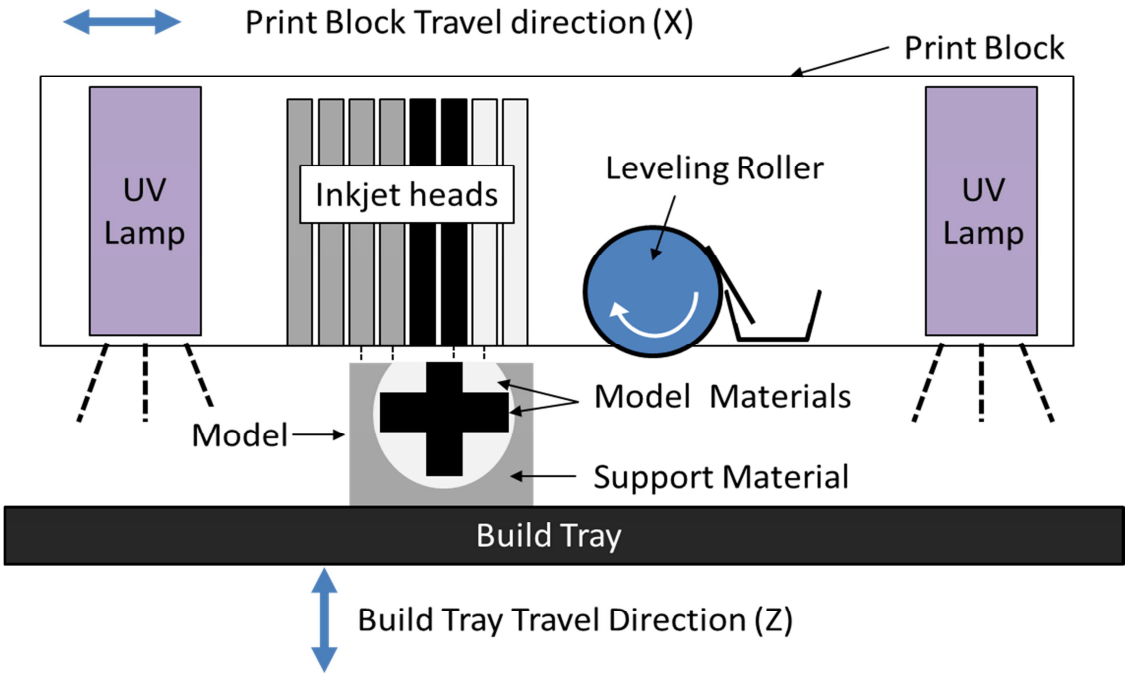

Figure 1-3: Stratasys PolyJet Print Head Block (adapted from Stratasys© Training Manual)

PolyJet is unique among AM processes in that it is designed specifically to deposit multiple materials within a single layer. From this, objects can be created with rigid, plastic-like sections attached to rubber-like or optically clear parts. This capability

has provided the opportunity to print more complex prototypes, just as rigid containers with rubber-like seals or rigid mechanisms with rubber-like joints.

The anatomy of the Stratasys Connex 350 is detailed in the image below. The printer is comprised of the print block, build platform, fluid material cartridges, fluid material lines, waste cartridge, and lid.

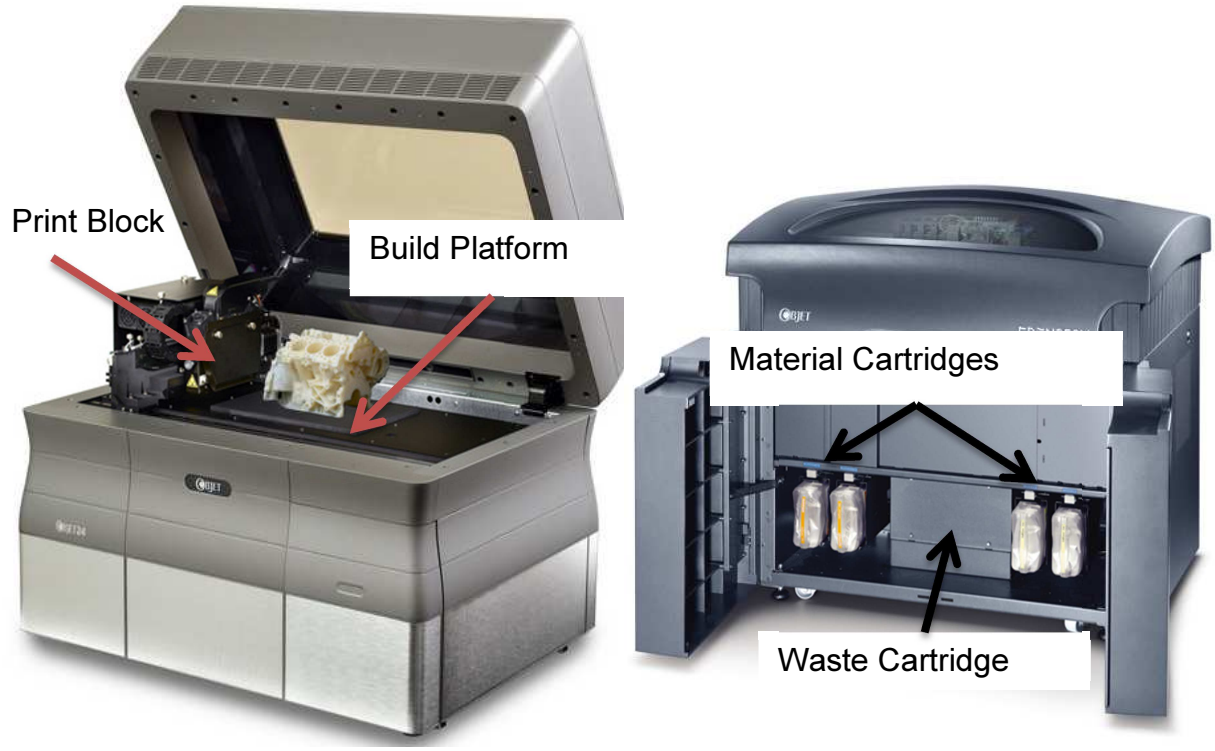

Figure 1-4: Stratasys Connex 350 PolyJet 3D printing machine [10]

The ability to process clear materials alongside other materials makes the PolyJet process an ideal candidate to incorporate the creation PUFs within its process. The process of incorporating PUFs production into PolyJet builds would proceed as follows (Figure 1-5):

1. Inject optically-detectable particles into clear PolyJet resin cartridge
2. Design a feature within the 3D model to incorporate the particle-doped resin

3. Print the 3D model with the particle-doped resin incorporated into the build

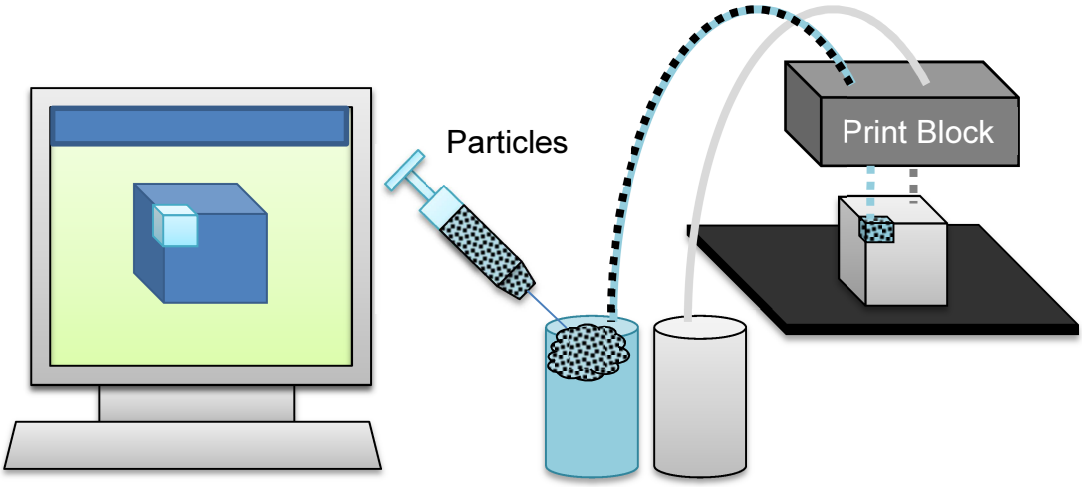

Figure 1-5: Procedure for Incorporating PUFs into PolyJet builds

Considering the required steps, it can be concluded incorporating PUFs within PolyJet builds has the potential to be immediately adaptable by current commercial PolyJet printers.

1.2.3 Quantum Dots

In order to deposit the particle-doped resin via inkjet, the particles must be small enough to pass through the inkjet nozzles, which are approximately 60 microns in diameter. Thus it is necessary to employ small particles, and nano-scale particles would be ideal for avoiding nozzle clogging. Quantum Dots (QDs) are a specific type of nanoparticle with unique optical properties that lend themselves well to this particular application. The salient property of a QD is that it absorbs ultraviolet (UV) light and emits the light in the visible spectrum. Traditionally, QDs are made of chalcogenides

(selenide or sulphate) of metals like cadmium or zinc (for example: CdSe and ZnS), but QDs composed of other materials also exist [10]. QDs range from 2 to 20 nanometers in diameter, and the color of the QD in visible and UV light is dictated by the size of the dot [10]. For example, a 2 nm QD particle will appear light yellow in visible light and glow blue under UV light. Figure 1-6 shows orange QDs in visible light, while Figure 1-6 shows the same QDs glowing yellow-green in UV light.

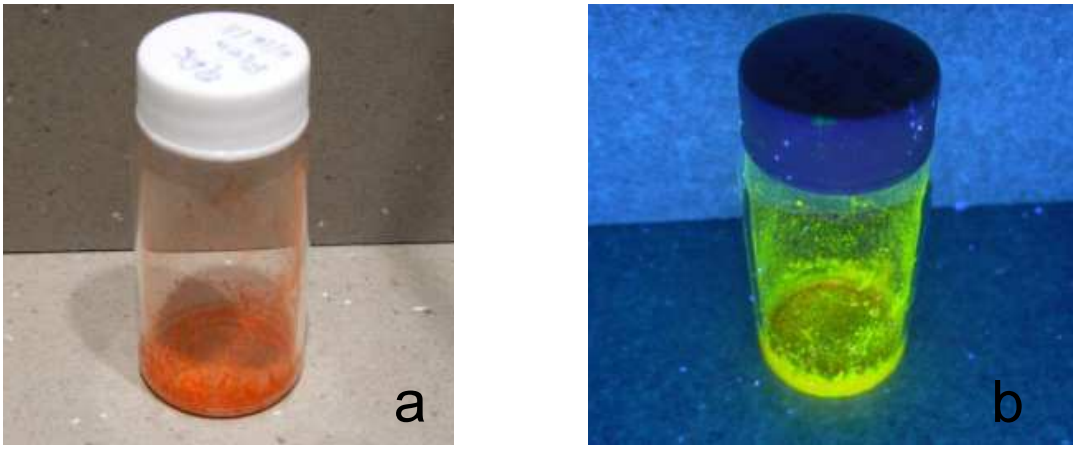

Figure 1-6: QD Powder in a) Visible Light (Orange Color) and b) UV Light (Yellow Color)

This particular alignment of optical PUFs comprised of QDs is a first in the field of cryptography, but overall the combination is obvious. The ability for a particle to transform an input wavelength of light is ideal for challenge-response type security since the challenge input signal (UV light) is differentiable from the system response signal (visible light). Also, as with the previously described optical PUF made of bubbles dispersed in a clear epoxy, any typical particle would only be able to block the input light signal. This design of merely blocking the input signal requires a specific PUF geometry, namely a sheet configuration in which the light source can shine completely through the

PUF into the detector. With QDs as the response particle, the PUF can be placed on the surface of an object and the input light source can be place adjacent to the response detector. Figure 1-7 describes the two configurations.

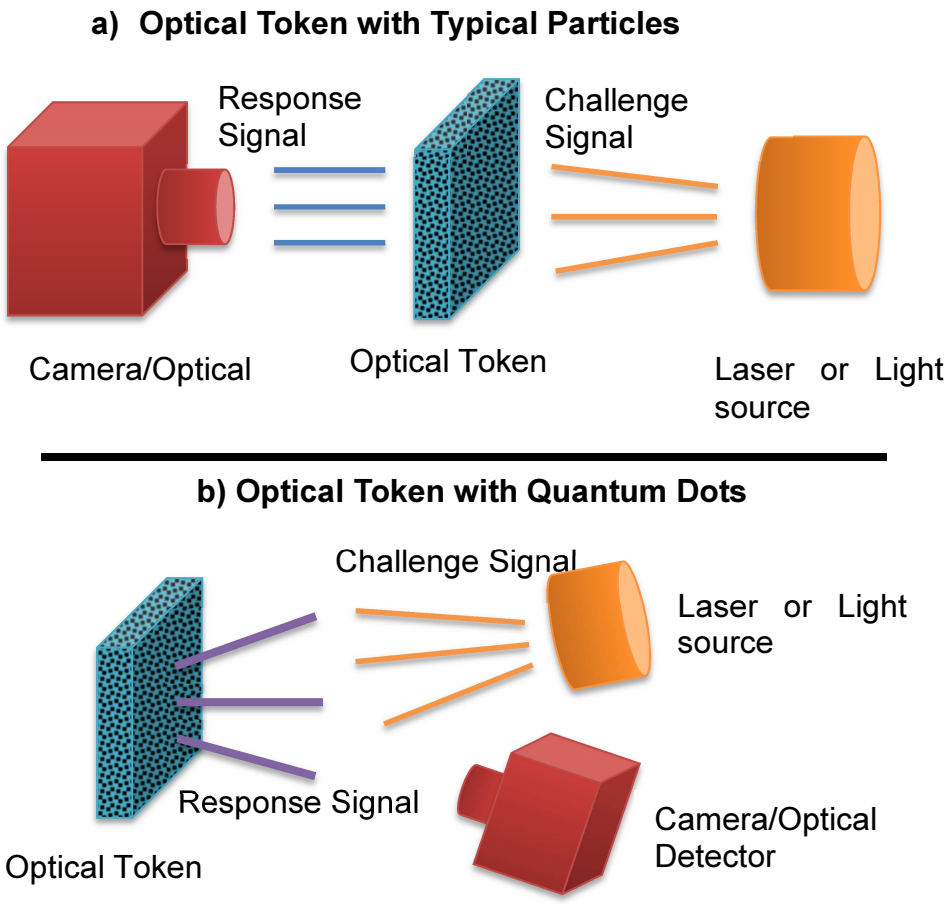

Figure 1-7: Procedure for Incorporating PUFs into PolyJet builds

QDs have been used in the areas of data storage and sensing devices (Chapter 3).QD nanoparticles are of particular interest in microscale patterning because of their size-dependent photoluminescence, narrow band of emission, and nonlinear optical properties [10–15]. The high-resolution patterning of quantum dots within bulk polymer,

specifically, has potential in photonic and biomedical applications as well as pressure and temperature sensing, cryptography, and programmable matter [14-20].

In summary, QDs emit discrete points of light which can be randomly dispersed when injected into a fluid. These two qualities align wholly with the basis of PUFs, which is the random arrangement of particles that are optically detectable.

1.3 Process Design Selection Overview

In summation, PUFs, QDs, and PolyJet have been chosen to serve as the platform of this investigation of creating security features within AM parts. PUFs were chosen as the desired security feature to be incorporated into AM because of their inherent unclonability. Specifically, optical PUFs, which take advantage of the stochastic arrangement of matter, were chosen because particles can be readily dispersed within AM media. PolyJet was chosen as the most-suited for PUFs due to the process's ability to process multiple materials, fluid feed material, and transparent media. Finally, QDs were chosen due to their size and unique optical properties. Figure 1-8 below summarizes the selection process:

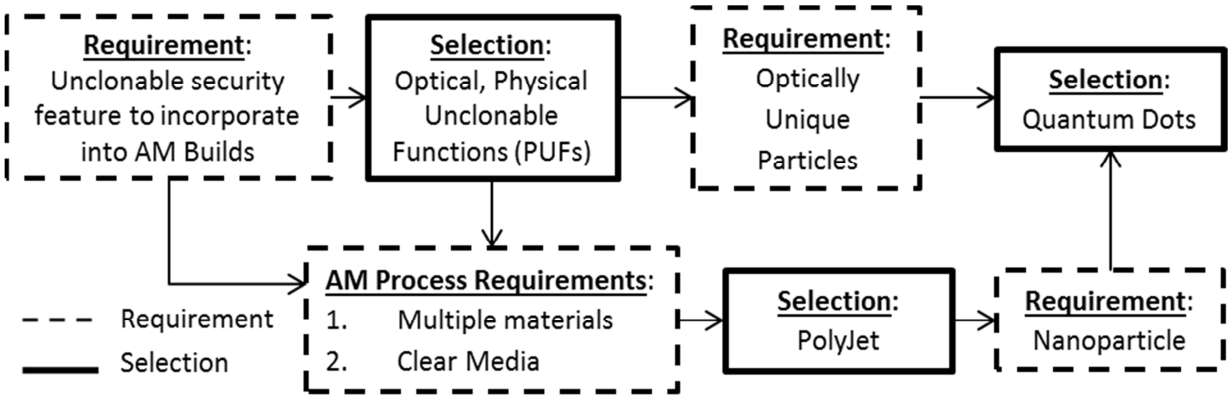

Figure 1-8: Summary of Process Design Decisions

1.4 Dissertation Outline and Research Contributions

The motivating application for this research is the creation of creating a security feature within AM builds, which would provide a means to combat counterfeiting and the illegal production of regulated geometries via AM. Given the previously-stated concepts for a potential solution (PUFs, PolyJet, and QDs), the corresponding overall project goal can be stated as follows:

Overall Project Goal: Create Physical Unclonable Functions via PolyJet 3D Printing of Quantum Dots

The primary research question, and overall research goal, that arises from this project goal is as follows:

Overall Research Question: How Do Quantum Dots Affect the PolyJet Process?

Within this overall project goal and research question resides specific sub goals and questions. Namely, the feasibility of the overall goal must be established and certain effects of the QDs on the PolyJet process must be characterized. First, verification of the visibility of the QDs within PolyJet resin must be achieved. Second, it must be proven that the QDs can be successfully ink-jetted as part of the PolyJet process. The corresponding qualifying questions are as follows:

Qualifying Question 1 (QQ1): What concentration of QDs within PolyJet media is necessary to provide readily visible fluorescence to the naked eye?

Qualifying Question 2 (QQ2): Can the Quantum Dots be added to the PolyJet media and successfully inkjetted without a significant change in jetting behavior?

Answering QQ2 requires studying the rheology of the QD-doped photopolymer as well as the inkjetting performance. Finally, the effects of the QDs on the photopolymerization part of the PolyJet process must be characterized, and this characterization is framed by the Primary Research Question:

Primary Research Question: How do QDs affect the photopolymerization of PolyJet resin?

This characterization and the subsequent answering of the Primary Research Question will constitute the significant research contribution of this dissertation. The following sections will describe in more detail the efforts toward answering QQ's 1 and 2 and the Primary Research Question.

1.4.1 Visibility of QDs with PolyJet Media

Chapter 2 is comprised of investigations and results related to QQ1, the visibility of the QDs within the cured PolyJet photopolymer. The investigations include creating thin films of QD-doped PolyJet media and investigating the sample under UV excitation with the naked eye, bright field microscopy, and fluorescent microscopy. Also, QD-doped PolyJet media is embedded within a PolyJet build to simulate an actual embedded PUF, and the QDs are optically analyzed in the same fashion. Finally, surface treatments and print settings are explored to demonstrate some means of improving the QD visibility if that improvement is needed in the future. Overall, the

conclusions from these visibility investigations demonstrate the feasibility of creating readable PUFs from QDs within the PolyJet process.

1.4.2 Inkjetting with Quantum Dots

Chapter 3 focuses on answering QQ2, which encompasses the effects of QDs on the inkjet process. In Chapter 2, the rheology and jetting behavior of the QD-doped PolyJet resin are investigated. First, a literature review of inkjetting with particle-loading fluids is provided, and the key rheological characteristics for predicating jettability are identified. Next, these key rheological characteristics are measured for varying QD concentrations, and the jettability of these concentrations is calculated. Finally, the jetting of the QD particles is performed with a single nozzle inkjet test stand, which demonstrates the practicality of adding QDs into PolyJet material cartridges.

1.4.3 Characterization of Photopolymerization with Quantum Dots

Chapters 4 and 5 contain the bulk of the contribution of this dissertation toward the goal of characterizing the effects of QDs on photopolymerization, which is in answer to the Primary Research Question. Chapter 4 includes a literature review of existing photocuring theory and characterization methods, while Chapter 5 communicates the modeling and experiments performed toward characterizing the effects of QDs on photopolymerization.

Beyond studying the effects of QDs on the PolyJet process lies the added tasks of adding QDs to the PolyJet material cartridges and actually printing the reading and encoding the QD pattern, however this step is beyond the scope of this dissertation.

1.5 Roadmap

Provided in Table 1-1 is roadmap that identifies the goals of this dissertation and the corresponding chapters and research phases. At the beginning of the roadmap in Table 2, it can be seen that the goal of Chapter 1 is to describe the problem, describe a solution to that problem, and describe the corresponding qualifying and research questions. The problem, specifically, is the need to incorporate security features within AM builds, and the solution is to add QDs to PolyJet media to create PUFs within PolyJet AM builds. This solution brings rise to two qualifying questions and one research question identified in Section 1.4. The work in Chapter 2 focuses on answering Qualifying Question 2, which deals with determining if the QDs are visible within PolyJet media. Chapter 3 includes a literature review of inkjetting with particles and experimentation that serves to answer QQ2: are the QDs inkjettable? Chapter 4 describes the literature review and experimental methods (equipment and procedures) used in this work toward answering the Primary Research Question: How do QDs affect Photopolymerization? Chapter 5 describes the experimental results of the research methods, the theoretical model formed based on the literature review, and a comparison of the model and the experimental results. Chapter 6 contains experimental data that illustrates the effects of intensity on the critical exposure of photopolymer, which constitutes the Secondary Research Question. The remaining chapter, Chapter 7, contains the conclusions from the experimental work and suggestions for future work toward creating PUFs via Polyjet of QDs.

Table 1-1: Roadmap

	Research Phase	Chapter	Goals
Introduction	Problem Identification Solution Proposal	**Chapter 1** Introduction, Motivation, and Project Outline	**Describe the problem** **Describe a solution** to the problem and the process for implementing that solution **Identify the qualifying and research questions** related to the proposed solution
Background & Feasibility Analysis	Information Gathering Preliminary Experimentation	**Chapter 2** Visibility of Quantum Dots within PolyJet Media (QQ1) **Chapter 3** Inkjetting with Quantum Dots in PolyJet Media (QQ2)	**Synthesize literature** related to the Qualifying Questions **Perform Experiments** to address Qualifying Questions 1 and 2 **Draw Conclusions** to address Qualifying Questions
Research Methods	Hypothesis Formulation Experimental Methods Hypothesis Validation	**Chapter 4** Literature Review of Photopolymer-ization Theory, Proposed Theoretical Model **Chapter 5** Experimental Techniques, Results and Critique and Modification of Theoretical Model **Chapter 6** Effects of Intensity on Critical Exposure	**Synthesize literature** related to the Primary Research Question **Identify gaps** in existing literature that prevent answering the research question **Form hypotheses** based on existing literature **Establish Methods** for validating the hypothesis **Perform Experimentation** to validate hypothesis
Summary	Conclusions Outlining Future Work	**Chapter 7** Project Summary and Future Work	**Draw Conclusions** based on experiment results **Identify significant contributions** **Summarize accomplishments** related to answering each of the research questions **Propose future work**

CHAPTER 2 QUANTUM DOT VISIBILITY WITHIN POLYJET MEDIA

2.1 Introduction

The work in this dissertation is focused toward creating security features within existing AM processes which can identify legitimate builds from counterfeits. PUFs are in the category of "challenge-response authentication," with the challenge being exposure to UV light and examination with an optical detection system, and the response being the pattern of the QDs within the PUF. To function as a security feature, it is crucial that the optical response of the PUFs to the "challenge" be readily detectable. Furthermore, to pursue the objective of creating PUFs within PolyJet artifacts, it is critical to consider the optical visibility of the QDs embedded within the cured part. Since the photopolymer surrounding the QDs also absorbs UV light, it is possible that the UV light meant to illuminate the QDs to elicit a security response will be absorbed by the surrounding polymer to an extent that makes detecting the QDs impractical. Thus, this chapter focuses on methods for optically detecting QD's dispersed in PolyJet media and methods for improving QD visibility within the media.

First and foremost, a range of QD concentrations must be explored to determine the minimum concentration necessary to produce fluorescence visible to the naked eye. This metric was chosen because concentrations with visible fluorescence would have sufficient amount of QDs to create PUF patterns. Thus, investigating cured, QD-doped PolyJet films is a convenient way to identify the appropriate sample concentrations for jetting and curing experiements. Determining this minimum concentration is critical to jetting and curing experimentation (Chapters 3-5) because of the cost of QD materials.

Thus, Qualifying Question 1 addresses the need to identify the minimum concentration of QDs:

Qualifying Question 1 (QQ1): What concentration of QDs within PolyJet media is necessary to provide readily visible fluorescence to the naked eye?

Detection of QD patterns within AM parts is critical to the security of the embedded PUFs, so factors that affect visibility both by the naked eye and by microscope must be explored. Variables within the production process itself can contribute to the visibility of the QDs within the PolyJet photopolymer. The variables in the production process of QD PoyJet PUFs includes functionalization and concentration of the QDs within PolyJet photopolymer, printer settings, PUF geometry, and post processing techniques. To frame the work exploring factors that affect visibility, QQ's 1.1 and 1.2 are formed:

Qualifying Question 1.1 (QQ 1.1): How do production variables affect the visibility of PUF patterns?

Qualifying Question (QQ 1.2): How do production variables affect the visibility of QDs by the naked eye?

First, the minimum concentration of QDs to produce fluorescence visible to the naked eye (QQ1) will be explored in Section 2.2. Then, variables affecting both microscopic and naked eye visibility (QQ's 1.1 and 1.2) will be addressed in Section 2.3. Since the work in this chapter stands to 1. Establish minimum concentrations for curing

and jetting experimentation in Chapters 3-5 and 2. to provide some insight into methods to improve visibility of the QDs, the analysis performed in this chapter is qualitative.

2.2 Qualifying Question 1: Minimum QD Concentration

A major variable in the samples used in this dissertation is the concentration of the QDs within the photopolymer. Adding QDs to the photopolymer affects the rheology of the PolyJet photopolymer media as well as the appearance of the cured media. Adding too few QDs would result in poor PUF patterning and visibility, and too many QDs would adversely affect the inkjetting properties of the photopolymer. A simple way to determine the upper limit of QD concentration is to observe a few concentrations under UV light with the naked eye.

QD concentrations were prepared by first synthesizing the QDs via chemical synthesis and then stirring and sonicating the mixtures until homogeneity was achieved [1]. Samples were created by exposing a small beaker of the uncured, QD-doped polymer samples to an 8-watt UV lamp for approximately 15 seconds (24 mJ/cm^2 dosage). This resulted in the films shown in Figure 2-1, which are two-to-three hundred microns thick and approximately 1 inch in diameter.

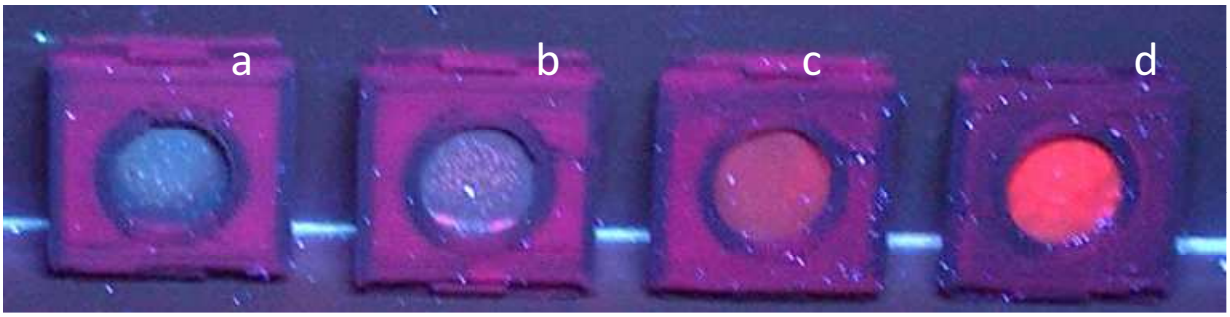

Figure 2-1: Film samples (in square, black fixtures) of varying QD weight percents under UV light: a) 0.02 wt% b) 0.1wt% c) 0.2 wt% d) 0.5 wt%

Upon observing these samples under UV light in a dark room, it can be seen that the QDs create a visible fluorescence with 0.2% mass concentration. A very strong fluorescence can be seen in the 0.5% sample. From this, it was determined that 0.5% mass concentration of QDs was sufficient to produce visible fluorescence to the naked eye, and that observing the effects of QDs in much higher concentrations is not necessary. In other words, since the salient purpose of the QD-photopolymer mixture is to create a pattern recognizable via microscope, it would not be useful to investigate concentrations beyond what is clearly visible to the naked eye. Therefore, for the visibility, rheology and jetting investigations, concentrations no greater than 0.5% will be observed. For the photopolymerization characterization in Chapters 4 and 5, concentrations of up 5 wt% are investigated since a broader characterization of the effects of QDs on photopolymerization is desired.

2.3 Qualifying Question 1.1 and 1.2: Production Variables that affect QD Visibility

Qualifying Questions 1.1 and 1.2 deal with process factors that could affect the visibility of the QDs on a macroscopic (e.g. naked eye visibility) and microscopic level. To establish the feasibility of creating PUFS with QDs in PolyJet media, understanding the process factors that can affect visibility is critical. Section 2.3.1 will discuss the different process variables explored, Section 2.3.2 will describe the sample preparation methods, Section 2.3.3 will describe analysis methods, and Sections 2.3.4 and 2.3.5 will discuss the visibility results on the macro and micro scales, respectively.

2.3.1 Process Variables

The “processing” of the QDs starts with the actual synthesis and functionalization of the QDs and ends with post-processing of the PolyJet prints with embedded QDs. Functionalization in this case denotes the modification of the QD particle surfaces toward improving compatibility between the QDs and the PolyJet polymer. Once the QDs are functionalized, they are mixed in varying concentrations with PolyJet VeroClear photopolymer via stirring and sonication until homogeneity in the mixture is achieved. Next the liquid samples are either embedded in PolyJet builds or deposited onto a substrate and subsequently cured. Finally, the PolyJet builds with embedded QDs can be polished and the surface treated to improve visibility. The remainder of this section will describe the various process steps in more detail.

Functionalization

Functionalization of the QDs was performed for the purpose of improving the compatibility between the QDs and the photopolymer, which would reduce agglomeration and settling seen in the QD-polymer mixtures. During functionalization, polymer ligands are attached to the surface of the QD particles and act as a bridge between the QDs and the surrounding polymer chains. By coating the surfaces of the particles and ultimately creating a distance barrier between the particles themselves, the QDs are less likely to be attracted to one another and agglomerate. Furthermore, the ligands help combat settling of the QDs. Finally, during curing, functionalization allows the QDs to be part of the polymer network instead of being trapped within [1]. The effects of the functionalization on visibility are discussed in Sections 2.3.3 and 2.3.4.

Printing Settings and Post Processing

VeroClear photopolymer used in this investigation is described by the manufacturer as “water clear.” PolyJet process itself, however, introduces imperfections on the surface of, and within, the additively-manufactured part that reduces its transparency. As listed in Table 2-1, four categories of techniques exist for improving the clarity VeroClear parts: system cleaning, printing settings, design techniques, and post-processing techniques.

1. Cleaning the material supply lines within the machine ensures that only translucent material will be deposited in the build.
2. The *printing techniques* that increase transparency are designed to minimize the amount of over-curing in the part, which contributes to decreased clarity.
3. Since the PolyJet process currently does not have the capability to selectively cure layer profiles, the entire build gets UV dosage even if a small portion of the build is getting printed at the time. Therefore, designing the part so that transparent portions of the part are not significantly lower than the total build height minimizes over cure that occurs as the UV light cures higher layers.
4. Post processing techniques such as polishing and lacquering improve the surface finish and clarity of VeroClear parts.

Table 2-1: Techniques for improving clarity of PolyJet VeroClear Parts [2-3] (Techniques considered in this research are highlighted in grey)

Cleaning Techniques	**Replace the resin using "High Performance"** replacement option: In contrast to the regular resin replacement option, the High Performance resin replacement option performs extra cleaning that will more fully ensure the complete depletion of non-transparent resin in the material feed lines, which contributes to the non-transparency of VeroClear prints.		**Clean the printing block** (roller bath and print heads): Cleaning the printing block removes non-transparent resins from the printheads and roller bath that may migrate into the VeroClear part during printing.
Printing Techniques	**Use a Matte finish:** The over-exposure of the VeroClear to UV light can negatively affect the translucency - printing with a Matte finish acts as a "sunscreen" against UV exposure.		**Print in High Speed Mode:** this mode reduces the amount of passes of the UV light by increasing the layer thickness from 16 microns to 30 microns.
Design Techniques	Avoid over-exposure of glossy parts by **printing objects with same Z-height**		**Use thin walls:** Less material means better transparency
Post Processing Techniques	**Allow a few days for the object to reach maximum clarity:** Allowing the part to rest for a few days will improve clarity along with polishing the surface.	**Polishing:** Polishing removes surface defects which contribute to opacity	**Lacquering:** Adding a lacquer to surfaces fills in cavities that contribute to opacity

Although the literature establishes some "best practices" for improving the clarity of VeroClear PolyJet prints, these methods are toward naked-eye clarity and not clarity on the microscopic level. Since optical PUFs are viewed via microscope, it is important that these methods be investigated for clarity on the microscopic level. In Table 2, the variables highlighted in grey (matte vs. glossy print settings, polishing and lacquering) are the two print settings that could affect the microscopics visibility of QDs within the polymer.

As shown at the bottom of Table 2-1, post processing techniques can also improve clarity in addition to print settings. The post-processing techniques that exist for

improving the clarity of VeroClear parts include polishing and lacquering [2]. Polishing the surface of VeroClear parts has the potential to improve visibility of the QDS because this process gets rid of surface defects that contribute to opacity. Lacquering, on the other hand, does not reduce surface defects but rather adds a coat of material, which has the potential to degrade visibility. These techniques are described in Section 3.3.3.

Geometry and Concentration

In designing PUFs, it is important to know the minimum thickness required to produce visibility of the PUF on the macro and micro levels. A geometry that is too thin might not be noticeable to the naked eye, and a geometry too thick would be a waste of QD material. Furthermore, too high of a concentration would make the QD patterns too crowded and indistinguishable, and too low concentrations would prevent the QDs from being visible to the naked eye. Thus, exploration of varying concentration and PUF geometries is performed in this work.

Summary of Variables

The following processing variables are explored in this chapter for their effects on visibility on the macro and micro levels:

1. Functionalization of the QDs prior to incorporating into PolyJet resin
2. QD Concentration within the resin
3. Geometry of the PUF
4. Printer Settings (Matte vs. Glossy)
5. Post Processing (polishing and lacquering)

Sample preparation and analysis methods will be discussed in Sections 2.3.2 and 2.3.3 and the visibility results for the naked-eye and microscope will be reported in Sections 2.3.4 and 2.3.5, respectively.

2.3.2 Sample Preparation

Functionalization

Functionalization was performed via chemical means at Virginia Tech [1]. After the QDs were synthesized and dried, the functionalization components were synthesized and the QD powder was incorporated. Once sufficient stirring was achieved, the coated QDs were dried once more into powder form.

Embedding Procedure

To fully investigate the visibility of QDs within PolyJet artifacts, QDs must be encased within printed PolyJet material and observed. This was accomplished by manually embedding a solution of QDs and PolyJet resin into a void of a printed part as it is being fabricated. Using a procedure outlined in prior work, samples were created with embedded QDs using the following steps (Figure 2-2) [4]:

1. Create a 3D model with empty volumes in the location of which the embedded fluid is desired to be placed
2. Initiate the PolyJet print
3. Pause the print at the appropriate layer
4. Open the printer and remove the support material that occupies the print in the areas that correspond to the empty volumes in the 3D model
5. Deposit the embedding fluid into the scraped volume

6. Cure inserted fluid with UV lamp
7. Close the printer and proceed with printing

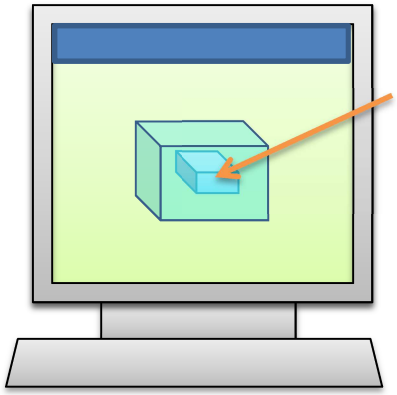

Steps 1-2: Design digital 3D model with some volume dedicated to embedding, and initiate print

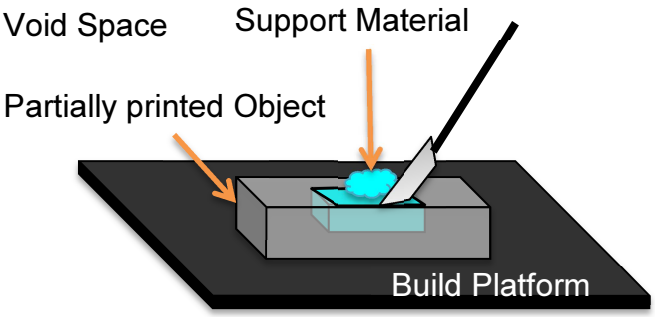

Steps 3-4: Pause the build and remove support material from void space

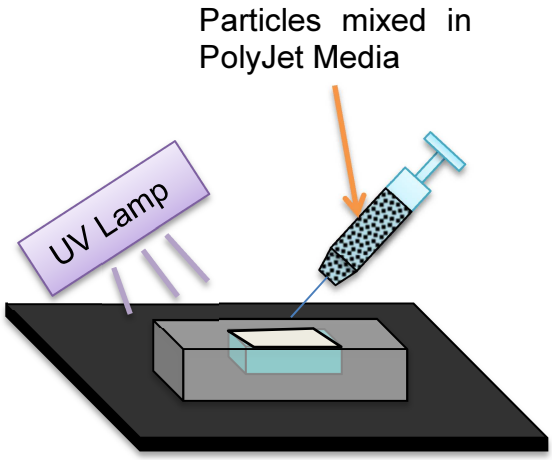

Step 5-6: Add nanoparticle fluid into void space and cure with UV lamp

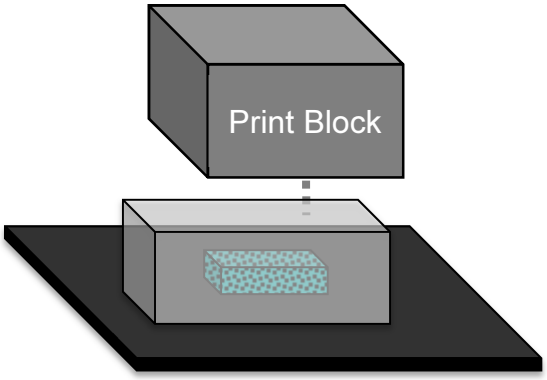

Step 7: Resume build, allowing the remaining build volume to encase the embedded QD mixture

Figure 2-2: Process for embedding QDs within PolyJet builds

Print Settings

Two different print settings were tested for their effects on visibility: the glossy print setting and the matte print setting. For the matte finish, support material is printed atop the top layer of the build and acts as “sunscreen” against over-curing (this layer removed post print using a high-pressure water jet). The glossy samples were left uncovered and received an additional does of UV light. Four samples were created: one sample was printed with a “matte finish” print setting and three samples were printed using the “glossy finish” print setting.

The matte and glossy print settings were polished and lacquered to see which combination of matte/glossy and polished/lacquered produced the best visibility. These combinations were observed via fluorescent microscopy (Section 3.2.3) and with a surfometer, which measures surface roughness.

Surface Treatment Sample Geometries

In order to test the effects of surface finishing techniques, it was necessary to design a test sample that could undergo surface finish treatments. Because it is difficult to selectively polish a surface (which is one of the surface finishing techniques), it was required that the samples be physically separate from one another (as opposed to applying many surface treatments to one sample surface). The surface finish samples were created using the embedding technique described in the previous section. To create the experimental samples, QD’s were synthesized, mixed in 5.0 wt% with PolyJet VeroClear photopolymer, and embedding into the PolyJet build. The dimensions of the test sample are illustrated in Figure 2-3 below.

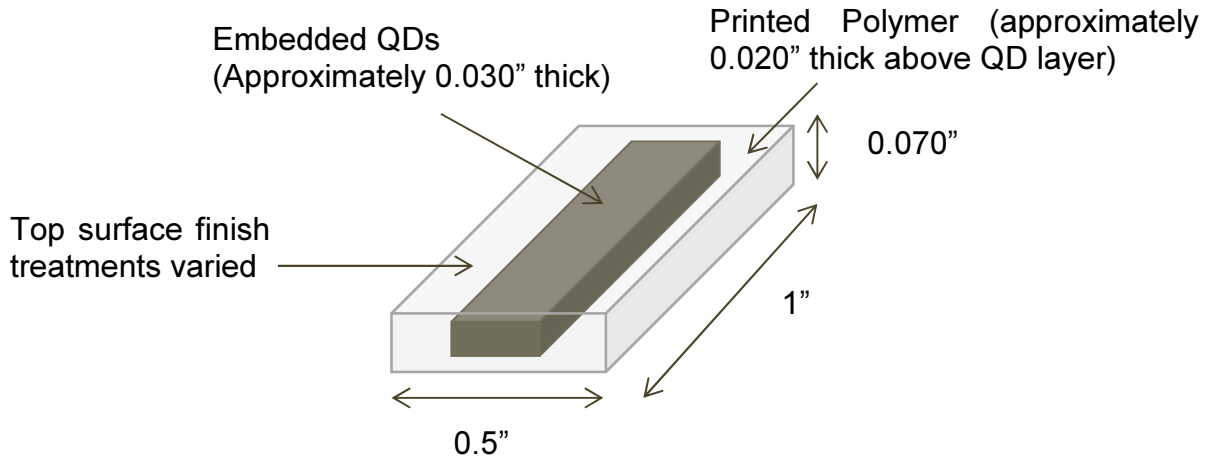

Figure 2-3: Diagram of Surface Finish Samples

Two of the three glossy samples were treated post-print: one by polishing (following PolyJet guidelines [2]) and the other by coating with a spray lacquer. The object of this test was to see what techniques provide the best surface finish, and subsequently the most clarity.

PUF Geometry and QD Concentration

The visibility of the QDs within printed VeroClear can be affected by the concentration of the QDs as well as the thickness of the QD layer. To analyze this, a test sample was designed with varying well depths and columns to accommodate 6 different concentrations of QDs. To create the experimental samples, QD’s were synthesized, mixed with PolyJet VeroClear photopolymer in varying concentrations, and embedding into the PolyJet build (as per Figure 2-2).

A test sample was designed with 6 columns of wells at varying depths. 18 different sample wells were created: six different concentrations were deposited at three

different well depths. The geometry and an image of the sample can be seen below in Figure 2-4:

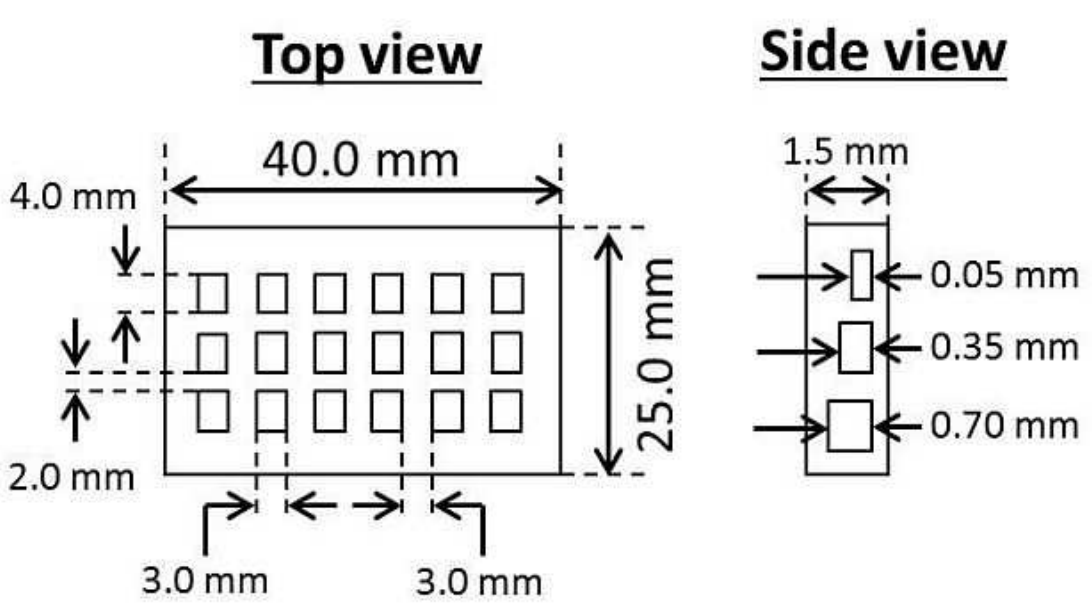

Figure 2-4: Diagram of Concentration and Well-Depth Sample Dimensions

Post Processing Techniques

Two post-processing techniques were tested for their effects on the visibility of QDs within PolyJet builds: polishing and lacquering. To polish the sample, several steps were taken. First, the surfaces were dry-polished with 200 and 300 grit sand papers to remove the larger surface defects. Next, wet sanding was done with 400, 600, and up to 1000 grit sandpapers. Wet sanding is accomplished by soaking the sandpaper in water prior to sanding. Micromesh sanding was accomplished by sanding the samples with micromesh sand paper and a polishing compound. Finally, the samples were buffed using a buffing wheel and more polishing compound. To lacquer the samples, an aerosol guitar lacquer was sprayed onto the sample surface and left to dry for 24 hours.

2.3.3 Analysis Methods

Bright Field and Fluorescent Microscopy

In order to view individual QDs, it is necessary to observe the samples under a microscope that can illuminate with UV light and detect fluorescent light. A fluorescent microscope is the ideal tool for observing individual QDs as they fluoresce. The fluorescent microscope used in this work is a Leica Microsystems DMI6000B inverted microscope equipped with Leica EL6000 external light source for fluorescence excitation. A TxR (Texas Red) filter cube was used for detecting emission of the QDs. The microscope can also be used for bright-field imaging by changing the light source and filter. Being able to view the QDs in this manner will give insight into how the surface finish techniques affect the visibility of QDs.

Naked Eye

Beyond the goal of addressing QQ1, some investigations were performed to understand the visibility of the QD fluorescence to the naked eye. Naked eye visibility matters for the practical reason of identifying the location of a PUF on an AM artifact. Therefore, brief inspection was performed to see how QD concentration, PUF thickness, print settings, and surface treatments affect the nake-eye visibility. These investigations serve as a starting point for future work in PUF design, but full, quantitative analysis is beyond the scope of this dissertation.

Surface Roughness Measurement

Since the surface finish plays an important role in clarity, it would be beneficial to understand the difference in surface roughness between the samples. Investigation of

surface roughness will be achieved using a high-precision surface roughness gauge know as a surfometer. The instrument utilizes a small, diamond-tipped probe with a piezo sensor to follow the contours of the sample surface and report data on the frequency and amplitude of surface defects. A surfometer is typically used on harder materials such as metals, but it was verified through the manufacturer that the SRG 4000 used in these experiments was capable of measuring hard plastic surfaces.

Summary of Methods

The methods in this chapter are directed toward investigating the visibility of the QDs within PolyJet polymer. Visibility is determined by the ability of an optical microscope to detect patterns created by the arrangement of QDs. Variables that might improve visibility include (i) printing parameters, (ii) post-processing techniques, (iii) QD concentration, and (iv) PUF geometry. Samples were created by injecting QD-doped PolyJet media via an embedding process that involves pausing a PolyJet build, removing support material, injecting the QDs, and resuming the build to encase the QDs. The remainder of this chapter will discuss the results of the visibility investigations.

2.3.4 Naked Eye Visibility Results

Embedding

Figure 2-5 is an image of a business card sized PolyJet print that was embedded with QDs using the procedure established in Section 2.3.2. Figure 2-5 is a demonstration that the embeddin technique works and that the QD fluorescence is visible from within a PolyJet build.

Figure 2-5: QDs Embedding in PolyJet Build under (a) UV light and (b) visible light

Although this technique makes the creation of artifacts with embedded QDs possible, it is very time-consuming and has many limitations. First, the features for embedding cannot be very fine and, subsequently, the fluid injection is difficult to achieve with fine features. The scraping tools used to remove support limit the ability to remove the support material, and the identification of the exact location of support material is difficult with fine features. Also, a complex feature is very difficult and time consuming to clean by hand. The biggest limitation of this approach, however, is the inability to create embedding features with any sort of three-dimensional complexity. Thus, the need for developing AM systems that can selectively place embedding materials within print layers is obvious. Overall, however, the results of the embedding experiment show that the QD glow of the embedded QDs can be seen with naked eye and that the embedding can be done without affecting surface finish of part.

Functionalization

Figures 2-6 and 2-7 contains images of functionalized and non-functionalized QD-polymer mixtures under UV and visible light, respectively.

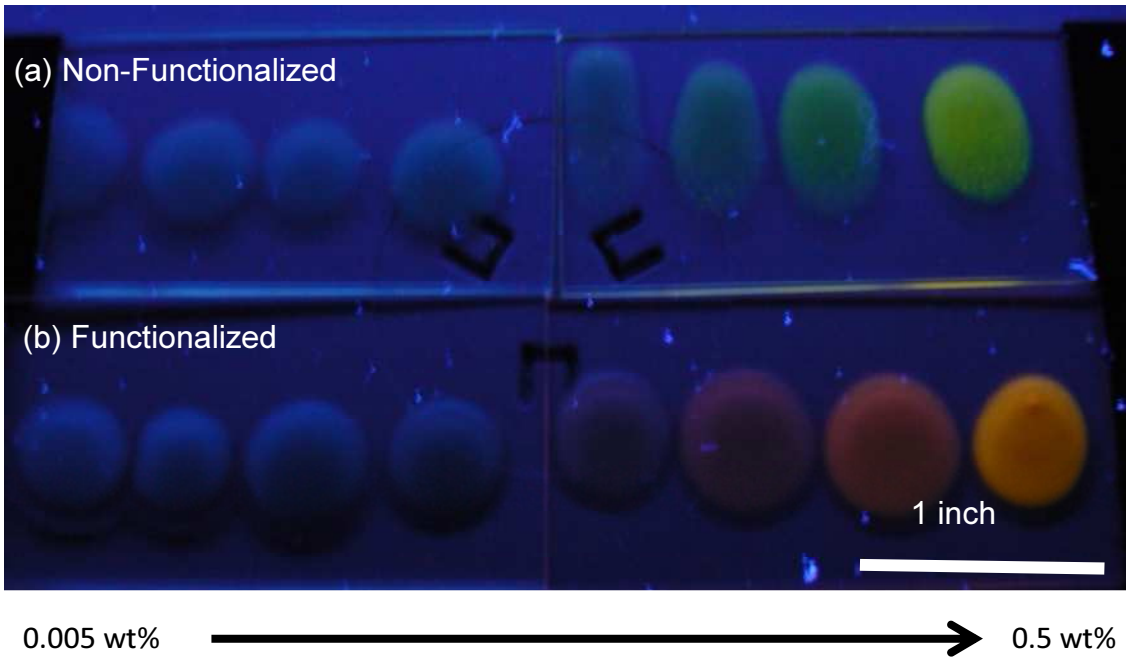

Figure 2-6: Images of (a) Non-functionalized and (b) Functionalized QDs under UV light

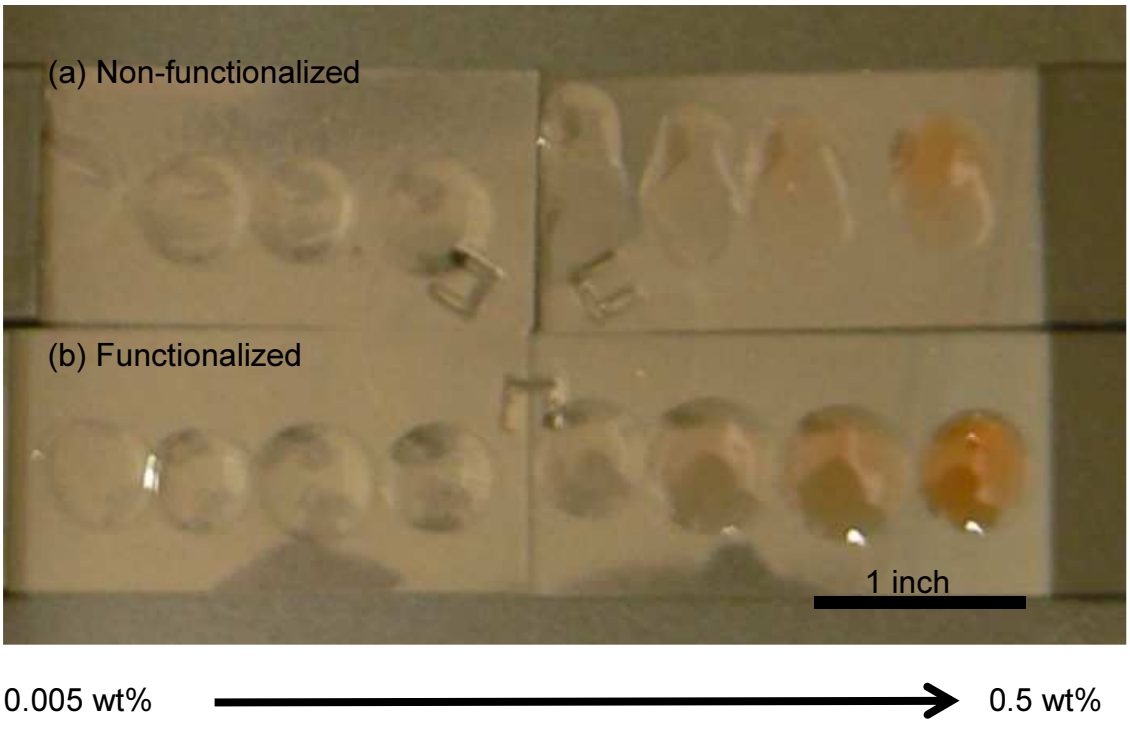

Figure 2-7: Images of (a) Non-functionalized and (b) Functionalized QDs under visible light

Concentrations ranging from 0.005 wt% to 0.5 wt% were deposited onto glass slides, cured, and then imaged with a DSLR camera. The most noteable difference between the functionalized and non-functionalized samples is the orange fluorescence of the functionalized dots and the green fluorescence of the non-functionalized dots. The reason for the change in color is not fully understood. The visibility of the different colors, however, does not appear to differ. Thus, it can be concluded that functionalization changes the color of the QD fluorescence but not the overall visibility to the naked eye.

PUF Geometry and QD concentration

As shown in Figure 2-8 and 2-9 below, 6 concentrations of QD-doped photopolymer were deposited in 3 different well depths:

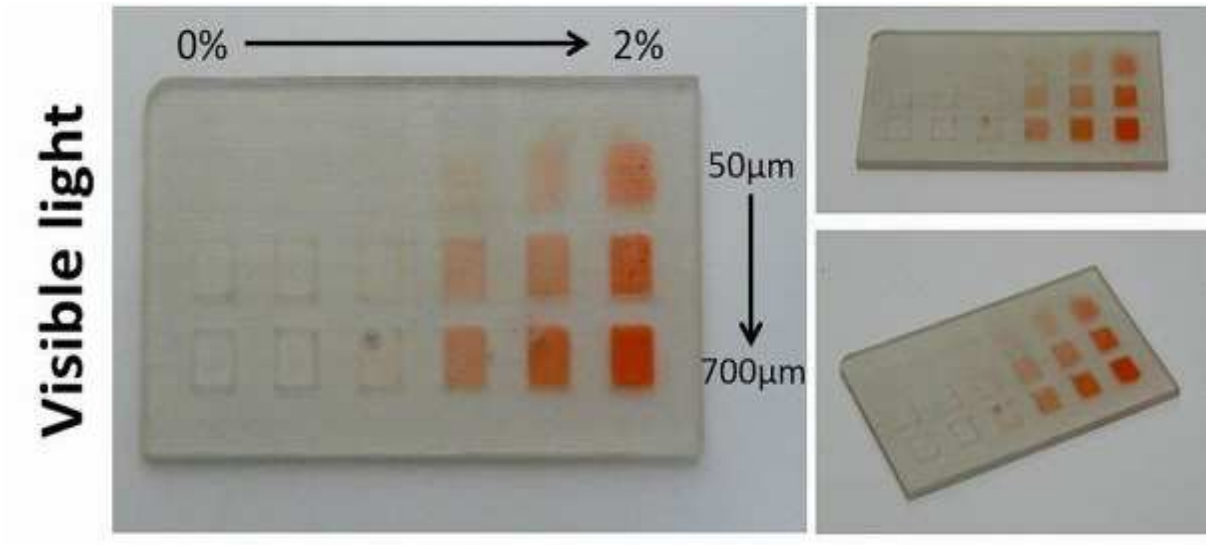

Figure 2-8: Image of Concentration and Well Depth Sample

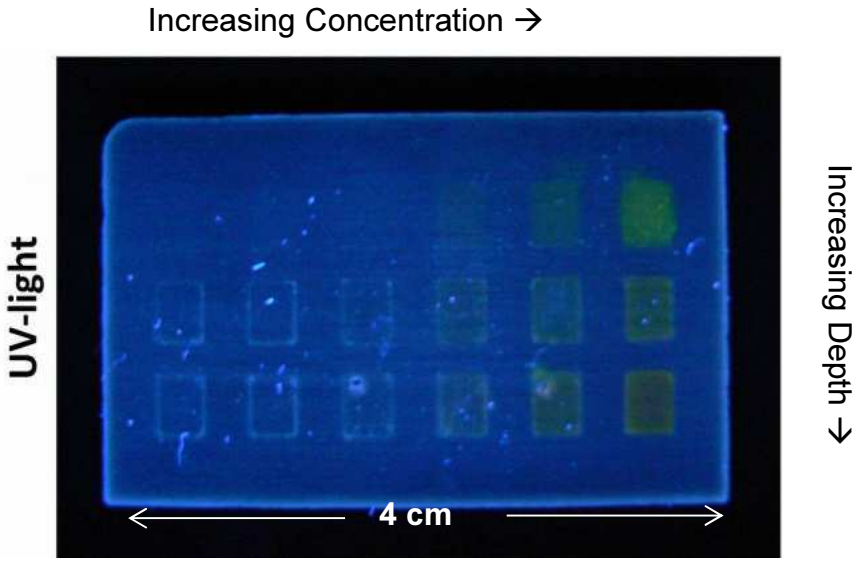

Figure 2-9: Concentration and Well Depth Sample (matte setting, not polished)

The top-right sample well is of most interest because it glows the brightest under UV light. This well corresponds to the shallowest of the 3 well depths but the highest concentration of QD's. Therefore, it can be concluded that higher QD-layer thickness does not lead to better visibility, but that higher concentration does contribute to better naked-eye visibility.

Surface Roughness Measurements

To understand the difference in resulting roughness between the surface treatments, Roughness measurements were taken using SRG 4000 roughness tester, and the results are compared in Figure 2-10 below. It can be seen that the matte finish sample is considerably rougher than the glossy samples, with the roughness of the glossy samples decreasing with both lacquering and polishing. Lacquering a glossy-printed sample does not appear to be as effective as polishing the sample in reducing

surface defects. This is probably due to the fact that lacquering is added via spray deposition, and resulting surface coating is nonuniform.

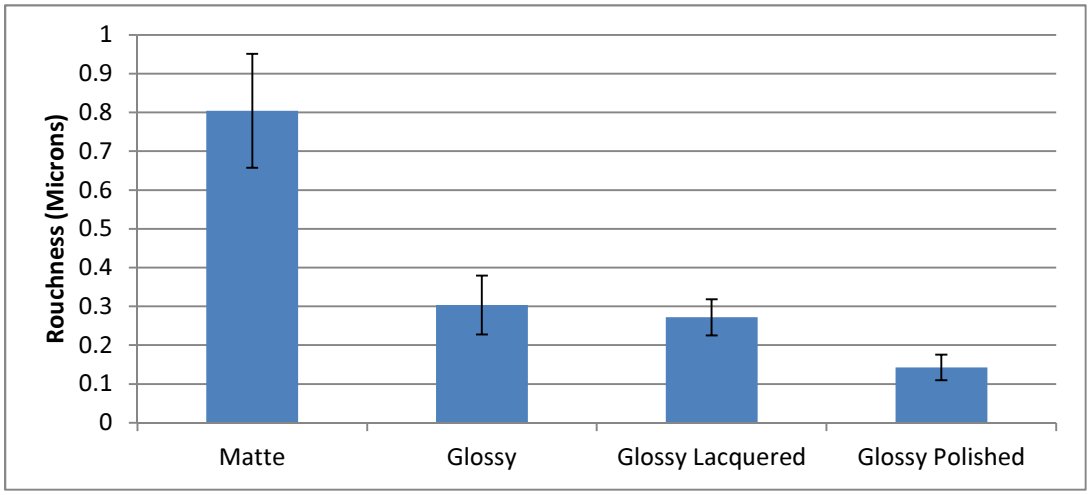

Figure 2-10: Roughness Averages (R_A) for Visibility Samples

Further exploration of the surface finishing should include polishing and lacquering Matte printed parts. However, pursuing an optimized combination of printer setting and surface finishing techniques is outside the scope of this dissertation.

Printer Settings and Post Processing

The visibility of the embedded QDs was investigated to see which surface finish was best for seeing the QD fluorescence (under UV light) with the naked eye. The imaging setup consisted of an 8-watt UV lamp and a DSLR camera, and the images were taken in a dark room. Figure 2-11a shows all the same arrangement as in Figure 2-11b, but the latter is under UV light.

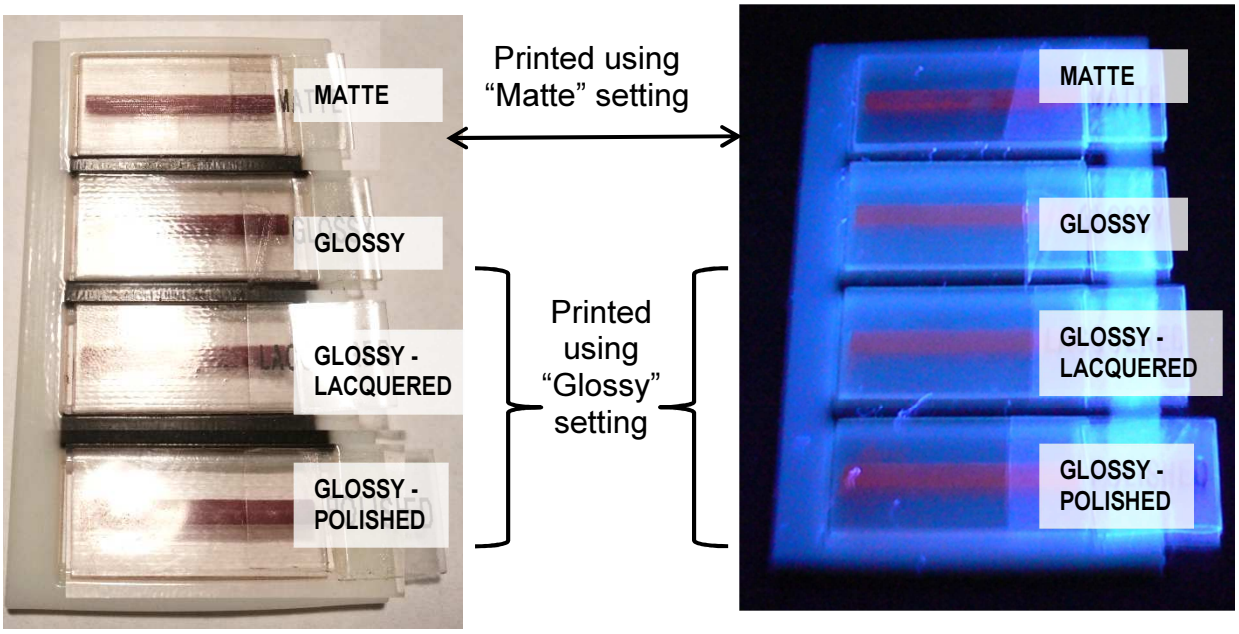

Figure 2-11: Surface finishes of the samples can be seen in the reflection of light (a) and the QD fluorescence can be seen under UV light (b)

The four samples are aligned within a black and white fixture. In visible light (Figure 2-11a), the fixture mounts appear black and the embedded QDs are brown. Under UV light (Figure 2-11b), the embedded QDs glow in a reddish color. Examining Figure 2-11b, it can be seen that the matte and glossy-polished samples have noticeably less "white glow" than the glossy and glossy-lacquered samples. Subsequently, the matte and glossy-polished finishes provided the better visibility of the quantum dots under UV light than the glossy and glossy-lacquered samples. It is hypothesized that the "white glow" is due to an over-cured layer that is present in the glossy samples but was removed during polishing of one of the glossy samples. Therefore, it can be hypothesized that over-exposure to UV light makes the QDs less viewable under UV light.

2.3.5 Microscopic Visibility Results

Functionalization

Figure 2-12 a and b are images taken with a fluorescent microscope of functionalized and non-functionalized QDs with cured PolyJet resin, respectively. The QD concentration is 0.5 wt% for each of these samples. Comparing these images it can be seen that the functionalization had an impact on agglomeration. The points of light created by the QDs in Figure 2-12a (functionalized) a visibly smaller than that of Figure 2-12b (non-functionalized). Thus, it can be concluded that the functionalization decreases agglomeration of QDs dispersed in Polyjet polymer.

To completely eliminate agglomeration of the QDs within PolyJet photopolymer, the QDs should be synthesized within the polymer itself or synthesized with the polymer as it is being created. However, the presence of agglomerates is advantageous in this application because the agglomerates are readily seen via optical microscopy while individual QD nanoparticles are not. Furthermore, the diversity in particle diameters adds to the complexity of the PUF and thus enhances its security. Thus, the functionalization performed in this work helps avoid too many large agglomerates while still maintaining diversity in agglomerate diameters.

Overall, the images in Figures 2-12 a and b reveal that the QDs are visible within the PolyJet photopolymer and produce speckle patterns visible via microscopy. These speckle patterns are the main, necessary characteristic of optical PUFs. Therefore, Figure 2-12 demonstrates that creating PUFs is possible via mixing QDs with PolyJet clear photopolymer and observing the speckle patterns via fluorescent microscopy.

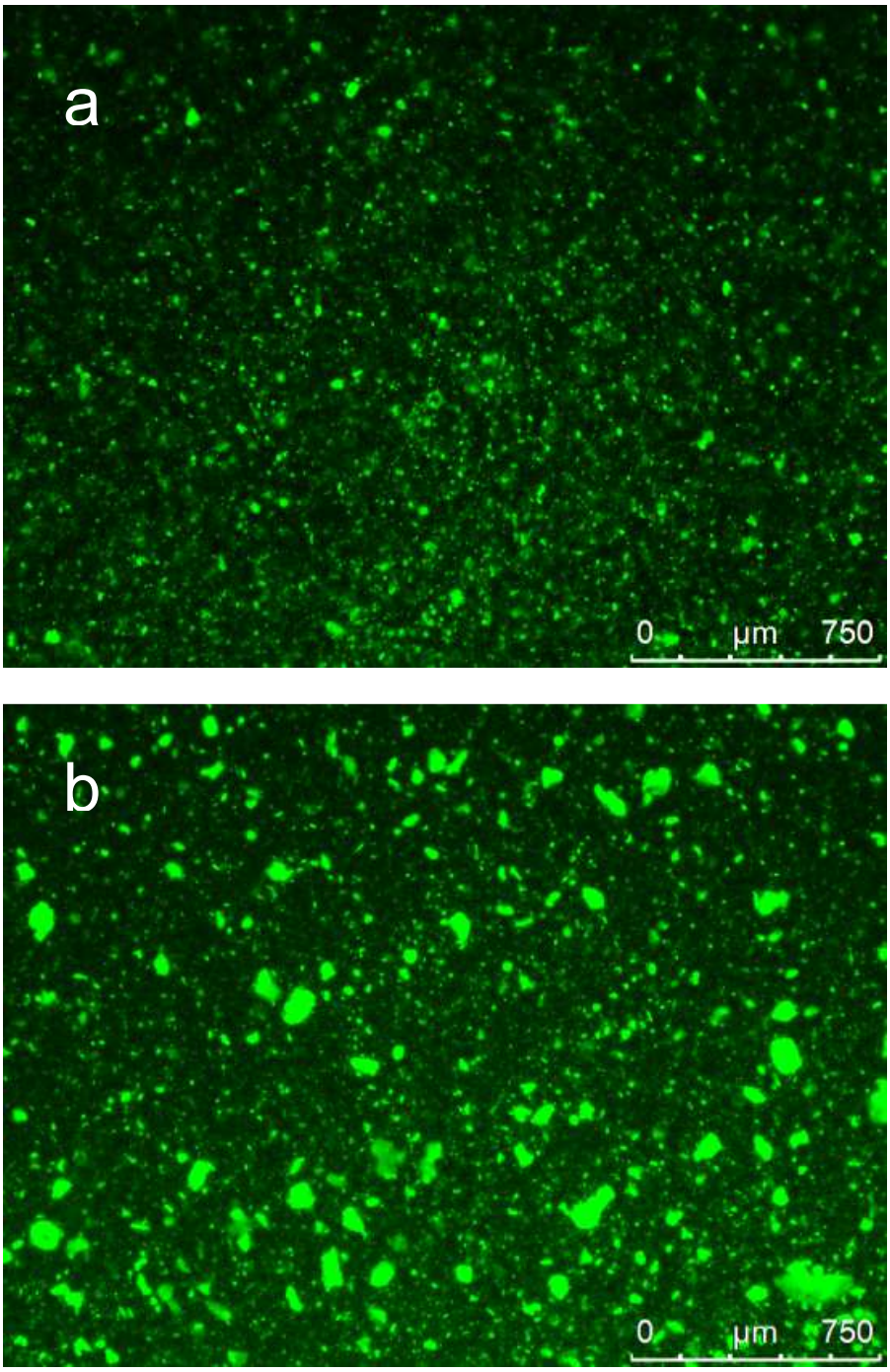

Figure 2-12: Fluorescent microscope images of (a) functionalized QDs and (b) non-functionalized QDs of 0.5 wt%

Print Settings and Post Processing

Figure 2-13 shows the four surface finish samples from Figure 2-11 under bright field light with a 5X magnification. It was hypothesized that the increased surface defects in the over-cured layer of the glossy and glossy-lacquered samples are what caused the “white glow” previously described.

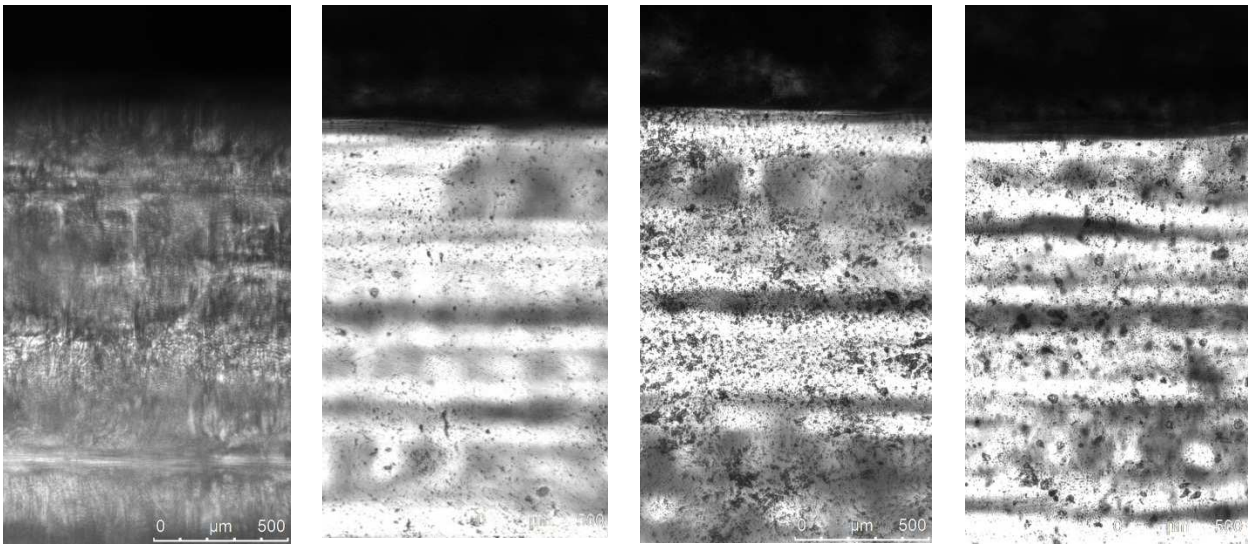

a) Matte Print Setting **b) Glossy Print Setting** **c) Glossy Print Setting, Lacquered** **d) Glossy Print Setting, Polished**

Figure 2-13: Samples with varying surface finishes investigated under bright field microscope (5X magnification)

The images in Figure 2-13 reveal that the matte setting contains the most surface defects, while the glossy print setting has the least. The glossy-lacquered and glossy-polished samples in Figure 2-13 c and d reveal a significant amount of surface defects compared with the glossy print sample. The surface defects caused by lacquering are due to small bubbles in the lacquer while polishing adds to the surface imperfection by revealing the defects that lie below the surface of glossy-printed parts.

After the matte images were taken, the matte sample was polished and then half of the sample was lacquered according to PolyJet guidelines for clarity [1]. The surfaces were also investigated via microscope and are displayed below:

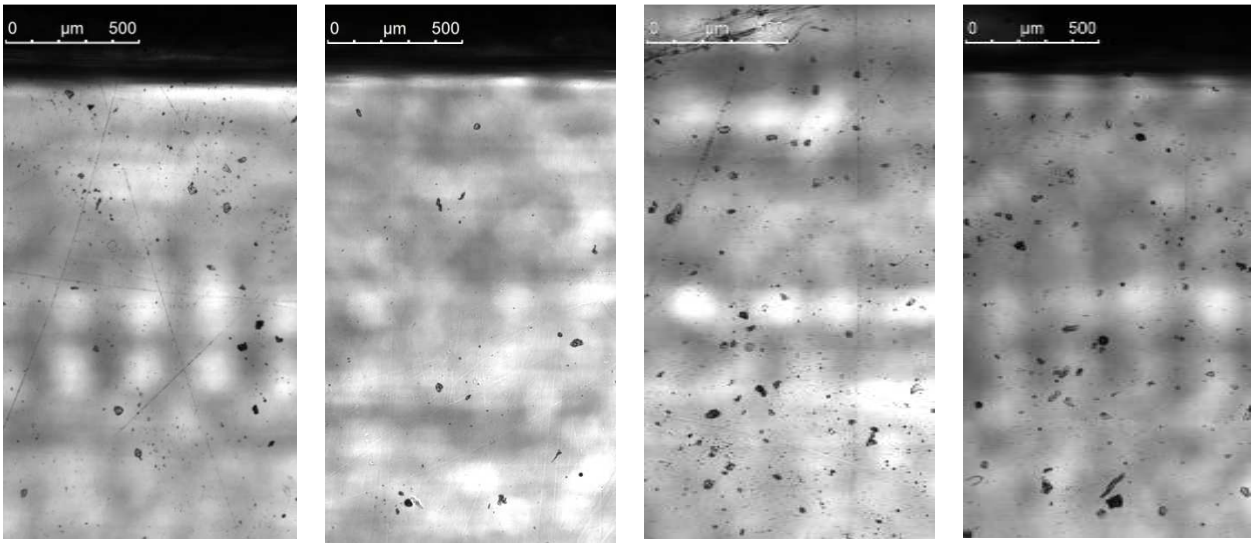

a) Matte Print Setting Polished (Best Case) **b) Matte Print Setting Polished & Lacquered (Best Case)** **c) Matte Print Setting Polished (Worst Case)** **d) Matte Polished & Lacquered (Worst Case)**

Figure 2-14: Matte printed samples under various surface treatments

For Figure 2-14, images were taken at two different areas of each sample section. Shown are two matte and two lacquer images (best and worst of each). It is noted that the best of the lacquer sample is far better than any of the samples previously imaged in that it has the fewest amount of surface defects. However, the worst of the two lacquer images shows as much or more surface defects than the matte polished sample. This variation in surface defects is attributed to the technique with which the lacquer was applied: perhaps the application allowed bubbles remain on the surface of the lacquer or perhaps the sample was not sufficiently shielding from dust

particles during drying. Whatever the case, it can be concluded that with the best technique of preparation and application, the matte printing finished that undergoes polishing and subsequent lacquer-coating has the best clarity as determined by the lack of surface defects in comparison with other samples.

As can be seen in Figure 2-15, the QDs are more visible under the matte finish than the glossy finish. Although the polishing of a glossy-printed sample does provide an almost equal amount visibility to that of the matte finish, the act of polishing itself is a time and labor-intensive endeavor. Ideally, to produce adequate visibility of the quantum dots, one could simply select the best setting on the printer, and no post-processing would be needed. To investigate this possibility, the matte and glossy samples were investigated under fluorescent microscopy and their visibilities were compared.

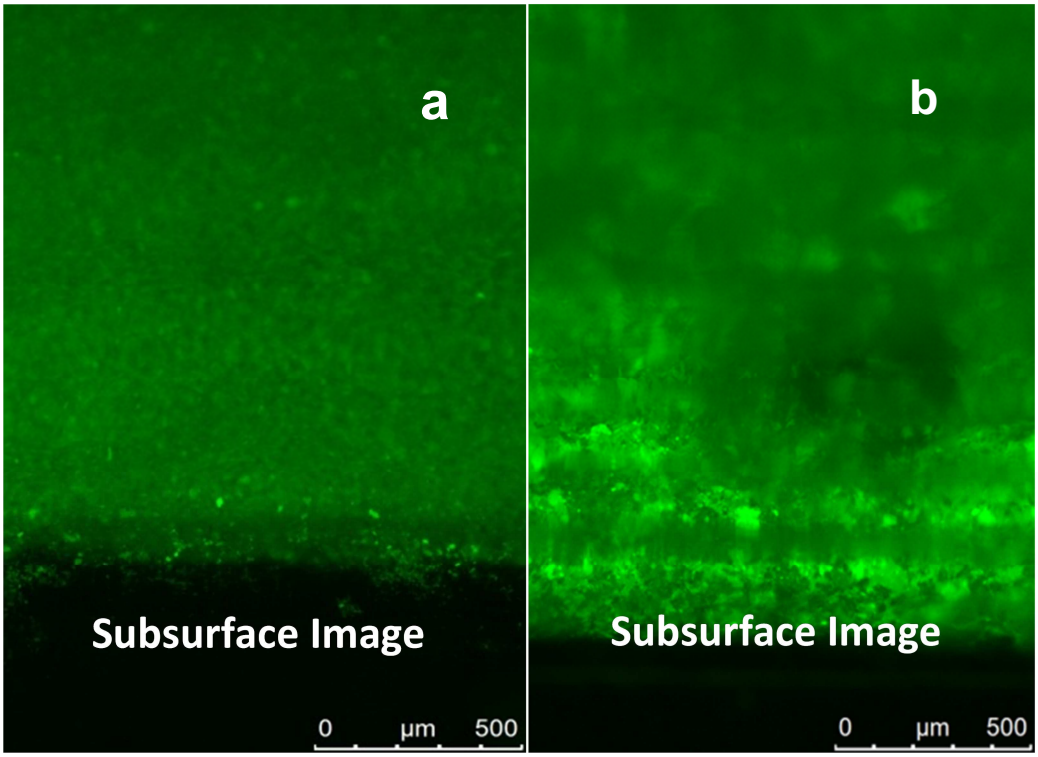

Figure 2-15: Samples under fluorescent microscopy with a) glossy print setting and b)matte finish print setting

The significant observation to be made from Figure 2-15 is that the QDs are visible under the glossy finish and not at all visible under the matte finish. Therefore, although the fluorescence of the QDs are more visible with the naked eye under a matte finish, the glossy finish is much better suited for providing a clear view of individual QDs and agglomerates. Future work with fluorescent microscopy will include re-printing and embedding the glossy samples discussed in this section, but avoiding the over-exposing that occurred due to printing the matte sample in the same build.

Further investigation of the surfaces of each sample was performed via microscopy and is discussed in the following section. Bright field microscopy images of the surfaces of the previously described samples are analyzed and their contributions to QD visibility are discussed.

Concentration

Samples ranging from 0.05 wt% to 0.5 wt% were imaged via fluorescent microscope, and the resulting images are displayed in Figure 2-14 a-d. In each of the images, a speckle pattern of QD agglomerates can be seen. As the QD loading decreases, the speckle pattern becomes less dense. The most noticeable difference in speckle patter density can be seen between the 0.5 wt% and 0.05 wt% concentrations (Figures 2-14 a and d). Overall, the images reveal that QDs in as low as 0.05 wt% concentrations can produce patterns suitable for the creation of PUFs.

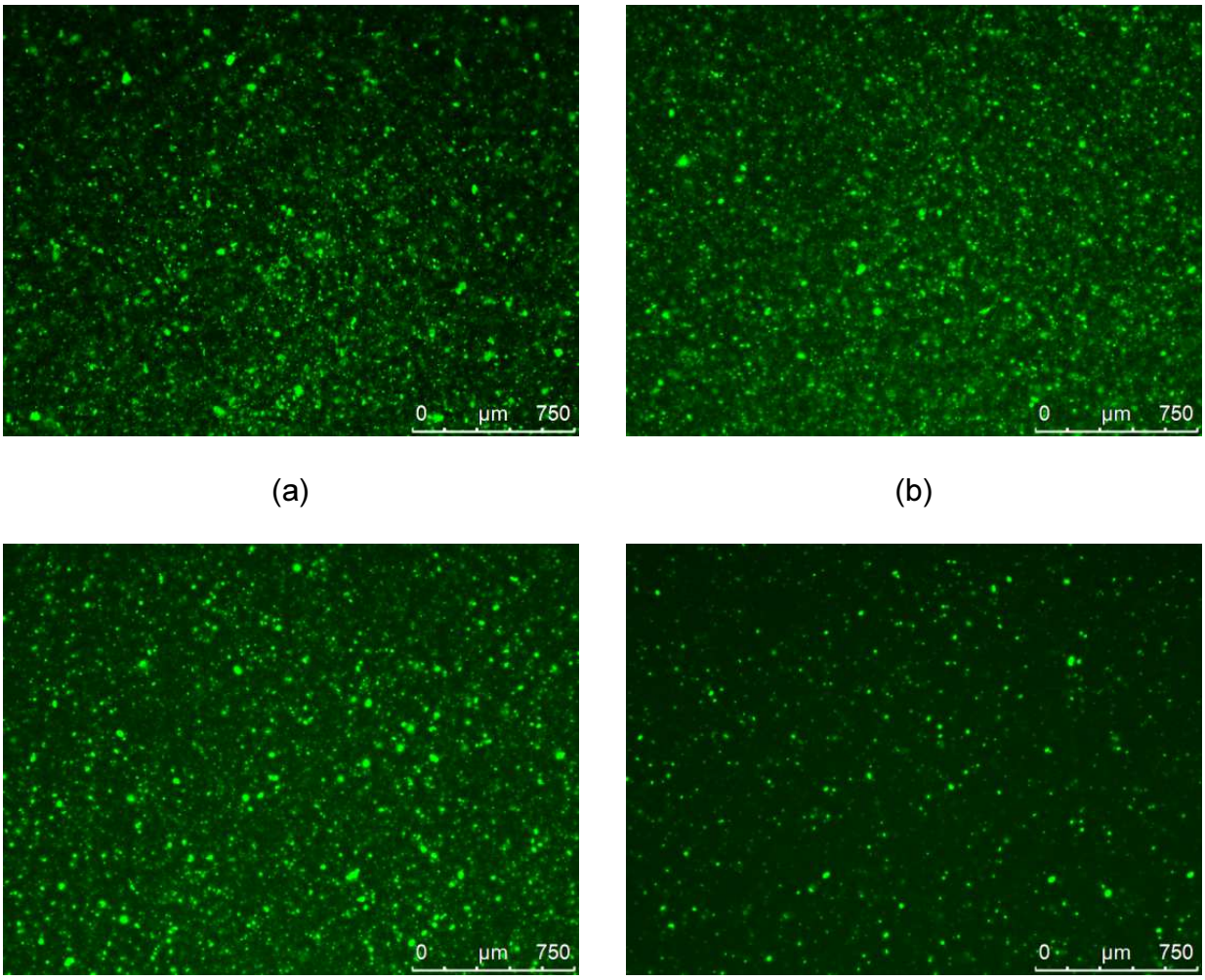

(a) (b)

(c) (d)

Figure 2-16: Fluorescent microscope imaging of (a) 0.5 wt% (b) 0.2 wt% (c) 0.1 wt% and (d) 0.05 wt%

2.4 Conclusions and Roadmap

The work described in this chapter is focused toward determining suitable concentrations of QDs within PolyJet media to produce visible fluorescence. The visible fluorescence is chosen as the benchmark for concentration since QD PUFs should be

detectable with the naked eye when illuminated by a UV lamp. Overall, the work in this chapter is focused toward answering QQ1:

Qualifying Question 1 (QQ1): What concentration of QDs within PolyJet media is necessary to provide readily visible fluorescence to the naked eye?

It was established in Section 2.2 that PolyJet polymers with at least 0.5 wt% QDs fluoresce under UV light visibly to the naked eye. Thus, sample concentrations for jetting and curing experimentation could be determined. Furthermore, processing variables that can affect the visibility of QDs within printed PolyJet media were explored. The visibility was investigated on both the naked-eye and microscope levels, addressing QQ's 1.1 and 1.2, respectively:

Qualifying Question 1.1 (QQ 1.1): How do production variables affect the visibility of PUF patterns?

Qualifying Question (QQ 1.2): How do production variables affect the visibility of QDs by the naked eye?

It was found that functionalization reduced QD agglomeration in 0.5 wt% loadings (Figure 2-12) and affected the color of fluorescence to the naked eye under UV light (Figure 2-7). As far as print setting and post processing techniques, it was found that polishing samples produced the best smoothness (Figure 2-10), however, the glossy finish (with no surface treatment) had the least amount of optical surface defects (Figure 2-12) Furthermore, varying PUF thickness and concentration showed that the highest

concentrations and thicknesses do not necessarily produce the most visible fluorescence (Figure 2-9). Most importantly, fluorescent microscopy revealed discrete points of QD fluorescence characteristic of PUFs in samples where QDs were embedded within PolyJet media. Overall, the results in this chapter demonstrate (1) the feasibility of creating PUF patterns with QDs dispersed in PolyJet media, (2) that printing settings and surface treatments have an effect on the visibility of the QDs on the macroscopic and microscopic levels, and (3) concentrations up to 0.5 wt% QDs are sufficient to produce fluorescence with the naked eye. Future work in the area of QD visibility should include looking further into PUF geometry to determine the optimal thickness and concentrations for visibility with and optical microscope; however, an optimization of PUF geometry is outside the scope of this dissertation.

Thus far in the dissertation, the motivation for creating PUFs via PolyJet of QDs has been described (Chapter 1) and the feasibility of viewing the QDs within the printed PolyJet media has been verified (Chapter 2). Chapter 3 will describe the work performed to address QQ2, which holds that the QDs must be ink-jettable in order to be processed via PolyJet. Table 2-2 contains the roadmap for the dissertation, outlining the research phases and goals associated with each chapter.

Table 2-2: Roadmap

	Research Phase	Chapter	Goals
Introduction	Problem Identification Solution Proposal	**Chapter 1** Introduction, Motivation, and Project Outline	**Describe the problem** **Describe a solution** to the problem and the process for implementing that solution **Identify the qualifying and research questions** related to the proposed solution
Background & Feasibility Analysis	Information Gathering Preliminary Experimentation	**Chapter 2** Visibility of Quantum Dots within PolyJet Media (QQ1) **Chapter 3** Inkjetting with Quantum Dots in PolyJet Media (QQ2)	**Synthesize literature** related to the Qualifying Questions **Perform Experiments** to address Qualifying Questions 1 and 2 **Draw Conclusions** to address Qualifying Questions
Research Methods	Hypothesis Formulation Experimental Methods Hypothesis Validation	**Chapter 4** Literature Review of Photopolymer-ization Theory, Proposed Theoretical Model **Chapter 5** Experimental Techniques, Results and Critique and Modification of Theoretical Model **Chapter 6** Effects of Intensity on Critical Exposure	**Synthesize literature** related to the Primary Research Question **Identify gaps** in existing literature that prevent answering the research question **Form hypotheses** based on existing literature **Establish Methods** for validating the hypothesis **Perform Experimentation** to validate hypothesis
Summary	Conclusions Outlining Future Work	**Chapter 7** Project Summary and Future Work	**Draw Conclusions** based on experiment results **Identify significant contributions** **Summarize accomplishments** related to answering each of the research questions **Propose future work**

CHAPTER 3 INKJETTING QUANTUM DOT-DOPED PHOTOPOLYMER

3.1 Introduction

PolyJet was chosen for the creation of PUFs due to its multiple material capability and clear resin (Section 1.3). PolyJet uses drop-on-demand inkjet technology to deposit photopolymer resin. As shown in Figure 3-1, drop-on-demand inkjet printhead deposit drops of printing media by means of the following occurrences: first, the printing media is supplied to the printhead chamber; second, a piezoelectric crystal receives a pulse of voltage and expands to create a positive pressure within the chamber; third, the positive pressure forces a small amount of the printing media out of the chamber through the nozzle, creating a droplet with some velocity.

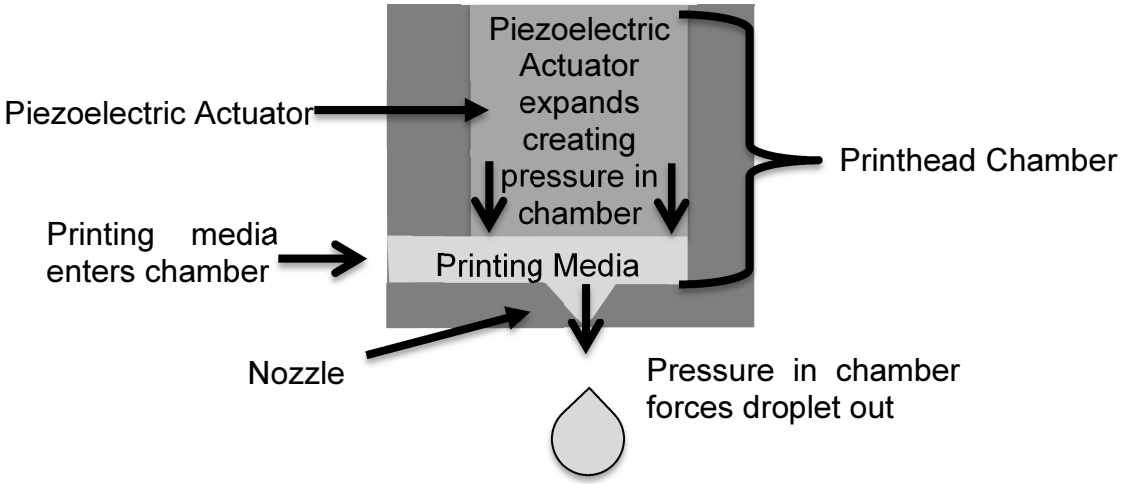

Figure 3-1: Diagram of a Drop-on Demand Inkjet Printhead

Adding particles to PolyJet printing media is likely to cause complications in the inkjet deposition portion of the 3D printing process. These complications include mainly nozzle clogging, but can also manifest themselves in the form of irregular droplet

shapes that affect the accuracy of the build [1]. In this chapter, factors that affect inkjet deposition will be explored toward answering Qualifying Question 2:

Qualifying Question 2 (QQ2): How do QDs affect the jettability of PolyJet media?

A literature review of the parameters that affect jettability and current work in jetting of particles is presented in Section 3.2. From this literature review, it is found that viscosity and surface tension are the main characteristics of a fluid that determines jettability [1-3]. Thus QQ's 2.1 and 2.2 are formed:

Qualifying Question 2.1 (QQ 2.1):

How do QDs affect the *surface tension* of PolyJet media?

Qualifying Question 2.2 (QQ 2.2):

How do QDs affect the *viscosity* of PolyJet media?

Measurements of surface tension and viscosity are taken using the procedures described in Section 3.3 and the results of the measurements are presented in Section 3.4. Although conducting rheological characterization will determine whether the fluid can be passed through an inkjet nozzle, the analysis of these properties will not reveal how actual droplet formation is affected. Therefore, QQ 2.3 is formed:

Qualifying Question 2.3 (QQ 2.3):

How do QDs affect the droplet formation of PolyJet media?

Demonstrating the feasibility of inkjetting QDs in PolyJet requires analysis of droplet formation of QD-doped polymer via an inkjet test stand. The procedure for creating and imaging inkjet droplets with the inkjet test stand is contained in Section 3.3 with the results reported in Section 3.4. Ultimately, the feasibility of successfully inkjetting QD-doped polymer in the PolyJet process will be determined via rheological calculations and analysis of inkjet deposition.

3.2 Literature Review

Because of the small size of the jetting chamber and the small diameter of the jetting nozzle orifice (60 microns), the rheology of the printing media is significant. Specifically, a highly viscous fluid and/or a fluid with a high surface tension would resist flow through the nozzle to a degree that cannot be overcome by the piezoelectric actuator. Similarly, if the surface tension of the fluid is too low, a splash of fluid will exit the nozzle instead of a cohesive droplet. Because of these risks, adding particles into inkjet printing media can affect the rheology of the media such that it is no longer ink - jettable. Therefore, the goal of this study is to discover the effects of quantum dots on photopolymer rheology and the associated jettability. Literature related to the effects of particles on fluid rheology and jetting is reviewed in the following sub-sections.

3.2.1 Rheology of Particle-Loaded Fluids

Prior research in nano-suspensions conclude that the primary rheological properties that affect inkjetting are surface tension and viscosity [1-3]. Rheology affects not only the jetting of the fluid, but the shape of the drop once it settles onto previously deposited layers of the PolyJet build. This section details existing knowledge on the effects of nanoparticles on the surface tension and viscosity of fluids.

Surface Tension

Surface tension is the force present at the interface of two fluids caused by the attraction between similar molecules. Surface tension is significant in determining the jettability of a fluid [1-3], and both the size and the concentration of the nanoparticles matter when determining the effect of particles on the surface tension of a fluid [4].

Nanoparticles can affect the surface tension through many different mechanisms. First, electrostatic forces between the nanoparticles cause attraction and contribute to increasing the surface tension. Van der Waals forces, which are intermolecular, can also cause an increase in surface tension [5]. In a study to determine the relationship between surface tension and nanoparticle loading, it was found that, with increasing concentration of nanoparticles, the surface tension of a fluid decreases, reaches a minimum, and then increases. The theory that explains this phenomenon is based on the assumption that particles accumulate at the interface between the liquid and gas [5]. Initially, as the particles increase in concentration, the cohesive energy between the similar particles of the fluid at the surface is interrupted by the nanoparticles, which are not similar to fluid particles and thus do not share attractive forces. As the concentration of nanoparticles increases, however, more particles become present at the surface and

Van der Waals and electrostatic attractive forces between the particles become significant.

The size of the nanoparticle in the fluid can also affect the surface tension, and it was found that larger particles created higher surface tension than smaller ones with the same mass concentration. This is thought to be due to the increased number of particles, that is, the same mass would contain a higher quantity of smaller particles than it would of larger particles, and the higher number of particles would create a higher number of "interruptions" between fluid particles at the fluid-gas interface and thus lower surface tension [5].

With this knowledge of how nanoparticles affect surface tension, it can be hypothesized that adding QDs to PolyJet photopolymer will decrease surface tension at low concentrations and increased surface tension at higher concentrations. Analysis of the actual effect of QDs on surface tension is presented in Sections 3.3 and 3.4.

Viscosity

The viscosity of a fluid is the fluid's resistance to deformation. With a high viscosity, the fluid has high resistance to deformation. A fluid with high viscosity requires more energy to eject from an inkjet nozzle. Therefore, adding QDs to PolyJet photopolymer could raise the viscosity to an amount that is unjettable, and the viscosity of the fluid should be tested.

The general approach to calculate the viscosity of a fluid containing particle loading under 0.01 volume fraction involves employing the Einstein equation, Equation 3-1 [6]:

$$n_r = 1 + 2.5f \tag{3-1}$$

where n_r is the relative viscosity and f is the volume fraction of hard sphere particles. Whether or not Equation 3-1 is applicable to nanoparticles has been called into question [7]. A study conducted with polystyrene nanospheres mixed into linear polystyrene molecules (polymer) found that the nanoparticles actually decreased the viscosity of the polymer (instead of increased as predicted by Equation 3-1). It was hypothesized that this decrease in viscosity was caused by the nanoparticles significantly increasing the free volume in the solution. In other words, since nanoparticles represent much less "attached" volume than larger particles, the particles in the fluid slide past each other more easily which results in lower viscosity [7].

Although the mechanism for decreased viscosity is surmised, the study admits that the model does not account for other mechanisms that affect viscosity, such as entanglement and enthalpic reactions, which are present when the nanoparticles and the carrier polymer are dissimilar (as previously stated, the nanoparticles and the polymer were both polystyrene) [7]. So, although this study shows that Equation 3-1 does not accurately predict the viscosity of fluids with nanoparticle loading, the equation will be used as an estimate. Overall and in response to QQ2.2, Equation 3-1 reveals that the viscosity should rise with increase in particle loading. Section 3.3.2 will describe the methods used to measure the viscosity as well as an estimation of their theoretical values based on Equation 3-1. The result of the viscosity measurements will be discussed in Section 3.4.2.

3.2.2 Inkjetting of Particle-loaded fluids

In addition to exploring the effects of QDs on the rheology of a fluid, answering QQ2 requires understanding the effects of QDs on the droplet formation (QQ2.3). Existing work in inkjetting of QDs and inkjetting of particles in general is presented in this section.

Inkjetting with Quantum Dots

Many QD applications have benefited from the selective placement that inkjet technology is capable of providing. Wood and authors have created pattern pixels for flexible displays by printing QD's in a solution via inkjet. The QD's were suspended in a solution of hexan, octane, and a polyisobutylene matrix material and delivered by a thermal inkjet picofluidic dispensing system in 50-300 picoliter drop volumes. The result was a flexible, electroluminescent, thin film with the layers of glass, indium tin oxide, inkjet-printed QDs, and phosphor paste [8].

Tekin and coauthors used inkjet nozzles to deposit QD-doped photopolymer into films to create a nanocrystal-polymer composite. A contribution from this paper includes the addition of 1-2% volume ethylene-glycol to subdue the "coffee-stain effect," that is, how particles will migrate toward the outside of a droplet when introduced to a surface (this is not favored when uniform distribution is desired) [9]. In a similar application, Haverinen and authors dissolved QD's in chlorobenzene to form their inkjet printing media. Their choice of a low-vapor pressure liquid as the main fluid of the printing media was also driven by the desire to also reduce the coffee-stain effect. The purpose of their research was to develop a simple process for creating light emitting diodes [10].

The approaches described above focused in the IJP of nanoparticles with solvents and relatively non-viscous(< 5 centipoise), low-molecular weight polymers as the carrier fluid [10-14]. These materials are beneficial for the creation of thin films. However, AM materials, which include viscous (~20 centipoise), high-molecular weight photopolymers (around 1 g/mL), are much better suited for forming nanocomposites into sizeable macrostructures and offer better mechanical properties [15].

To summarize, the literature review conducted to identify existing knowledge on the effects of QDs on the rheology or inkjetting of fluids revealed no findings. No mention of solids loading, rheological properties, or challenges in printing the QD-doped fluid were given in these works. It is assumed that, in the works presented, QDs were added to printing media in such low concentrations that rheology and inkjet-nozzle clogging were not considered. Thus, answering QQ2.3 will rely on knowledge in the area of inkjetting of particles in general, which is discussed next.

Inkjetting with Particles

As previously stated, adding particles to inkjet media will change the rheology (viscosity and surface tension) of the fluid and potentially render the fluid un-jettable. This section focuses on strategies for predicting jettability based on measurable rheological characteristics and current work in jetting fluids with particles and QDs.

Much work has been done in the area of micro-patterning nanoparticles toward the development of polymer electronics, micro-optical components, complex nanocomposites and others [16-20]. Inkjet printing is a particularly effective method of patterning nanomaterials on the microscale. Nanomaterials incorporated into printing media can be selectively patterned and can also be placed among other materials to

form complex composites [21]. Brian Derby has provided an extensive review of work related to inkjet of highly particle-loaded printing media [6]. His research has yielded a model that suggests that the ratio of the square root of the Weber number to the Reynold's number called the Ohnesorge number (*Oh*, Equation 3-2), can dictate printability.

$$Oh = \frac{\mu}{\sqrt{\gamma \rho \frac{d}{2}}} \tag{3-2}$$

where ρ is density, *d* is the nozzle diameter, γ is surface tension, and μ is viscosity. Equation 3-2 suggests that the most important variables in predicting jettability are viscosity, surface tension, density, and nozzle diameter. Derby cites that jettability generally occurs when the inverse of the Ohnesorge number (1/*Oh*) is less than 10 and greater than 1. Equation 3-2 has been used to predict jettability of wax that is highly loaded with sub-micron sized alumina particles for the creation of ceramic artifacts via direct 3D printing [6]. Although disagreements exist about the accuracy of the Ohnesorge number in predicting jettability [22], it is still considered a fundamental equation in inkjet modeling [23].

In depositing ceramic-doped photopolymers, Derby cites the ability to jet fluids with up to 40 vol% solids loading [23]. Since QDs are favored for the unique optical properties and not mechanical properties, loadings much less than 40 vol % will be needed. Furthermore, it was shown in Chapter 2 that QD concentrations as low as 0.2 weight percent produce sufficient fluorescence to be identified by the naked eye as well as ample clustering of the particles visible to fluorescent microscopes. Equation 3-1 predicts that, for 1.0% volume fraction of particles, a 2.5% change in viscosity will be

seen, which should not be significant enough to affect jettability. Thus, for the purposes of creating PUFs, it can be predicted that the addition of QDs in sufficient concentrations will not affect the jettability of PolyJet photopolymer. The methods used to verify this hypothesis are described in Section 3.3

3.3 Analysis Methods

Thus far in Chapter 3, a literature review of the potential effects of particles on rheology and jetting properties of fluids has been presented. This section (Section 3.3) describes the analysis methods used in answering Qualifying Question 2 and the sub questions QQ 2.1-2.3. First, Section 3.3.1 describes the procedure for measuring surface tension of QD-doped PolyJet media of various QD concentration via tensiometry to address the effects of QDs on surface tension (QQ 2.1). Second, Section 3.3.2 describes viscosity measurement of QD-doped samples in varying concentrations via a rheometer, which addresses QQ 2.2. Finally, the experimental procedure for testing the inkjet deposition of QD-doped polymer is described in Section 3.3.3 toward answering QQ2. Table 3-1 outlines each QQ and the respective experimental method and section in which the method is described.

Table 3-1: Qualifying Questions and corresponding Analysis Methods and Section Numbers

Qualifying Question (QQ)	Analysis Method	Section Number
QQ 2.1: How do QDs affect the *surface* tension of Polyjet media?	Tensiometry	Section 3.3.1
QQ 2.2: How do QDs affect the viscosity of Polyjet media?	Rheometry	Section 3.3.2
QQ 2.3: How do QDs affect the droplet formation of PolyJet media?	Inkjet deposition and imaging via inkjet test stand	Section 3.3.3

3.3.1 Surface Tension

Surface tension was measured using the Wilhelmy Plate Method with a 20mm-length aluminum plate. In this method, a small plate with a known surface area and surface roughness is pulled through the surface of the sample fluid (See Figure 3-2 below). The resistance to this pulling motion is measured with a microbalance, and the surface tension is calculated from this data.

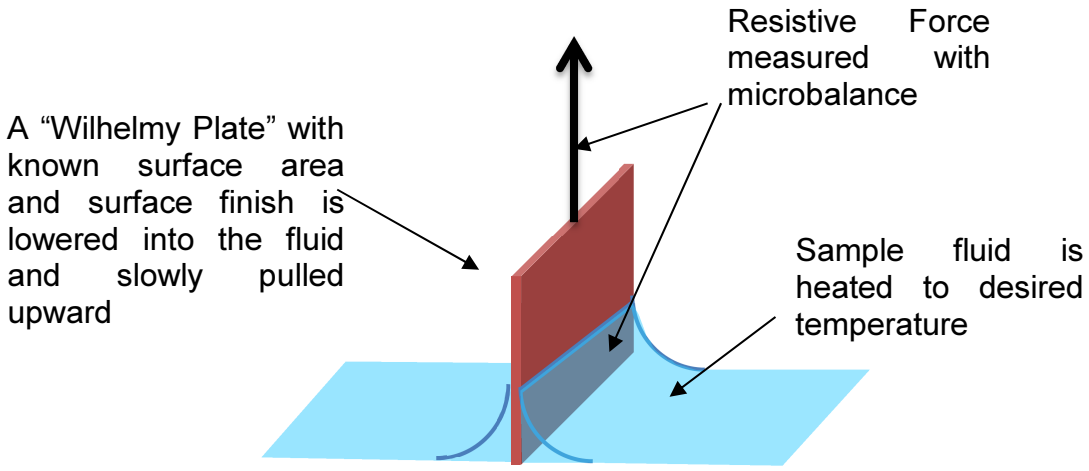

Figure 3-2: Wilhelmy Plate Method for measuring surface tension

The samples were heated to approximately 72 ℃ (Stratasys PolyJet printing temperature) before taking the surface tension measurement. Seven samples were measured three times each. The following concentrations were measured: 0.005, 0.01, 0.02, 0.05, 0.1, 0.2, and 0.5 weight percent (wt %). The results of the surface tension measurements are discussed in Section 3.4.1.

3.3.2 Viscosity

Viscosity of each prepared sample was measured using an AR-2000 model rheometer configured with a 40mm diameter, 2° angle rheometric cone. The sample is

loaded onto a temperature-controlled base plate, and the rheometric cone is lowered onto the sample at a precise distance from the base plate, sandwiching the fluid sample. The instrument spins the cone, measures the resistance to rotation, and calculates the viscosity from this measurement. Figure 3-3 below is a simplified depiction of this instrument.

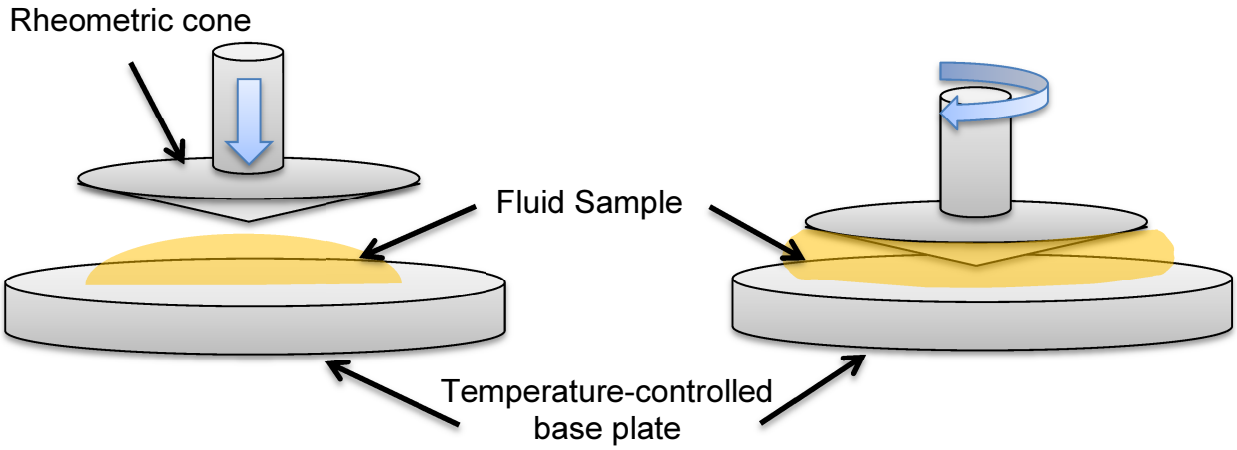

Step 1: Rheometric cone is lowered onto fluid sample

Step 2: Rheometric cone spins, resistance to rotation is measured, and viscosity is calculated

Figure 3-3: Viscosity measurement using a rheometer

The samples are measured at a temperature of 72 degrees Celsius and shear rate of 10 sec^{-1}. This shear rate was chosen based on preliminary results that showed a settling-out of the viscosity readings after this shear rate was reached. Just like with the surface tension measurements, 7 samples were measured with 3 measurements per sample. The same concentrations were used for viscosity measurements as was used in the surface tension measurements (0.005, 0.01, 0.02, 0.05, 0.1, 0.2, and 0.5 wt%). The experimental results from these viscosity measurements are discussed in Section 3.4.2.

3.3.3 Jetting

Because the jetting nozzle is small (60 micron diameter on a Stratasys Connex 350), the fluid properties of the printing media significantly affect the ability of the printhead to eject droplets. Viscosity or surface tension that is too high can prevent droplet ejection or even cause nozzle clogging. Thus, it is necessary to perform the jettability calculations discussed in Section 3.2.2.

Upon predicting that the QD-doped polymer was within the jettable range of the 1/*Oh* number (Section 3.4.1), an inkjet test stand (MicroFab Technologies, El Paso, TX) was used to observe droplet formation. As shown in Figure 3-4, the test stand setup consists of a single, 60 micron inkjet nozzle, a fluid reservoir, pressure and temperature-regulating electronics, and a strobe and coupled camera, which images the jetted fluid. The fluid reservoir on the jetting apparatus contains external heaters that were used to heat the nozzle and reservoir to the photopolymer printing temperature (72 ℃). The reservoir also regulated to maintain a slight vacuum to prevent the fluid from freely falling through the nozzle.

In the reservoir, the fluid passes through a 7 micron filter before entering the nozzle chamber. A pulse is created in the nozzle via a cylindrical piezoelectric crystal that surrounds the glass tubular nozzle, and a droplet is forced out of the nozzle. Images are then taken of the droplet as it exits the chamber via a strobe and camera that are synced with the jetting piezoelectric crystal.

Because of the very small solids loading of QDs (0.5 wt% and lower) and because of the literature review citing much higher solids loading being jettable (up to 40% solids loading) [23], it is hypothesized that inkjet droplet formation of the QD-

doped, PolyJet photopolymer will not differ significantly from droplet formation of plain PolyJet photopolymer. The results of the inkjet deposition trials will be discussed in Section 3.4.3.

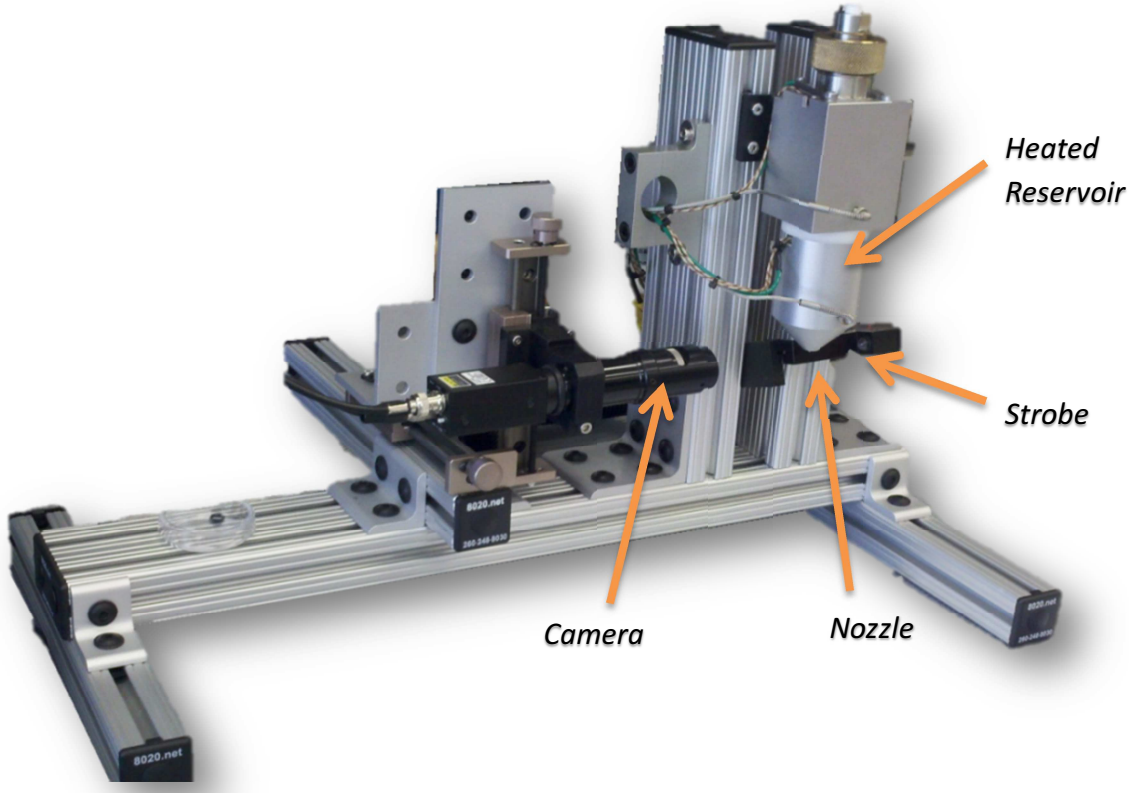

Figure 3-4: MicroFab Inkjet Test Stand

3.4 Results

Thus far in Chapter 3, a literature review has been presented and the methods have been described toward addressing QQ's 2.1, 2.2, and 2.3. These QQ's deal with the effects of QDs on surface tension, viscosity, and droplet formation via inkjet. Section 3.4 will describe the results of the characterization and their impact on the QQs.

3.4.1 Surface Tension

Three samples were measured via tensiometry for QD concentrations ranging from 0.005 wt% to 0.5 wt%. Results of surface tension measurements are reported in Figure 3-5. The QD concentrations are reported in weight percent (wt%) on a logarithmic scale (x-axis) against the values for surface tension (y-axis), reported in milinewtons per meter (mN/m). The deviation of surface tension values measured for pure PolyJet polymer are reported in the grey band in Figure 3-4 and range from approximately 20.25 to 20.75 mN/m.

The data in Figure 3-5 reveals that the addition of QDs in 0.5 wt% did cause a significant increase in surface tension. Calculations to predict the impact of this increase in surface tension are discussed in Section 3.4.3.

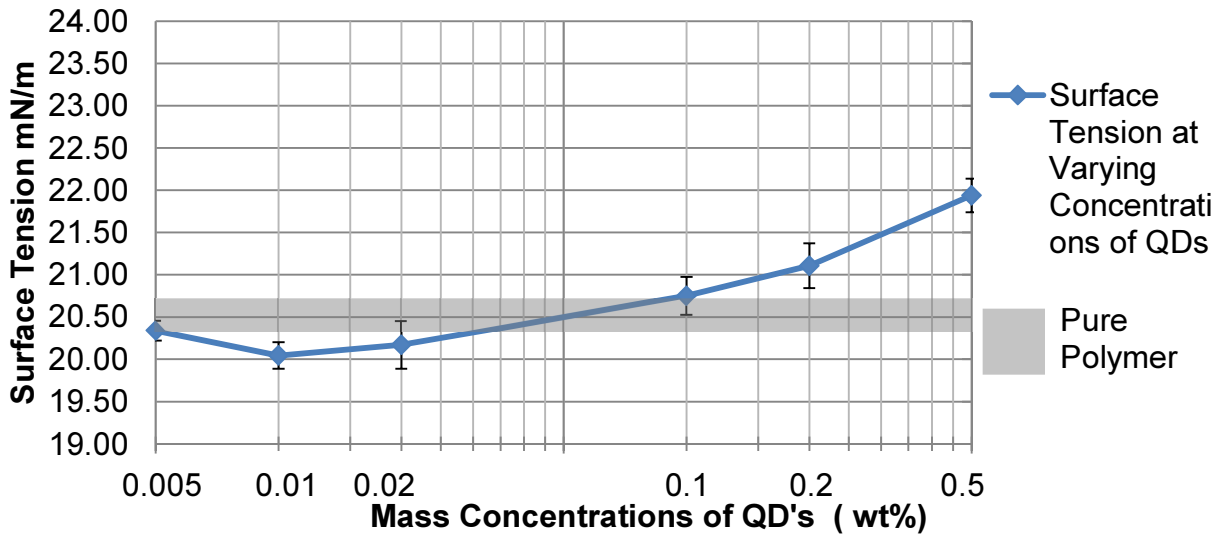

Figure 3-5: Surface Tension of and Varying Concentrations of QD's

3.4.2 Viscosity

For the viscosity measurements, three samples were measured from each test concentration at a shear rate of 10 seconds^{-1} and the printing temperature of the Objet Connex, which is 72 ℃. Using Equation 1, it is predicted that adding 0.5 wt% QDs to the control polymer will increase the viscosity by 0.23%. Experimental results showed an average of 0.15% increase in viscosity, with the average measured viscosity of the control polymer and the suspension with the highest QD loading (0.5 wt%) being 0.01982 ± 0.0012 Pa•s and 0.01985 ± 0.0015 Pa•s, respectively. Figure 3-6 shows one standard deviation from the average viscosity (of 3 samples each) collected for pure polymer highlighted in grey. As shown, the average viscosity for all sample concentrations lies within one standard deviation from the average viscosity found for pure polymer. Although an increase average viscosity can be seen for the 0.02 wt% sample, the overlap of the error bars signifies that there is no significance in this higher average value.

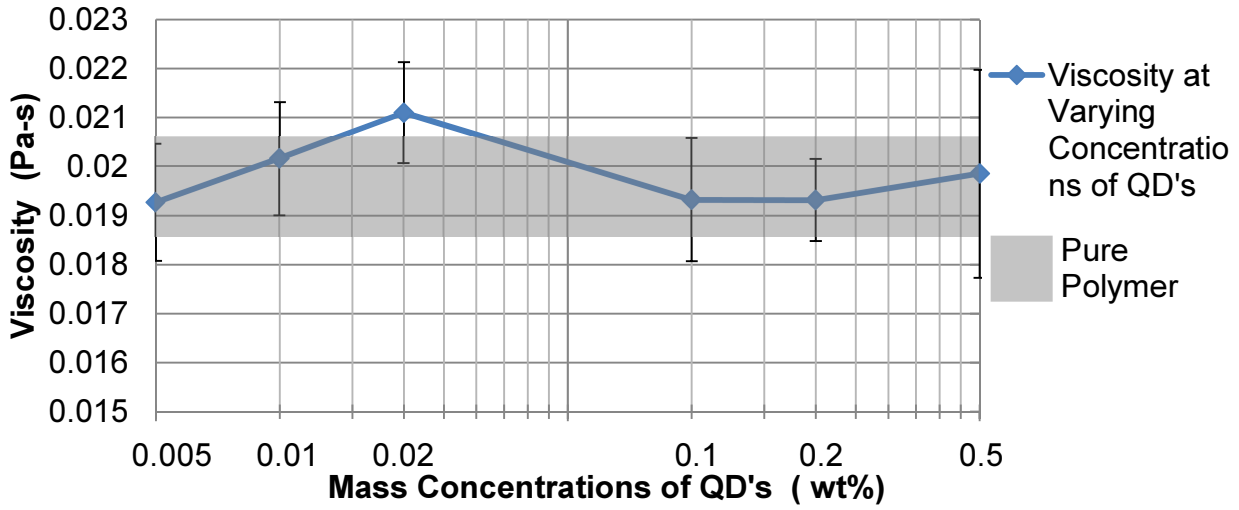

Figure 3-6: Viscosity of QD's + Photopolymer

3.4.3 Jetting

The ability to create droplets via inkjet is predicted by Equation 3-2 [6]. For nozzle diameter of 60 microns, a fluid density for VeroClear of 1.08 g/ml, and with the rheological experiments reported in Section 3.4.1, the inverse of the Ohnesorge number (1/*Oh*, Equation 5) was found to be 1.75 for pure polymer and range from 1.75 to 1.92 for the varying concentrations of QDs. Figure 3-7 below contains a plot of the resulting 1/*Oh* values.

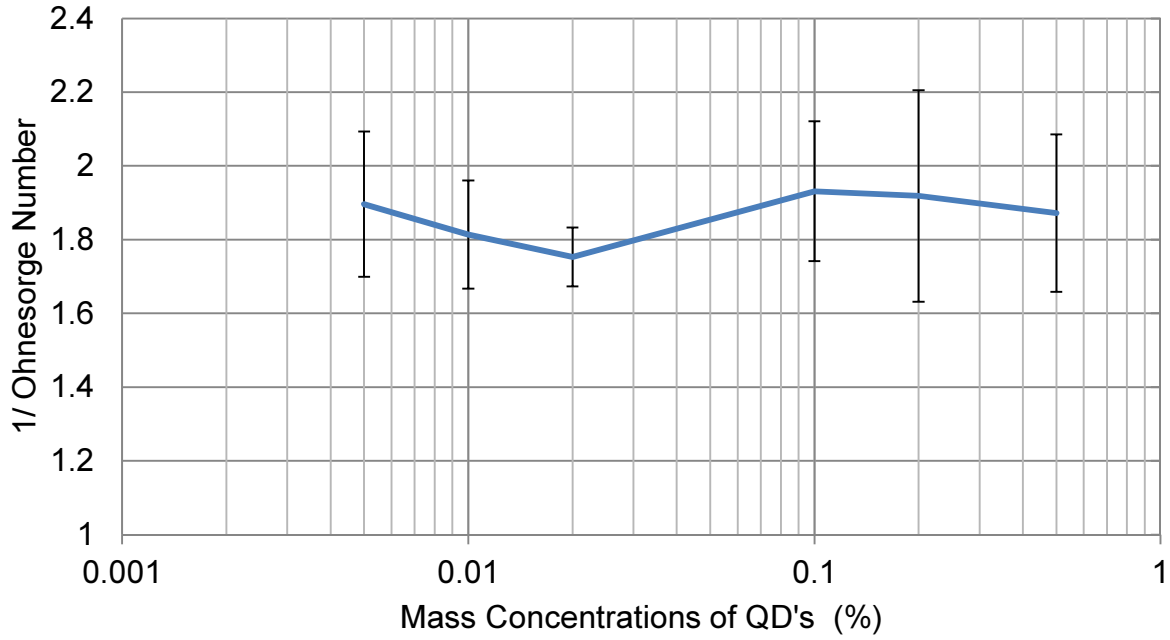

Figure 3-7: 1/Ohnesorge number for each QD concentration, calculated from surface tension and viscosity data.

As seen in Figure 3-7, the value for 1/Oh varies between the values of 2 and 1.6. Since 1/*Oh* is within the printable range (less than 10 and greater than 1) for all concentrations, it can be concluded that the addition of QDs at such low concentrations does not shift the rheology of the photopolymer out of the printable region.

After verifying via jetting calculations that the QD-doped PolyJet photopolymer is jettable, jetting tests were performed with an inkjet test stand (Figure 3-3). Jetting images were taken with varying voltage and dwell settings as shown in Figures 3-8a and b below. The data for 0.5 wt% sample was imaged since this concentration had the largest deviation from pure polymer rheological measurements (Figure 3-4) and thus the highest probability that jetting abnormalities would be seen. In the pulse profile sent to the piezo in the inkjet nozzle, voltage governs the energy behind the pulse and the dwell setting governs the duration of the pulse. These two parameters are typically varied to determine the waveform that produces optimum droplets in terms of volume, shape, and velocity [20]. Figure 3-8 contains the imaging data collected for a range of voltages verse dwell values for pure polymer and 0.5 wt% QD polymer.

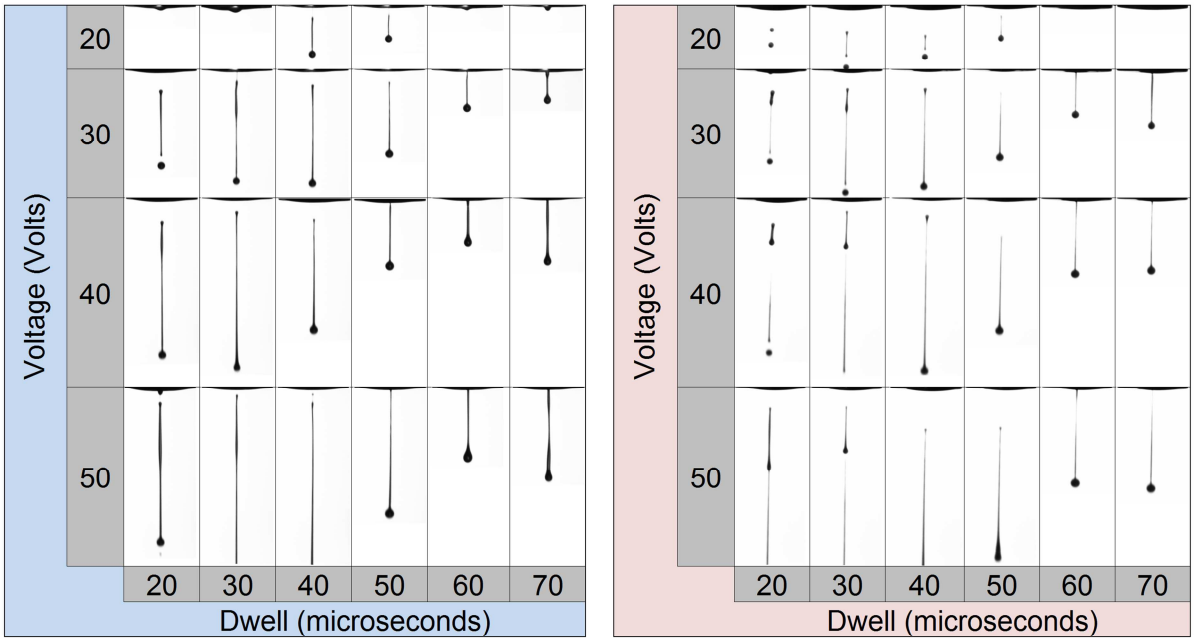

(a) Pure Photopolymer (b) 0.5 wt% QD's in Photopolymer

Figure 3-8: Images of (a) pure photopolymer and (b) with 0.5 wt% QD's - drops formed for varying values of voltage and dwell

Figure 3-8 contains an array of drop images created using varied voltage and dwell settings. All images in Figure 3-8 were taken at a jetting frequency of 600 hertz and at 200 microseconds after the beginning of the pulse. At the top of each droplet image is the tip of the inkjet nozzle, which used as a reference point for the images. Comparing the individual drop images, it can be seen that some drops are farther away from the nozzle than others. A drop that is further from the nozzle has a greater velocity, and increased droplet velocity is a function of the input voltage to the piezo. The structure of the drop consists of the drop and the tail, the drop being the circular, front end of the fluid mass, and the tail being the fluid that trails behind the main drop mass. As dwell increases, the tail becomes shorter and eventually recedes into the drop mass. However, due to the interaction of the fluid with the ejection pressure wave, some tails separate from the drop mass to form satellite drops, as prominently shown in Figure 3-8b for a dwell of 20 microseconds (first column).

Measurement of the drop masses and velocities were attempted, but meaningful results could not be obtained with the test stand software. In other words, Therefore, qualitative assessment of the images is needed to determine the impact of QDs on droplet formation. Upon comparing Figure 3-8 a and b, some differences between the pure polymer droplets and the QD-doped droplets are noted. First, the drop volumes for the QD-doped polymer are visibly smaller than for pure polymer, which can most clearly be seen by observing the difference in the tail thickness between the two. Also, for two settings of voltage and dwell (20 volts, 20 and 30 microsecond dwell times), the QD-doped polymer succeeds in droplet ejection while the pure polymer does not.

Sources of variation in the imaging include contrast settings, brightness of the backlit LED (this tended to waver over time), and pressure irregularity in the reservoir. These sources of variation within the test stand setup itself created a challenge in producing consistent results, and although the difference may seem significant, these results are within the observed typical variation of the jetting device when jetting this particular polymer. An example of a significant difference in the pure polymer and the QD-doped polymer would be the complete inability to eject droplets at any one of the data points taken. Since droplets were formed with QD-loaded polymer for the majority of settings for which pure polymer produced droplets, it can be concluded that the jetting characteristics of the photopolymer is not significantly affected by the presence of quantum dots in up to 0.5 wt% concentrations.

Figure 3-9 contains overhead images of deposited QD-doped inkjet droplets in 0.5 wt% QD loading under (a) visible light and (b) UV light. In contrast to Figure 2-7 that shows an even distribution of QDs for QD-doped polymer embedded in PolyJet build geometries, Figure 3-8 reveals evidence of some migration of the QDs into groups within the ink jetted droplets. This phenomenon can be explained by the aforementioned “coffee stain” effect, which is the migration of particles within droplets due to surface tension effects [10]. However, individual QD agglomerates and patterns characteristic of PUFs can be distinguished within the droplets. Overall, the evidence in Figure 3-8 validates the feasibility of inkjet deposition of QD-doped PolyJet photopolymers for the purpose of creating PUFs.

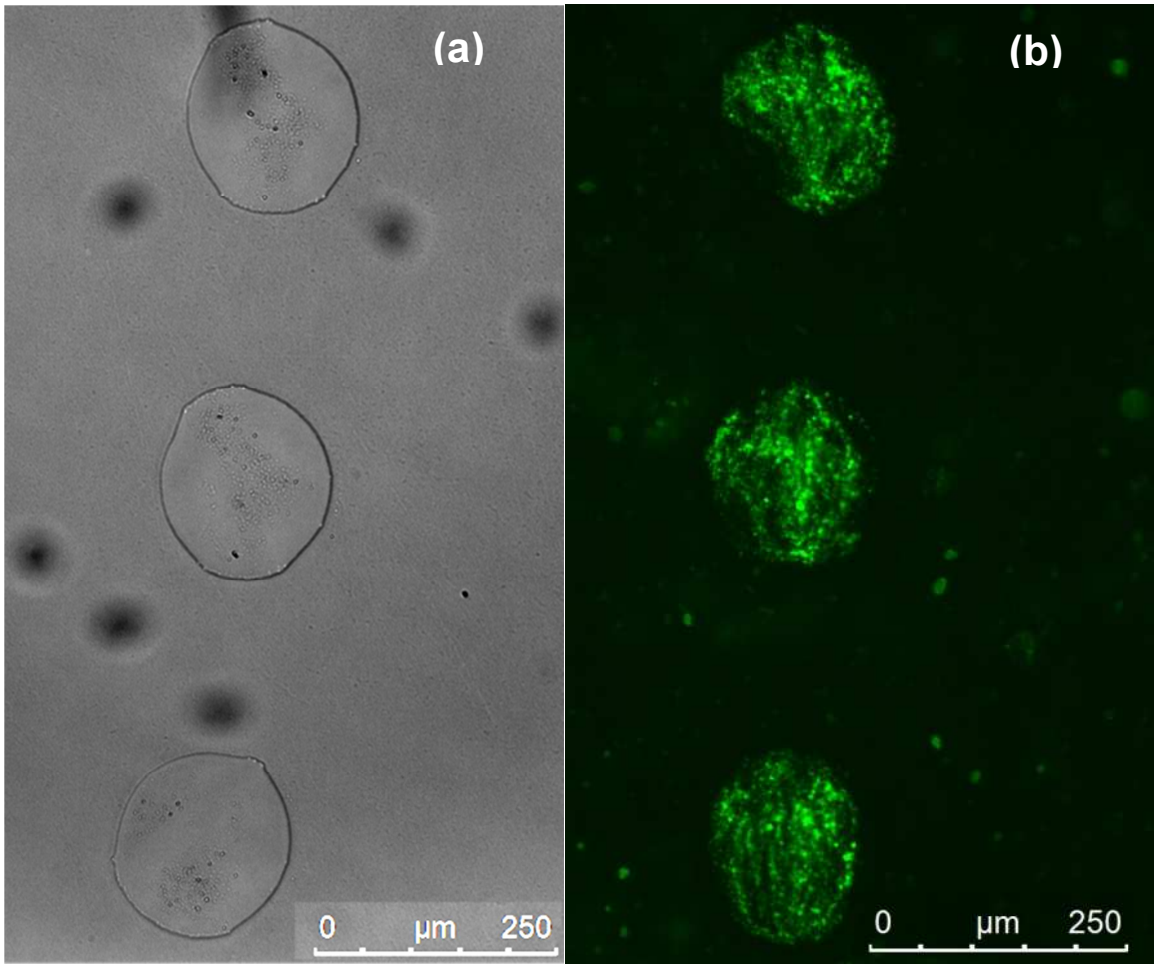

Figure 3-9: Overhead image of inkjet drops of Quantum Dot-doped photopolymer deposited onto a substrate shown under (a) visible light and (b) UV light

3.5 Conclusions

The focus of this chapter was to address Qualifying Question 2:

Qualifying Question 2.1 (QQ 2.1):

How do QDs affect the *surface tension* of Polyjet media?

A literature review was performed to the required rheological properties for jettability, and rheological measurements were performed. It was found that surface tension and

viscosity are the primary rheological characteristics that govern jettability. Thus, QQ's 2.1 and 2.2 were formed:

Qualifying Question 2.1 (QQ 2.1):

How do QDs affect the *surface tension* of PolyJet media?

Qualifying Question 2.2 (QQ 2.2):

How do QDs affect the *viscosity* of PolyJet media?

Viscosity and surface tension measurement were taken from QD-doped PolyJet poly of varying QD concentrations. Calculations were made based on the measured rheological properties, and from these calculations the determination was made that the QD-doped PolyJet photopolymer would be jettable in concentrations in at least as much as 0.5 wt%. Jetting was then performed for this concentration, and it was determined that no significant difference in jetting performance could be seen between the pure and the 0.5 wt% QD-doped PolyJet photopolymer. Therefore, it can be concluded that adding QD's in up to 0.5 wt% should have no significant effect on the jetting quality of the PolyJet process. Finally, the deposited inkjet droplets in Figure 3-7 reveals that QD agglomerates can be seen in distinguishable patterns characteristic of PUFs. The work presented in this chapter was published in the peer-reviewed journal, *Advanced Engineering Materials* [24].

3.6 Roadmap

Thus far in the dissertation, Qualifying Questions 1 and 2 have been addressed in Chapters 2 and 3, respectively. In Chapter 2, the visibility of discrete points of QD fluorescence were investigated as well as possible strategies for improving visibility of the printed PolyJet media. In Chapter 3, the jettability of the QDs was predicted in the form of rheological measurements and jetting calculations. Jettability of the QD-doped fluid was also demonstrated experimentally via a single nozzle inkjet test stand. Chapters 4 and 5 of this dissertation will investigate how QDs affect the photocuring of the AM resin toward answering the Primary Research Question.

Primary Research Question: How do QDs affect the photopolymerization of PolyJet resin?

A roadmap of this dissertation is provided in Table 3-2.

Table 3-2: Roadmap

	Research Phase	Chapter	Goals
Introduction	Problem Identification Solution Proposal	**Chapter 1** Introduction, Motivation, and Project Outline	**Describe the problem** **Describe a solution** to the problem and the process for implementing that solution **Identify the qualifying and research questions** related to the proposed solution
Background & Feasibility Analysis	Information Gathering Preliminary Experimentation	**Chapter 2** Visibility of Quantum Dots within PolyJet Media (QQ1) **Chapter 3** Inkjetting with Quantum Dots in PolyJet Media (QQ2)	**Synthesize literature** related to the Qualifying Questions **Perform Experiments** to address Qualifying Questions 1 and 2 **Draw Conclusions** to address Qualifying Questions
Research Methods	Hypothesis Formulation Experimental Methods Hypothesis Validation	**Chapter 4** Literature Review of Photopolymer-ization Theory, Proposed Theoretical Model **Chapter 5** Experimental Techniques, Results and Critique and Modification of Theoretical Model **Chapter 6** Effects of Intensity on Critical Exposure	**Synthesize literature** related to the Primary Research Question **Identify gaps** in existing literature that prevent answering the research question **Form hypotheses** based on existing literature **Establish Methods** for validating the hypothesis **Perform Experimentation** to validate hypothesis
Summary	Conclusions Outlining Future Work	**Chapter 7** Project Summary and Future Work	**Draw Conclusions** based on experiment results **Identify significant contributions** **Summarize accomplishments** related to answering each of the research questions **Propose future work**

CHAPTER 4 THE ROLE OF LIGHT SCATTERING IN PHOTOPOLYMERIZATION

Thus far in the dissertation, the visible and rheological properties of Quantum Dots (QDs) within PolyJet photopolymer have been examined to demonstrate the feasibility of incorporating QDs within the PolyJet process. In Chapter 2, it has been shown that QD agglomerates can be seen via fluorescent microscopy in patterns that could be used for creating Physical Unclonable Functions (PUFs). In Chapter 3, it was shown that QD-PolyJet photopolymer mixtures can be processed via inkjet without noticeable affects toward inkjet droplet formation. This chapter will focus on the final step in the PolyJet process, photopolymerization, to guide the development of a hypothesis for the Primary Research Question:

Primary Research Question:

How do QDs affect the photopolymerization in an AM context?

QDs have the potential to affect the photopolymerization process in two different ways. First, the QDs may extinguish the light energy exposed to the photopolymer via absorption or scattering as is typical of particle behavior. Second, the QDs may play a role in photopolymerization due to their unique ability to transform light energy from one wavelength to another. To understand the potential roles of QDs in photopolymerization, a review of prior work in photopolymerization modeling is presented in this chapter. Table 4-1 below summarizes the topic combinations investigated and the corresponding sections of this chapter.

Table 4-1: Topics covered in the Literature Review

	General Applications	Additive Manufacturing Applications	Theoretical Modeling
QDs in Photopolymers	Section 4.1.1	Section 4.1.2	*Research Gap*
Particles in Photopolymers	*(Not investigated)*	Section 4.1.3	Section 4.2.3
Particles in Transparent Media	*(Not investigated)*	*(Not investigated)*	Section 4.2.2

Sections 4.1 and 4.2 describe relevant applications and theoretical models, respectively, while Section 4.3 contains the proposed hypothesis based on the presented information. Overall, this chapter will summarize existing knowledge related to the effects of particles and QDs on photopolymerization and a hypothesis for the effects of QDs on photopolymerization based on the literature review will be presented.

4.1 Processes with Particle Loaded Photopolymers

Relevant applications have been pursued in areas dealing with film casting QDs in photopolymers, micropatterning with QDs in photopolymers, and Additive Manufacturing (AM) processes utilizing particles and photopolymers. This section will summarize progress made in these applications and identify information relevant to answering the Primary Research Question.Section 4.1.1 details current applications utilizing QD-photopolymer including film-casted optical electronics, which focus primarily on the optical performance of the QDs within photopolymers. Section 4.1.2 deals with producing microfabricated optical electronics from QDs and photopolymers, and these applications focus primarily on improving the ability to pattern QD's for the purpose of creating electrical components.

Finally, Section 4.1.3 details current AM processes that utilize particles and photopolymers, and the theoretical models developed in these applications will be noted and discussed in further detail in Section 4.2.

4.1.1 Quantum Dot Behavior in Photopolymers

Many electrical applications benefit from the compact energy transformation that QDs are capable of providing. Additionally, photopolymers are widely used in the areas of electronics due to their near-instantaneous solidification. Thus, QDs have been introduced into photopolymers for the creation of micro-LEDs, micro-sensors, data storage devices, and photovoltaics. Characterization of quantum dot behavior within photopolymers has been well researched in the area of optical data storage and optical sensing [1-8]. Li and authors have drop-casted eraseable, thin-film data storage devices using a QD-doped photopolymer and were able to reduce flouresent power as well as change the refractive index of the QD-photopolymer mixture. The authors report that this is the first attempt at creating “erasable multimode three dimensional (3D) bit optical data storage in a CdS QD-doped photorefractive polymer [9].”

Jorkaala and Stennenen have investigated the optical properties of ZnSe QDs within polyvinyl alcohol photopolymer and have concluded that the nanocrystals increase optical output when temperature is decreased [2]. Lui and authors reported that by controlling the spacing between the QD’s via holographic assembly, the defraction efficiency of the photopolymer/QD solidified mixture can reach 100 percent. This enables the creation of centimeter-sized, transmission Bragg gratings, a type of photosensor, which they created by casting QDs dispersed in photopolymer into films [4]. These are just a few of many efforts to study the interaction between quantum dots

and photopolymer in the cured state for use in photosensing and optical data storage [1-8].

To differentiate these works from the work in this dissertation, it must be noted that the focus of these works was to characterize the behavior of QDs within *cured* photopolymer; the authors did not consider the effects of QDs on the curing process. Thus, prior art in creating optical components does not fully intersect with the goal of this dissertation. However, these works constitute the most applicable knowledge in the area of QDs in photopolymers and further illustrate the gap in theoretical modeling of the effects of QDs on photopolymerization.

4.1.2 Quantum Dots 3D Microfabrication

Sun and authors have successfully created 3D microstructures out of Cadmium Sulfide (CdS), Quantum Dot-doped photopolymer composites via two photon polymerization [10-11]. Their method of fabrication involves patterning light energy via laser onto a build stage which is slightly submerged below the surface of a vat of a QD-photopolymer mixture. Once the layer of polymer above the stage is cured, the stage lowers further into the vat of resin, and the next layer is cured on top of the first layer. The process continues until all layers have been created. The microstructures created in the work by Sun and authors include log-piles, the geometry of which is tuned for maximum photoluminescence, and the famous 3D microbull and microlizard (famous among micro stereolithography research). The artifacts created have a build envelope on the order of 10 microns and have feature sizes on the order of half a micron. Similar work with lithography of QD-doped photopolymer reveal features sizes as small as 2 microns [12].

In Sun and authors' work, the Cadmium Sulfide (CdS) QDs are created in situ in a polymer matrix, meaning that QD precursors are mixed among the photopolymer precursors, and the photopolymer and QDs are chemically synthesized together. Applications targeted by Sun and authors' work are currently limited to micro-3D optical displays. The focus of Sun and authors' work is to narrow the particle size distribution of the CdS nanoparticles during the synthesis. By narrowing the size distribution of the particles, a narrower emission spectrum can be achieved, which would result in higher emission intensity at the resulting emission bandwidth.

To differentiate the contributions of Sun and authors' work and the work presented in this dissertation, the goals of each must be examined. First, the goal of this dissertation is to contribute knowledge toward the creation of PUFs in PolyJet builds. With the goal of creating PUFs in mind, variation in the size distribution of the QD agglomerates is desired. Such variation would add complexity to each PUF and ensure visibility of at least the larger agglomerates under a fluorescent microscope. Furthermore, a goal of this dissertation is to propose a process in which QDs can be added to an already commercially available photopolymer, which is suitable for PolyJet equipment. An in-situ synthesis of QDs within a photopolymer suitable for Polyjet would be a good focus for future work but is outside the scope of this dissertation. Furthermore, the major goal of this dissertation is to contribute knowledge toward the characterization of the effects of QDs on photopolymerization. While Sun and authors do achieve 3D structures out of QD-photopolymer composite material, characterization of the photocuring process was not undertaken.

4.1.3 Particles in AM Photopolymers

Photopolymers used in Stereolithography (SL) constitute one of the original AM processes developed in the 1980's. SL is an AM process that utilizes an ultraviolet (UV) laser in conjunction with a build platform which lowers into a vat of photopolymer with each layer of the build (See Chapter 1). Particles can be added to SL photopolymer to create composites, and most commonly added to SL media are ceramic powders for the creation of load-bearing members and casting molds. First, the powder is mixed into the SL resin with some dispersant and other additives to create a suspension. After adding the slurry to the SL vat, the build platform is lowered just below the surface of the slurry, and a wiper blade coats the build platform. Next, the UV laser cures the layer of slurry into the desired two dimensional shape, the build platform lowers and gets recoated, and the process continues until the part is completed. What is removed from the vat is considered a green part, which is afterward processed in a furnace to burn out the polymer and sinter the ceramic particles. Sintering involves heating the particles just below their melting temperatures so that the particles begin to fuse but do not flow.

Ceramic powders have been added to SL resin in as much as 60 volume percent (vol%) [8-13]. Alumina powder as well as silicon nitride have been added to SL resin to create structural objects while silica is added to SL resin to create molds for casting applications [9]. Studies on the effect of powder on stereolithography focus on the effects of opacity [15], on the effects of high index of refraction of the powders [16-18], and on the general curing behavior of the SL resin with the addition of the ceramic powders. Theoretical models developed during these investigations will be discussed in Section 4.2.

4.2 Theoretical Frameworks for Photopolymerization with Particles

Thus far, applications involving photopolymerization with particles have been discussed in absence of their theoretical models. This section will discuss general light scattering by particles theory, general models for predicting light scattering by particles, and current models for describing photopolymerization with particles. First, the discussion of general light scattering theory will include the types of light scattering and scattering which is present in QDs. Second, general mathematical models related to light scattering by particles will be presented, and the main components of the models will be noted. Finally, current theoretical models that describe photopolymerization will be presented along with models that include the influence of particles on photopolymerization.

4.2.1 Introduction to Light Scattering

Types of Light Scattering

Particle matter responds to light energy by absorbing, reflecting, or scattering it. Fundamentally, the physics of the reaction is determined by the fate of the light photons that strike the matter [19-21]. If the light energy is absorbed, the photon is turned into some other form of energy, such as thermal energy. A reflected photon simply bounces off of the particle matter and away from the particle's medium. A scattered photon, however, gets it trajectory altered and remains within the medium in which the particle resides. Since, technically, light energy does not terminate within the particle itself when absorbed, but rather it is converted into another type of energy, the light is never truly absorbed but rather ends up being scattered into some form or another. Therefore, the

terms “absorbing” and “scattering” are both referred to as “scattering” in the literature [33].

Scattering can be elastic or inelastic depending on whether the photon’s energy is conserved or not. Raman scattering is an inelastic type of scattering in which the photon loses or gains energy and actually undergoes a wavelength shift into a higher or lower frequency of light [21, 34]. Two types of Raman scattering occur: when a longer wavelength shift occurs, it is called a Stokes shift, while the contrary is called an anti-Stokes shift [35]. Elastic scattering of light by particles is dependent on particle size. Rayleigh scattering occurs when the diameter of the particle is small in comparison with the wavelength of light it is scattering, and Mie scattering occurs when the particle diameter is much larger than the wavelength of light. Rayleigh scattering is wavelength dependent, and spectral transmission analysis will result in an asymptotic relationship between wavelength and absorbance [37]. Thus, analysis of a suspension’s spectral transmission via spectrophotomer will provide information on the dominant scattering mechanism. This critical experiment is described in further detail in Chapter 5.

Scattering by Quantum Dots

Raman scattering occurs in QDs and, Stokes-shifting is the mode in which QDs convert UV light into visible light [36]. However, due to the inability a QD to accommodate a finite number of photons, Raman scattering contributes a very small portion of the total scattering that occurs in a QD-doped medium. Therefore, other scattering mechanisms must be considered when predicting QD light scattering.

Understanding the interaction of QDs and light energy requires some background knowledge in electron energy states. First, a QD is a semiconducting material, which

has electrical properties between that of a conductor and an insulator [19, 22]. The difference between a semiconductor, conductor, and insulator is due to the energy gap between the valence and conduction electron bands in these materials [23]. The valence band is where electrons typically reside but can be excited into the conduction band with enough energy [24]. The result of exciting an electron into the conduction band is electrical conduction. For an insulator, the gap between the conduction and valence band is large, and the resulting energy required to excite an electron into the conduction band is also large. In contrast, the valence and conduction bands of a conductor overlap, allowing free movement of electrons into the conduction band with little excitation. A semiconductor, therefore, has an intermediate-sized band gap that results in both insulating and conductive properties, depending on the amount of incident excitation energy [25-26].

In addition to electrical behavior between that of insulators and conductors, QDs also have excitation properties between that of bulk material and atoms. QDs get their name “quantum” from these properties, meaning that they are of the size for which quantum effects are present [3, 20-22, 27]. More specifically, whereas electrons in bulk material can travel in all three dimensions, the electrons in quantum dot energy gaps are confined in all three spatial directions, resulting in a discrete, quantized spectrum of energy [28]. This discrete, quantized energy spectrum is what causes the size-dependent fluorescence of QDs and the larger the particle, the lower the fluorescent energy. Thus, the smaller QDs emit the high-energy blue light while the larger QDs emit the low-energy red light [22].

QD fluorescence occurs due to excitation of valence electrons into higher energy bands and then subsequent photon emission from the electron returning to the lower energy state. Excitation of QDs can be instigated by electrical charge or an optical charge; most commonly, the energy from UV light is used to cause QD fluorescence. Just as the fluorescence of a QD has a narrow band of emission, the absorption of a QD has a narrow range of light that is absorbed. Consequently, the diameter of a QD can be determined by observing the absorption spectrum of the QD [29]. For example, a QD with a diameter of 4.5 nm will show absorption and resulting excitation peak at 600 nm wavelength, while a QD with a diameter of 2.1 nm will peak at 498 nm wavelength [28,30].

QD excitation characteristics become significant when it becomes possible for excited QD particles to interact with the ingredients in photopolymers [13-14]. Photoinitiators are a main ingredient in photopolymers and produce free radicals when excited by a photon of a certain wavelength of energy. Certain sizes of QDs can absorb the photons needed by photoinitiators, which would result in impeded photopolymerization. Barichard and authors have used holographic techniques to determine the role of red QDs in the polymerization process in combination with a co-photoinitiator. Comparing tests with and without the co-photoiniator, they found that QDs can serve as a photoinitiator but are not very effective in this role. Furthermore, the QDs can only serve as a photoinitiator when a tertiary amine is present, which is a particular type of monomer. In summation, the findings of Barichard's work reveal some involvement of the QDs in the polymerization process but do not attempt to model the involvement. Thus, developing a model to predict the influence of QDs on

photopolymerization must rely on general light scattering theory as well as current theory in the influence of particles on AM photopolymers.

Although no photopolymerization studies have been conducted specifically with PolyJet photopolymer, Barichard and authors noticed a decrease in the curing rate of photopolymer due to the presence of QDs [13-14]. The physico-chemical role of the QD in the inhibition of photopolymerization in grated sensors was the main focus of their work. They found that QDs can serve as photoinitiators, but are very weak compared to typical compounds used for this purpose. The conclusion of the study revealed that the co-initiators are supposedly becoming trapped on the surfaces of the QDs, which reduces the polymerization rate.

Barichard's recent findings mark the first investigation of the relationship between QD particle loading and photopolymerization rate. Although a trend can be seen in the data, a mathematical model has not been produced to characterize this relationship. This research gap guides the scientific contribution of this dissertation:

Scientific Contribution:

Answering the Primary Research Question by predicting the effect of QDs on photopolymerization will contribute new knowledge to the area of QD-loaded photopolymers. Developing a theory to predict the effects of QDs on photopolymerization will serve applications involving sensing, displays, and composites in addition to creating PUFs via PolyJet.

4.2.2 Light Extinction Theory

QDs may inhibit photopolymerization by preventing the exposing light from reaching critical photopolymer components. As opposed to the chemical role QDs may play in photopolymerization, the interference with the incident light may be treated as a general light scattering scenario. The Beer-Lambert Law empirically describes the extinction of light as it passes through a medium and can be expressed most generally in the following differential form [31-32, 38-40]:

$$\frac{dI}{dz} = -\gamma I \tag{4-1}$$

where *I* is light intensity, z is the direction in which the light is traveling through the medium, and γ is the extinction coefficient. The relation maintains that the change in light intensity in a medium as a function of depth depends on the product of the incident intensity of the light and the absorbing characteristics of the medium. If there is no change in the medium as a function of depth (z), then the Beer-Lambert equation can be integrated into the following form:

$$I(z) = I_o \exp(-\gamma z) \tag{4-2}$$

where I_0 is the incident intensity of the light source. The extinction coefficient γ is the operating term in Equation 4-2 and is discussed in more detail in the next section.

Extinction Coefficient

Defining the amount of light absorbed within a media lies with defining the extinction coefficient, γ, of the media. The general form of the extinction coefficient for particle-doped media is as follows [33]:

$$\gamma = \int_0^\infty \pi r^2 Q_{ext} N(r) dr \tag{4-3}$$

Where πr^2 is the particle cross section, Q_{ext} is the extinction efficiency factor, $N(r)$ is the number of particles per unit volume, and r is the average particle radius. Thus, the extinction coefficient takes into account particle size, concentration, and extinction efficiency. Combining the product of the number of particles per unit volume with the cross-section of a particle (πr^2) from Equation 4-3 constitutes what is known as the extinction cross section. The extinction cross section and the extinction efficiency factor will be discussed in the following sections.

Extinction Cross Section

Particles dispersed within a media have a cross section with respect to the incident light that directly influences the scattering efficiency of those particles. The cross section is the 2D area of the particles from the perspective of the light source and is reported as a percent of the total cross sectional area of the particle-doped media [33,41]. From the terms in Equation 4-3, the extinction cross section is shown in Equation 4-4:

$$extinction\ cross\ section = \int_0^\infty \pi r^2 N(r) dr \tag{4-4}$$

where, as previously mentioned, r is the particle radius and $N(r)$ is the number of particles per unit volume. Taking an average radius and converting the number of particles per unit volume ($N(r)$) to volume fraction,ϕ, the extinction cross section can be simplified to Equation 4-5:

$$extinction\ cross\ section = \frac{3\phi}{4r} \tag{4-5}$$

From this point forward in the theoretical models in the literature, the particle radius term is converted to the particle diameter, d. By converting radius to diameter, converting volume fraction to weight percent (wt%), and taking the simplified extinction cross section from Equation 4-6, the extinction coefficient can be simplified to Equation 4-6 [38]:

$$\gamma = \frac{3\rho_{media} wt\% Q_{ext}}{2\rho_{particle} d} \tag{4-6}$$

This form of the extinction coefficient is the form that is typically used in simplified scattering models. While the extinction cross section component is straight-forward, determining the extinction efficiency term, Q_{ext}, requires some understanding of the scattering mechanisms present within the media. Determining the extinction efficiency term will be discussed in the following section.

Extinction Efficiency Term, Q

The extinction efficiency term is the primary means of predicting a medium's ability to absorb or scatter light. The efficiency term includes both scattering and absorbing efficiency (Equation 4-7):

$$Q_{ext} = Q_{sca} + Q_{abs} \tag{4-7}$$

Thus, to determine the full coefficient, the type and amount of scattering and absorption must be determined. For particles that are much larger than the wavelength of light passing through, Mie theory best dictates the scattering efficiency. The general formula for Mie scattering is shown in Equation 4-8 [33]:

$$Q_{mie} = 2 - \frac{4}{\rho} sin\rho + \frac{4}{\rho^2(1 - cos\rho)} \quad (4\text{-}8)$$

Where ρ is defined as follows:

$$\rho = \frac{2\pi d}{\lambda_o} \Delta n \quad (4\text{-}10)$$

with *d* being the particle diameter, λ_o being the incident light wavelength, and Δn being the different of index of refraction between the particles and the media. Equation 4-9 covers the whole domain of ρ and produces a dampened sinusoidal curve, the maxima's of which are used to determine the optimum ρ values to achieve extinction.

Simpler equations for specific boundary conditions have been formed for the scattering efficiency coefficient [33, 43]. Since the work in this dissertation is focused on a specific particle diameter (*d*), incident wavelength (λ_o), and difference index of refraction of the QDs and the photopolymer (Δn), simpler equations selected by the boundary conditions may be used to formulate the scattering efficiency term, *Q*. These boundary conditions are characterized by two parameters, the ratio of particle diameter to incident light wavelength, x, and the difference in index of refraction between the particles and the medium (Δn). These two parameters are defined as shown in Equations 4-11 and 4-12.

$$x = \frac{2\pi d}{\lambda_o} \quad (4\text{-}11)$$

$$\Delta n = n_{particles} - n_{solution} \quad (4\text{-}12)$$

The index of refraction term is defined as $\Delta n = n_{particle} - n_{media}$. The ratio of the particle size to the wavelength of light is called the *size parameter* where r is the radius and λ is the wavelength. Once Δn and x are determined, Q_{ext} can be determined from

existing extinction coefficient formulas. The parameters x and m are mapped into a diagram of boundary regions as shown in Figure 4-1.

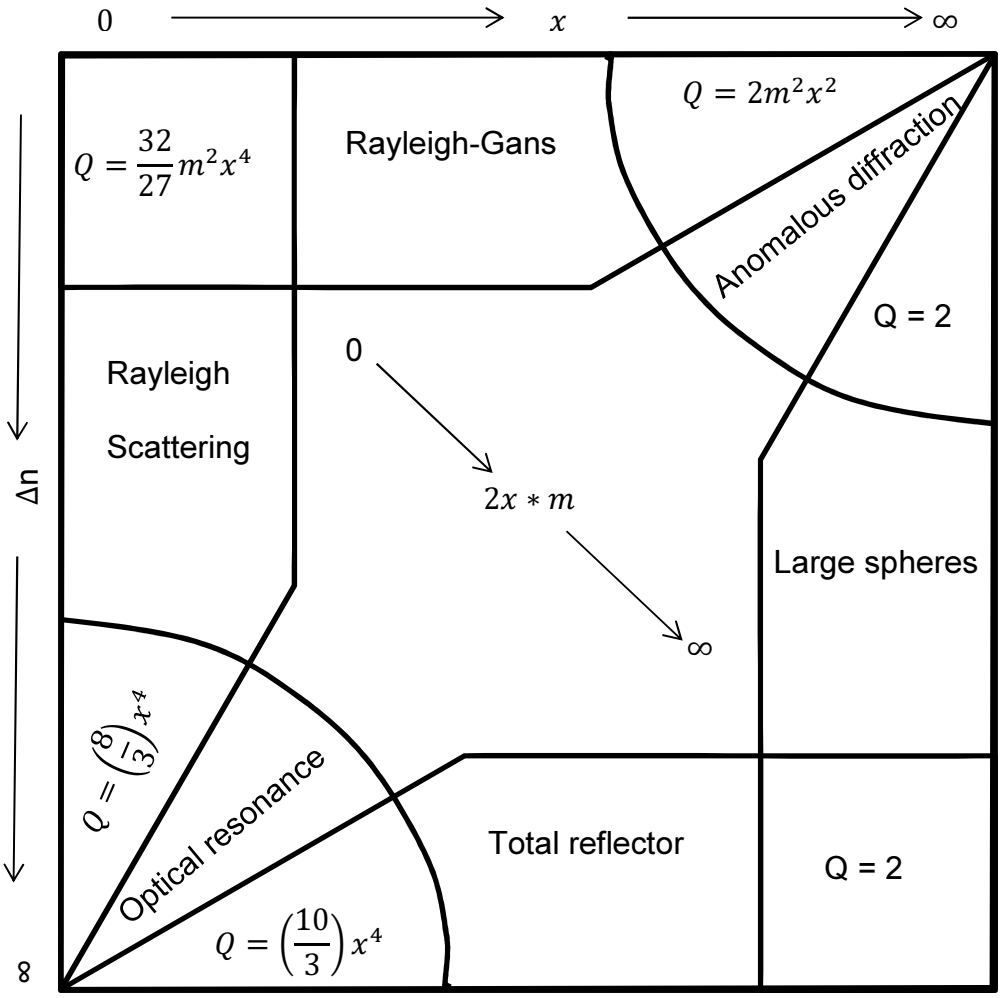

Figure 4-1: Boundary regions for extinction coefficient [33, 43].

Within Figure 4-1, three main parameters create the divisions in the boundary region diagram: particle size, index of refraction, and phase shift. The vertical divisions are created by the particle size regions, small, medium, and large particles. The horizontal divisions are for the difference in index of refraction, and the semi-circular divisions are the regions in which the wavelength of light undergoes a phase shift. Thus, by calculating the size parameter, x and the index of refraction difference, m, the

extinction coefficient Q_{ext} can be determined. For example, for spheres which are small compared to the wavelength of incident light, Rayleigh scattering theory is appropriate, and the Rayleigh coefficient of scattering efficiency is as shown in Equation 4-13 [33]:

$$Q_{Rayleigh} = x^2 m^2 = \left(\frac{2\pi d}{\lambda_o}\right)^2 \Delta n^2 \tag{4-13}$$

Thus, selecting the extinction efficiency of a medium depends on the ratio of the particle diameter to the wavelength of incident light as well as the difference in index of refractions of the particles and the medium. The experimental methods for determining the average particle diameter and the refractive indices of the QDs and the media will be described in Chapter 5.

4.2.3 AM Photopolymerization Models

Thus far in the dissertation, light scattering theory has been described without considering photopolymerization theory. To create a theoretical model that considers light scattering theory in photopolymers, the photopolymerization process must be understood. Polymerization occurs when monomers (organic compounds) are energized such that they "link" to other monomers to form "polymers" (hence the term "polymerization"). *Photo*polymerization occurs when the activating energy comes from a light source. To complete this reaction, monomers, photoinitiators, and photo inhibitors come into play. The process happens in three stages: initiation, propagation, and termination. First, light of the appropriate wavelength initiates the process by striking the photoinitiators which then create free radicals [39]. A free radical is a particle that has an unpaired valence electron and is reactive with other materials because of this

“dangling” covalent bond. The free radicals then react with the monomers to create a propagating reaction that links the monomers together [38].

When photopolymers are exposed to the appropriate wavelength of light at a sufficient intensity, photopolymerization begins for the mass of polymer that is exposed to the light. Since the light energy is absorbed by the photopolymer as the light penetrates it, only the polymer above a certain depth receives enough energy to crosslink. This depth of crosslinked polymer is known as the cure depth and is predicted using current photopolymerization theory used in AM.

To explain current AM photopolymerization theory, the Beer-Lambert Law presented in Equation 4-1 (Section 4.2.1) is arranged into the form shown in Equation 4-14.

$$z = \frac{1}{\gamma}\ln\left(\frac{I_o}{I(z)}\right) \tag{4-14}$$

The curing of photopolymers can be characterized using this form of the Beer-Lambert Law, with $I(z)$ paralleling the critical exposure (E_c), I_o being the incident light intensity (E_o), z being the cure depth (C_d), and 1/γ being the depth of penetration term (D_p). Rewriting the equation according to these new terms, the Beer-Lambert equation becomes what is known in the field of AM as the Jacobs equation [39-40]:

$$C_d = D_p\ln\left(\frac{E_o}{E_c}\right) \tag{4-15}$$

where C_d is the cure depth, D_p is the depth of penetration, E_o is the incident exposure dose, and E_c is the critical exposure dose. The critical exposure is the minimum amount of exposure energy needed to initiation photopolymerization, and the depth of penetration is the depth to which photopolymerization occurs given a certain amount of

light. This arrangement is used to predict cure depth of a photopolymer from a given intensity with the depth of penetration and critical exposure terms being defined for each specific polymer. In cases where D_p and E_c are not defined (e.g., when developing a new photopolymer) and must be determined, the cure depth is measured for various exposure values and plotted in a graph of the log of exposure verses the cure depth. The usefulness of the Jacobs equation comes from forming a working curve from cure depth samples, and this working curve is used to experimentally determining critical exposure (the *x*-intercept) and depth of penetration (the slope of the log-linear trend line). Figure 4-2 is a depiction of a working curve [39-40].

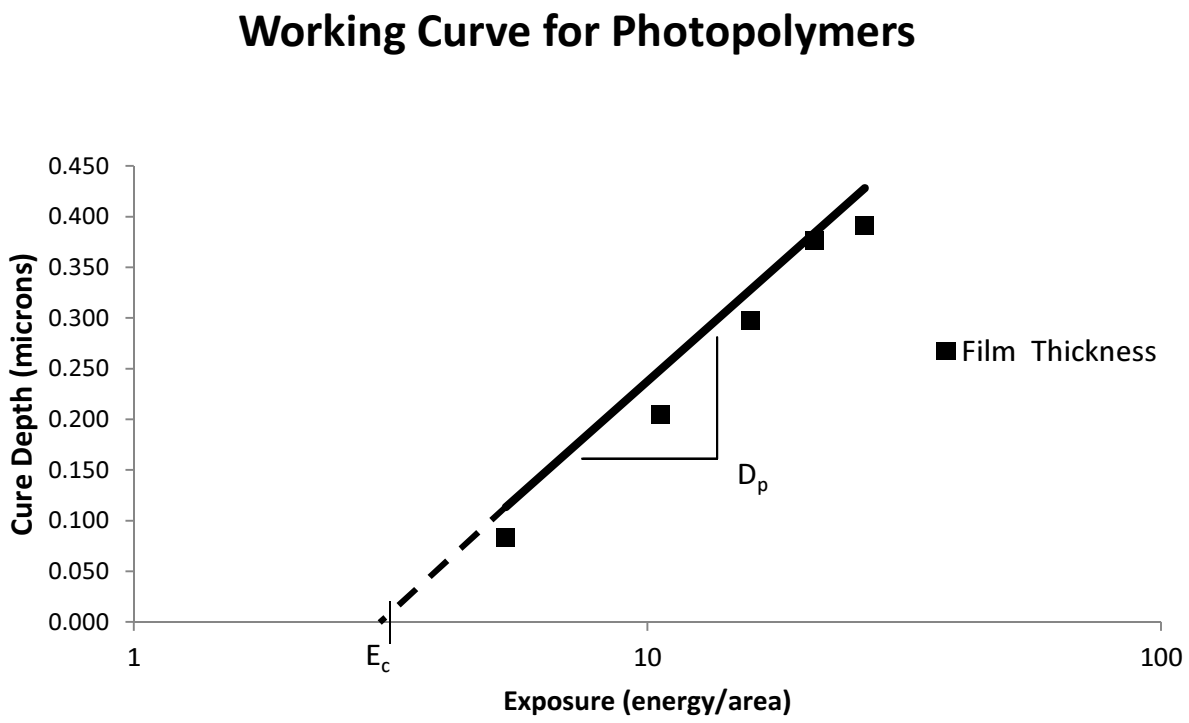

Figure 4-2: Example Photocuring Working Curve.

To create a working curve, thin film samples on the order of a few hundred microns thick are created by controlled exposure to UV light. By varying exposure dose,

film samples of varying thicknesses are created. Upon measuring these samples, their thickness is plotted on the *y*-axis of the plot against the log of the exposure dose on the *x*-axis. The line that continues through each of the points is the working curve. The *y* intercept of the working curve is dictated by the Jacob's equation to be the critical exposure, and the slope of the working curve is the depth of penetration. Thus, from this plot, the amount of energy needed to initiate cure (e.g., critical exposure) along with the approximate depth of penetration light can be determined for an individual polymer, which can be used to predict the depth of cure (layer thickness) given a certain UV dose [29-30].

Macro Vs. Micro Absorption Models

Predicting the curing behavior of photopolymers traditionally is approached on either a micro or macro level, meaning the modeling is either specific to photoresist composition or the model simplifies photopolymer curability into up to two separate terms, respectively [31]. The micro-type models are based on the volume concentration of each photopolymer ingredient and the subsequent probability that a photon will strike a photoinitiator, produce a free radical, and then finally cause monomers to crosslink. The influence of dies, which absorb photons, and other materials that absorb free radicals are taken into account. Halloran and authors have created a model (Equation 4-16) that predicts cure depth based on specific components of their photopolymer mixtures including photoinitiators, photoinhibitors, dyes, and monomer types [32]:

$$C_d(E) = \frac{1}{\frac{1}{l_{sc}}+(1-\emptyset)(c_p\varepsilon_p+ c_D\varepsilon_D)}\left(lnE - ln\left[(1-\emptyset)\frac{h\nu}{\Omega}(\gamma_Q Q + \gamma_D c_D)\frac{1}{c_p\varepsilon_p}\right]\right) \qquad (4\text{-}16)$$

where $c_p\varepsilon_p$ is the absorption of the photoinitiator, $c_D\varepsilon_D$ is the absorption of inert dyes, Q is the concentration of inhibitors, $\emptyset$ is the volume fraction of solid material, Ω is the quantum yield for photogeneration, and the other terms dictated similar photoreactive properties of the photopolymer. Halloran's formulation is useful for situations where photopolymer ingredients are known and well characterized. However, for this work, where a commercially available polymer is used and the composition is largely unknown, developing a model of this kind is impractical.

In contrast to the micro-level models, modeling has been performed for particle-loaded photopolymers without consideration for the specifics of the photopolymer composition. These macro-level models lump the photo-sensitivity of the photopolymer into two terms, critical exposure and depth of penetration. This type of theoretical model was used by Griffith to model the effects of ceramic particles on photopolymerization on AM photopolymers and will be discussed in the next section.

Extinction Efficiency in Photopolymerization Models

Griffith and authors propose a theoretical model to predict the cure depth of ceramic-doped AM photopolymer that focuses on the simplified extinction efficiency term, Q [38]. While Q terms were considered from Mie and Rayleigh-Gans models, Griffith ultimately develops an empirical coefficient represented in Equation 4-17.

$$Q_{ext} \propto \left(\frac{2\pi d}{\lambda_o}\right)^i \Delta n^2 \tag{4-17}$$

Just like the simplified Q term in Equation 4-13, Griffith's extinction coefficient Q_{ext} is a function of the difference in index of refraction between the particles and the media and is also a function of the ratio of the particle circumference to the wavelength

of light [31, 33, 42]. Griffith incorporated this Q_{ext} term into the depth of penetration term of the Jacobs Equation (Equation 4-15) to create Equation 4-18 [38]:

$$C_d \propto \frac{2d}{3Q\emptyset}\ln\left(\frac{E_o}{E_c}\right) \tag{4-18}$$

$$Q = \left(\frac{2\pi d}{\lambda_o}\right)^i \Delta n^2 \tag{4-19}$$

Where d is the average particle diameter, E_o is the given exposure of light, E_c is the critical exposure of the photopolymer, $\emptyset$ is the volume fraction of particles in the media, and Δn and $(2\pi d/\lambda_o)^i$ are the refractive index difference and the particle size-wavelength ratio. The term i is specific to the particle-polymer mixture and is determined via optimization techniques. Equation 4-18 constitutes one of the first attempts at incorporating light scattering theory into an AM photopolymerization model. Griffith's model will be leveraged to form a hypothesis to predict the effects of QDs on PolyJet photopolymer presented in the next section.

4.3 Primary Research Hypothesis

Based on the literature presented, a hypothesis can be formed that incorporates light scattering theory and AM photopolymerization models. Table 4-2 contains the critical relationships between scattering efficiency and photopolymerization toward forming the Primary Research Hypothesis.

Table 4-2: Progression of Current Theory Toward Hypothesis

1. Integrated form of Beer Lambert Law	Equation No.
$$I(z) = I_o \exp(-\gamma z)$$	(4-2)
2. Integrated form of Beer Lambert Law solved for z, penetration depth	
$$z = -\frac{1}{\gamma}\ln\left(\frac{I_z}{I_o}\right)$$	(4-20)
3. General Form Scattering Efficiency	
$$\gamma = \int_0^\infty \pi r^2 Q_{ext}(r) N(r) dr$$	(4-3)
4. Take Average Radius of Equation 4-3	
$$\gamma = \pi r^2 Q_{ext} n$$	
5. Convert to Weight Percent (*wt%*) and Diameter, *d*	
$$\gamma = \frac{3 d \rho_{particle} wt\% Q_{ext}}{2\rho_{media}}$$	(4-6)
6. Rayleigh Scattering Coefficient	
$$Q_{Rayleigh} = x^2 m^2 = \left(\frac{2\pi d}{\lambda_o}\right)^2 \Delta n^2$$	(4-13)
7. General Form AM Photopolymerization Model (Cure Depth Equation)	
$$C_d = D_p \ln\left(\frac{E_o}{E_c}\right)$$	(4-15)
8. Griffith Model for Cure Depth of Ceramic-Doped AM Photopolymers	
$$C_d \propto \frac{2d}{3Q\emptyset}\ln\left(\frac{E_o}{E_c}\right), \qquad Q = \left(\frac{2\pi d}{\lambda_o}\right)^i \Delta n^2$$	(4-18) (4-19)

Equation 4-2 contains the integrated form of the Beer Lambert Law for the scattering of light with particle doped media. Equation 4-20 in the Table 4-2 is Equation 4-2 solved for the depth term, *z*. Comparing Equation 4-20 with equation 4-15, a similarity can be seen. Equation 4-20 illustrates that the depth to which light penetrates is inversely proportional to the scattering efficiency of the particles within the media. Equation 4-3 contains the general form of scattering efficiency, which is altered to accommodate weight percent loading into Equation 4-6. Equation 4-6 further illustrates the inverse relationship between particle loading and the depth of penetration. Understanding the relationship between cure depth (C_d) and depth of penetration (D_p) presented by the Jacob's equation in Equation 4-15, Griffith presents Equation 4-19, which is a form of the Jacob's equation that incorporates light scattering theory. Ultimately, Griffith uses a light scattering term to replace the depth of penetration term. For this research it is proposed that QDs will affect the depth of penetration in a similar manner, namely that the depth of penetration can be predicted using light scattering theory. Since QDs are nanoparticles, and are thus smaller than the wavelength of the light, Rayleigh scattering is appropriate and Equation 4-13 should be applicable. This combination of theoretical models constitutes the Primary Research Hypothesis.

Primary Research Hypothesis: The effect of QDs on the depth of penetration term for photopolymers can be predicted by Rayleigh light scattering theory.

$$D_p = \frac{2\rho_{media}}{3d\rho_{particles}Qwt\%}; \quad Q = Q_{rayliegh} = \left(\frac{2\pi d}{\lambda_o}\right)^2 \Delta n^2 \qquad (4\text{-}20), (4\text{-}21)$$

Experimentation in Chapter 5 will be focused on validating this hypothesis and exploring any additional effects that the QDs might have on photopolymerization that have not been discovered in prior literature.

4.4 Roadmap

This chapter reviews existing work in QD-photopolymer systems and current modeling photopolymerization with particles. The current work in these areas does not intersect by means of providing a model for the photopolymerization of with QDs. However, relevant modeling has been performed in the area of light scattering by particles and scattering of light by particles in AM photopolymers. Thus, the scientific contribution of the work in this dissertation is to gain an understanding of the effects of QDs on photopolymerization, in the form of the Primary Research Hypothesis. The remainder of this dissertation will include the experimental methods to validate the hypothesis, experimental results, a comparison of the hypothesis and the experimental results, and the conclusion from this work. A roadmap is provided below to outline the chapter contents.

Table 4-3: Roadmap

	Research Phase	Chapter	Goals
Introduction	Problem Identification Solution Proposal	**Chapter 1** Introduction, Motivation, and Project Outline	**Describe the problem** **Describe a solution** to the problem and the process for implementing that solution **Identify the qualifying and research questions** related to the proposed solution
Background & Feasibility Analysis	Information Gathering Preliminary Experimentation	**Chapter 2** Visibility of Quantum Dots within PolyJet Media (QQ1) **Chapter 3** Inkjetting with Quantum Dots in PolyJet Media (QQ2)	**Synthesize literature** related to the Qualifying Questions **Perform Experiments** to address Qualifying Questions 1 and 2 **Draw Conclusions** to address Qualifying Questions
Research Methods	Hypothesis Formulation Experimental Methods Hypothesis Validation	**Chapter 4** Literature Review of Photopolymer-ization Theory, Proposed Theoretical Model **Chapter 5** Experimental Techniques, Results and Critique and Modification of Theoretical Model **Chapter 6** Effects of Intensity on Critical Exposure	**Synthesize literature** related to the Primary Research Question **Identify gaps** in existing literature that prevent answering the research question **Form hypotheses** based on existing literature **Establish Methods** for validating the hypothesis **Perform Experimentation** to validate hypothesis
Summary	Conclusions Outlining Future Work	**Chapter 7** Project Summary and Future Work	**Draw Conclusions** based on experiment results **Identify significant contributions** **Summarize accomplishments** related to answering each of the research questions **Propose future work**

CHAPTER 5 PHOTOCURING EXPERIMENTAL METHODS AND RESULTS

This chapter details experimental methods and results toward characterizing the effects of QDs on the photopolymerization of PolyJet VeroClear photopolymer. In addition, the experimental results will be compared with the Primary Research Hypothesis presented in Chapter 4. The Primary Research Hypothesis describes the scattering efficiency of the QDs within the photopolymer and predicts the depth of penetration of QD-loaded photopolymers.

Primary Research Hypothesis: The effect of QDs on the depth of penetration term for photopolymers can be predicted by Rayleigh light scattering theory.

$$D_p = \frac{2\rho_{media}}{3d\rho_{particles}Qwt\%}; \quad Q = Q_{rayliegh} = \left(\frac{2\pi d}{\lambda_o}\right)^2 \Delta n^2 \qquad \text{(4-20), (4-21)}$$

Where D_p is the depth of penetration, d is the average particle diameter, Q is the scattering coefficient, λ_o is the wavelength of incident light, *wt%* is the weight percent of QDs, and Δn is the difference in refractive indices of the QDs and the media.

In this chapter, Section 5.1 describes the experimental methods used to characterize the QDs and the photopolymerization of QD-doped photopolymer. Section 5.2 describes the results of the photocuring experiments, and Section 5.3 contains a comparison between the Primary Research Hypothesis and the experimental data. Finally, Section 5.4 describes methods and findings related to the effects of intensity on the critical exposure of the photopolymer, which was also explored due to unique results obtained during the photocuring experimentation.

5.1 Experimental Methods

The methods described in this section focus on characterization of the curing of QD-doped resin and characterization of QDs towards scattering properties, refractive index, and particle and agglomerate size. To validate the Primary Research Hypothesis, one needs to know the diameter and the refractive index of the QDs at the wavelength of cure (365 nm). Furthermore, the dominant scattering mechanism (e.g. Rayleigh or Mie) is identified via spectrophotometry. Procedures for obtaining these values for QD properties are presented in Section 5.1.1.

The polymerization of QD-doped polymers is characterized toward identifying values for the Jacobs equation (Equation 4-15) [1]:

$$C_d = D_p \ln\left(\frac{E_o}{E_c}\right) \tag{4-15}$$

where C_d is the cure depth, D_p is the depth of penetration term, and E_o and $E_c$are the incident and critical exposures, respectively. Since the input into this equation is the incident exposure and the output is the cure depth, the terms characteristic to the individual polymer are the depth of penetration and critical exposure of the photopolymer. The critical exposure and depth of penetration are determined by plotting film thicknesses verse exposure values, which constitutes the working curve of a photopolymer (Section 4.2.3). As described in section 5.1.2, the working curves are formed by creating and measuring cure-depth samples via microstereolithography (μSL).

The experiments described in this section are conducted to validate the Primary Research Hypothesis. These methods along with their respective components of the Primary Research Hypothesis are summarized in Table 5-1.

Table 5-1: Summary of research methods toward answering the respective components of the research hypothesis.

Primary Research Hypothesis

$$D_p = \frac{2\rho_{media}}{3d\rho_{particles}Qwt\%}; \quad Q = Q_{rayleigh} = \left(\frac{2\pi d}{\lambda_o}\right)^2 \Delta n^2 \qquad \text{(4-20), (4-21)}$$

Jacob's Equation relating Cure Depth (C_d) and Depth of Penetration (D_p)

$$C_d = D_p \ln\left(\frac{E_o}{E_c}\right) \qquad \text{(4-15)}$$

Term	Variable/Parameter	Experimental Method or Parameter Value
$\left(\frac{2\pi d}{\lambda_o}\right)^2 \Delta n^2$	Rayleigh Scattering Coefficient (small particles)	SEM to determine average particle size, spectrophotometer to verify Mie scattering
d	Average Particle Diameter	SEM analysis of QD-doped cure depth samples revealed the average size of QD agglomerates. Spectrophotometry reveals peak absorbance wavelength, which can be traced to the average nanoparticle diameter.
D_p	Depth of Penetration	Extrapolated from Workings Curves, which are formed by plotting cure depth verses exposure. Cure depth samples were created with a microstereolithography apparatus.
E_c	Critical Exposure of QD-doped Polymer	
E_0	Incident Exposure of Pure Polymer	Value of PolyJet lamp intensity (20 mW/cm^2)
C_d	Cure Depth	Measured films created via Microstereolithography
$\rho_{\text{particles}}$	Density of Particles	Density of CdSe, 5.82 g/cm^2 [2]
ρ_{media}	Density of Polymer	1.08 g/cm^3, measured
λ_o	Wavelength of Curing Light	Peak Wavelength of PolyJet Lamp (365nm)
Δn	Difference in Refractive Index of polymer and QDs	UV Refractometer, Literature Review [3]
$wt\%$	QD Weight Percent	Values of 0.5, 1, 2, and 5 wt% determined by visibility tests in Chapter 2

5.1.1 QD Characterization

QDs have the potential to influence photopolymerization by scattering the light energy intended for exposure. The scattering efficiency of a particle depends on the size, absorption and scattering characteristics, and the index of refraction difference between the particle and the fluid in which it resides (Section 4.2.2). First, the absorption and scattering properties of the QDs are determined by spectrophotometry. Spectrophotometry measures the amount of light transmitted through a medium verses the wavelength of light. Analyzing the trend in transmission verses wavelength reveals the dominant scattering mechanism (scattering by large particles or small). Second, the presence and size of the QD agglomerates are determined by imaging on a Scanning Electron Microscope (SEM). The size of the agglomerates further verifies the dominant scattering mechanism revealed through spectrophotometry.

Finally, the refractive index is measured with a UV refractometer. This section deals with the methods to characterize the QDs in terms of scattering and absorption mechanisms, particle size, and refractive index.

Spectrophotometery

Spectrophotopmetery was used to characterize transmission of a range of UV light wavelengths through the QD-doped photopolymer. A spectrophotometer contains a light source, wavelength filters, and a detecting device for detecting the intensity of light. The instrument is initialized by charting the intensity of light through the spectrum of wavelengths. After the sample is inserted, the instrument then measures the intensity travelling through the sample and reports an absorbance value based on the difference between the initialization data and the sample data. Samples of varying QD loadings

were analyzed in the spectrophotometer to determine the dominant scattering mechanism.

The data obtained from a spectrophotometer is absorbance verses wavelength. An absorbance curve that is mostly linear corresponds to Mie scattering while an asymptotic curve corresponds to Rayleigh scattering [4]. Thus, the profile of the spectrophotometer data will determine the type of scattering in the QDs and the resultant mathematical model. The QDs can still maintain their nanometer (nm) size fluorescent properties while being assimilated into much larger agglomerates. Also, the QDs have a specific wavelength peak that corresponds to the individual QD particle diameter, regardless of the presence of agglomeration. In other words, the peak wavelength of the absorbance profile signifies the size of the QDs. For example, a QD with a diameter of 3 nm will have a peak absorbance of light around a 550 nm wavelength [5]. Thus, the spectrophotometer data will reveal the dominant scattering mechanism as well as verify the QD particle size.

Scanning Electron Microscopy (SEM)

As stated in Chapter 4, the average particle agglomerate size of the QDs in the photopolymer determines the type of light scattering that occurs in the particle-doped medium (Rayleigh or Mie scattering). Also, the particle size is part of the modeling equation for determining scattering efficiency.

Ideally, the particle size distribution in a medium can be measured via dynamic light scattering (DLS). DLS takes advantage of Brownian motion, the size-dependent, natural vibrations of particles, to obtain the particle sizes. DLS was not used in this work due to several reasons. First, to accurately measure particle size via DLS, stable

dispersion of the particles must be obtained. In other words, any settling of the particles would alter the results of the measurement. From stability measurements (Appendix), it is known that the QDs do settle over time in the fluid, and that larger QD agglomerates do exist and settle quickly. Another reason DLS was not usable for the QD-VeroClear mixture was the viscosity of the VeroClear was too high. In order to measure the Brownian motion of the particles, the fluid must have low enough viscosity that the particles can freely move. In this work, it was surmised that the extent of agglomeration was heavily dependent on the interaction between the photopolymer and the QDs. Therefore, the agglomeration due to the interaction of the QDs with the polymer would not be represented by a dispersion of the QDs in a different liquid of lower viscosity, such as toluene. Thus, an alternative method for determining the size of the QD agglomerates is needed.

As an alternative to DLS, Scanning Electron Microscopy (SEM) was performed on cured QD-photopolymer samples to determine the particle sizes present within the films. Since QDs are semiconductors, they are visible to the SEM. Recycled stair-step samples from the micro stereolithography cure-depth experiments (Section 5.1.1) were used in this measurement. To prepare the films for SEM imaging, the samples were frozen in nitrogen and fractured. Afterward, the samples were coated in gold via vacuuming and vapor deposition. Pure polymer, as well as 2.0 wt% QD samples, were imaged in magnification ranging from 75x to 500x. To quantify particle sizes, a section of an image was isolated and the particles were measured by counting the number of pixels across their diameter. The pixels were related to the distance scale on the image, and the particle size distribution was determined.

Refractive Index

The refractive index (RI; also known as “index of refractive”) is a measure of the speed that light travels through a medium with relation to the speed of light in a vacuum. The difference in the RI between the photopolymer and the incorporated particles majorly influences the scattering properties of the particle-doped photopolymer. Since the photocuring is driven by a UV lamp with a peak wavelength of 365 nm and RI is wavelength dependent, the RI of the QD-doped photopolymer must be measured at this wavelength. To perform the RI measurement at 365μnm, a Filmetrics thin-film measuring system was used. The QD-polymer concentrations were prepared by mixing dry, powdered QDs into VeroClear polymer by weight percent. The mixtures were stirred for 15 minutes, sonicated for 5 minutes, and restirred for 5 minutes. Weight percentages of 0.5 wt%, 2.0 wt%, 5.0wt%, and 10.0 wt% were prepared along with the control sample of pure VeroClear. The samples were coated onto silcon wafers via spin coating and then cured under UV light. The remaining uncured residue was rinsed away with isopropyl alcohol. The samples were then measured for thickness with a micro-contact measurement system. Using this thickness value combined with the speed through which the light passes through the sample yields the value for refractive index.

The methods in this section describe the procedures needed to quantify QD characteristics toward validating the theoretical model presented in Chapter 4. The following section describes the methods related to characterizing the effects of the QDs on photopolymerization.

5.1.2 Photocuring Characterization

Photopolymerization can be characterized by in-situ monitoring of the viscosity of the curing polymer, which is achieved by an instrument called a photorheometer. In addition, polymerization can be characterized by measuring the thickness (cure depth) of polymer films created by controlled doses of UV exposure and plotting the film thicknesses verses the exposure dose. The plot of cure depth verses the natural logarithm of the exposure dose is known as the Working Curve of the photopolymer. The working curves are based on the Jacob's equation, Equation 4-15 (repeated here for convenience):

$$C_d = D_p \ln\left(\frac{E_o}{E_c}\right) \tag{4-15}$$

where C_d is the cure depth, D_p is the depth of penetration term, and E_o and $E_c$are the incident and critical exposures, respectively. As shown in Figure 4-2, the data point for film thickness create a straight line on the log plot. The slope of that line constitutes the depth of penetration of the exposure light source, and the x-intercept of the line (where cure depth equals zero) constitutes the critical exposure of the photopolymer under a given light source.

Cure-depth films can be created by a mechanical exposure method, such as a UV lamp with a mechanical shutter or UV conveyor, or a digital exposure method, such as a microstereolithography machine. Selecting an appropriate polymerization characterization method depends on two parameters: the intensity of the light source and the amount of QD-doped polymer required to create a sample. As for the intensity parameter, curing properties of photopolymers are dependent on the intensity of the curing light (discussed more in Chapter 6) [6]. Both the lamp and shutter apparatus and

UV conveyor have intensities that differed greatly from the 20 mW/cm^2 intensity of the UV lamp on the PolyJet machine (1.6 mW/cm^2 and 100 mW/cm^2, respectively). Furthermore, neither mechanical method used the QD-doped sample volume efficiently (Table 5-2). As for the photorheometer, filters on the light source limit the emission to outside a peak emission of 365nm. Since the Polyjet polymer is designed to be compatible with a broader range of wavelengths (see absorption data in Figure 5-4), curing with an LED light source would not produce results characteristic of the PolyJet process.

As for sample volume, due to the expense of QDs it is necessary to find a characterization method that uses the QD-doped polymer sample efficiently (provided the most data points for the least amount sample volume). Between microstereolithography and the photorheometer, the former can create samples with multiple thicknesses per exposure while the latter can only produce 1 thickness/data point for a similar sample volume.

The criteria for selecting a photopolymerization characterization method is summarized in Table 5-2. Considering these points, the μSL setup was selected as the primary method for characterizing photopolymerization of QD-doped Polyjet photopolymer.

Micro Stereolithography

As previously stated, microstereolithography was chosen as the method for characterizing photopolymerization due to its broad emission range and efficiency in using sample volume. A micro stereolithography apparatus (μSLA) is an AM process that uses a projector and lenses to project small 2D images onto the surface of a vat of

Table 5-2: Selection Criteria for Photopolymerization Characterization Method

Methods to → Characterize Photopoly-merization ---------- Criteria (below)	**UV Conveyor**	**Photo-rheometer**	**Microstereo-lithography Apparatus**	**Lamp and Shutter Mechanism**
Similar output to PolyJet lamp • 20 mW/cm^2 intensity • broad UV spectrum	**Unfavorable** Intensity is too high: 100 mW/cm^2	**Favorable** Adjustable intensity, but filters make emission spectrum too narrow	**Most Favorable** Adjustable intensity and similar spectral output	**Unfavorable** Intensity is too low: 1.6 mW/cm^2
Sample material required per data point		**Unfavorable** Requires 0.3 ml per sample, 1 data set per sample **(0.3 mL per data point)**	**Most Favorable** Requires 0.5 mL for 5 films with 5 thicknesses each (0.5 mL for 25 data points, **0.02 mL per data point**)	

photopolymer (Figure 5-1). To create this projection, UV light is collimated via optical lenses and reflected onto a dynamic mask, such as a digital mirror device. The dynamic mask is controlled by a computer to reflect a certain image. The reflected image is then reduced via more optical lenses and projected onto the resin surface. By reducing a digital projector image, which has high-pixel volume, into a very small area, the process achieves very high resolution. Thus, three dimensional geometries with features on the order of a few microns can be created with the μSLA process.

To create film samples that are both small but measurable, a new sample geometry was designed. The new design incorporates multiple exposures into a single sample, creating a stair-step geometry. Figure 5-2 illustrates the exposure process.

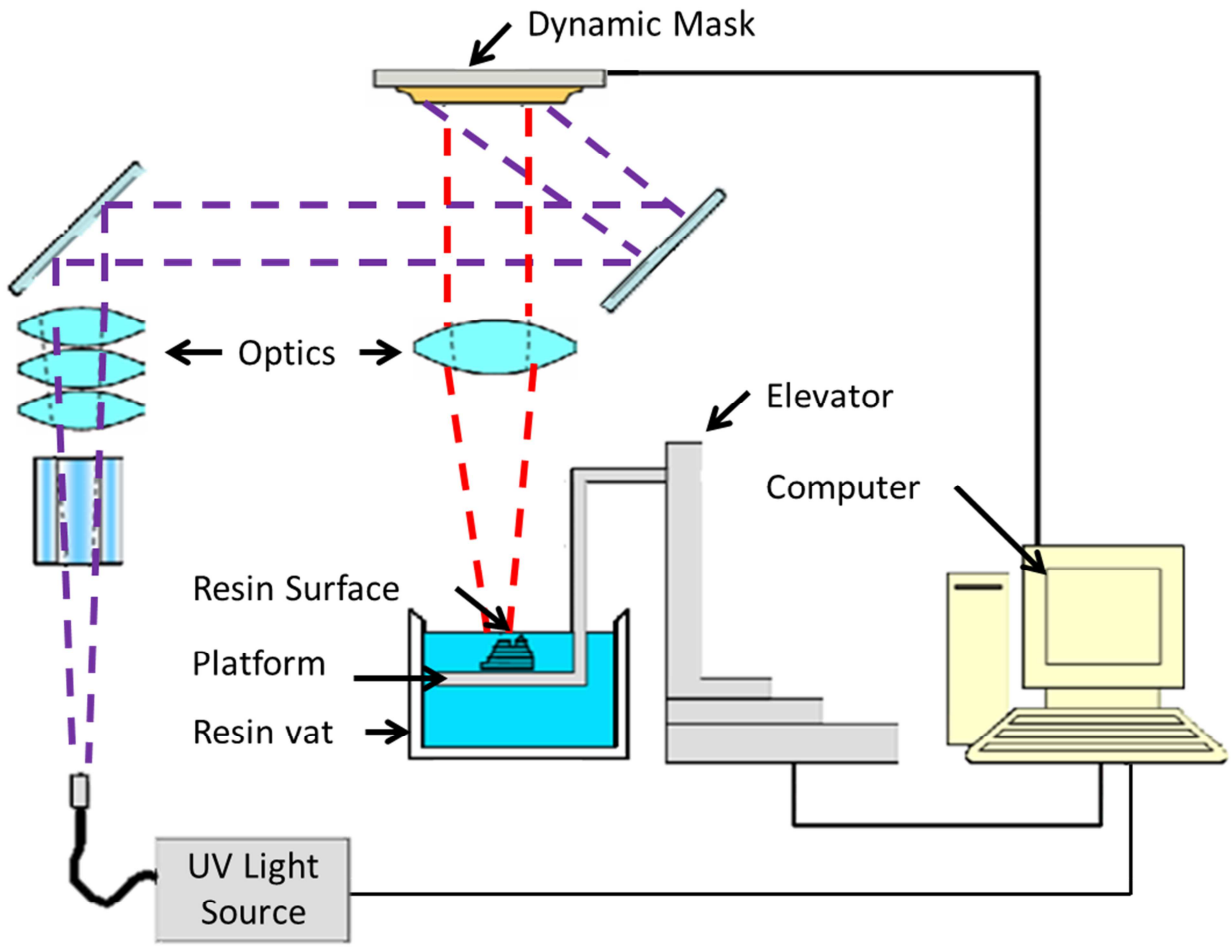

Figure 5-1: Masked Projection Microstereolithography

Each sample gave five data points of thickness for a variety of exposures. Five samples were created for each polymer, resulting in 200 data points for each QD concentration. A possible alternative to creating the stair-step sample would be to create a sample with a single stair height and measure multiple heights along the length of the sample. However, curling was found to be a significant problem on the thicker samples, causing the sample to shift during measurement.

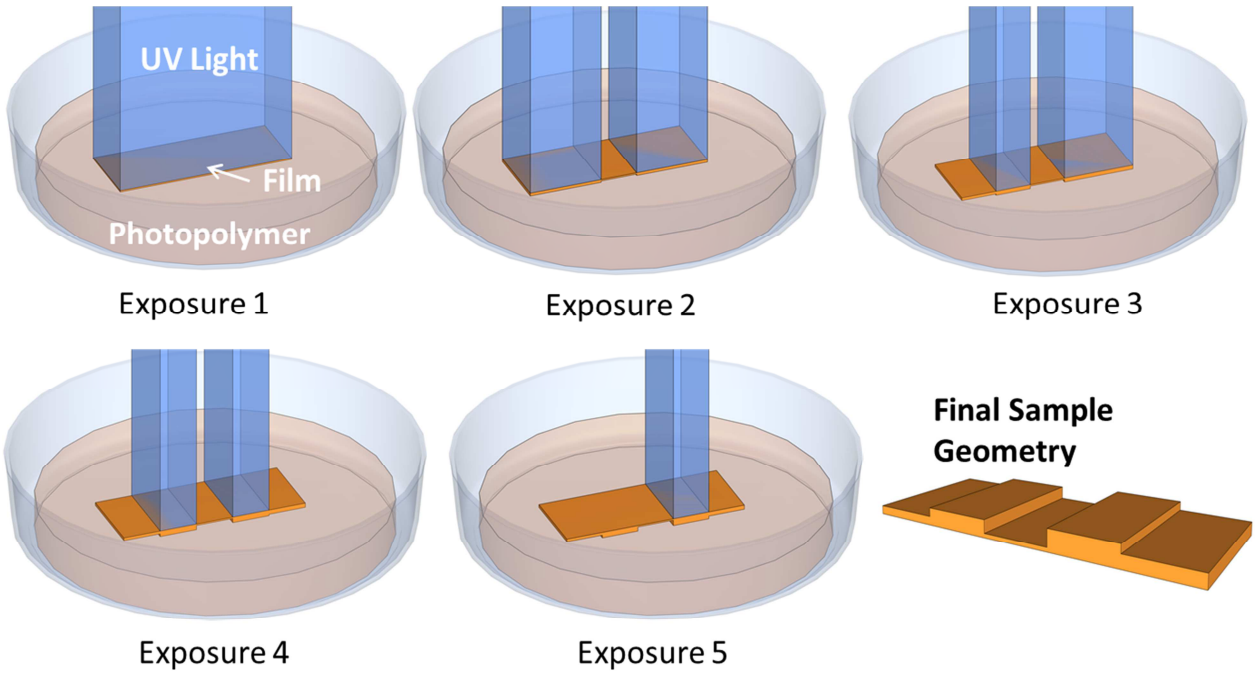

Figure 5-2: Multiple exposures levels given to create the stair-step geometry (sample is floating and not attached to a build platform).

Creating samples with varied step heights not only combats the curling in single-height samples but also provides a means to test multiple exposures per step height. The thinnest section of "stair" was placed in the middle of the sample to combat curling. Also, double sided tape was used to help keep the samples flat.

For each stair-step sample, the intensity of the UV projection was calibrated to approximately 20 mW/cm^2 with a UV dosimeter. The QD-doped polymer samples were injected into a small well and exposed. Once created, the samples were removed from the well and blotted dry. The step heights are measured with a Dino Lite Pro digital handheld microscope and plotted against their exposure values to create a working curve for the photopolymer.

5.1.3 Experimental Methods Summary

Methods to characterize the QDs within PolyJet photopolymer include spectrophotometer, SEM imaging, and UV refractometery to determine QD scattering, particle size, and index of refraction, respectively. To characterize photopolymerization of QD-doped photopolymer in the form of working curves, a microstereolithography apparatus was used to create cure depth samples via controlled exposure. The methods used in experimentation are focused toward finding values to verify the Primary Research Hypothesis.

5.2 Experimental Results

Experimental results were obtained using the methods described in Section 5.1. This section details the results obtained for producing the working curves for the QD-doped photopolymer as well as QD particle and agglomerate size and dominant scattering mechanism. The values obtained in this experimentation are directed toward verifying the Primary Research Hypothesis to describe the effect of QDs on photopolymerization.

5.2.1 QD Characterization

The QDs were characterized in terms of particle size, agglomerate size, and dominant scattering mechanism. Spectrophotometer data revealed that Mie scattering was the dominant scattering mechanism and that the individual QD diameter was 2.4-2.6 nanometers in diameter. Since Mie scattering dominated, it was apparent that the individual QDs had agglomerated (despite functionalization), and the size of the agglomerates needed to be obtained. The QD agglomerates were observed via Scanning Electron Microscopy (SEM) and the average agglomerate diameter was

obtained by analysis of the SEM images. SEM images also revealed some interesting phenomena in the photopolymerization with the QD agglomerates that has not been discussed in previous literature.

Spectrophotometery

Samples of PolyJet photopolymer with varying concentrations of QDs (8 different concentrations, including pure polymer) were analyzed via the spectrophotometer. The resulting data, shown in Figure 5-3, provides an understanding of the absorption profiles of the different samples across a range of wavelengths of light (300 nm to 700 nm).

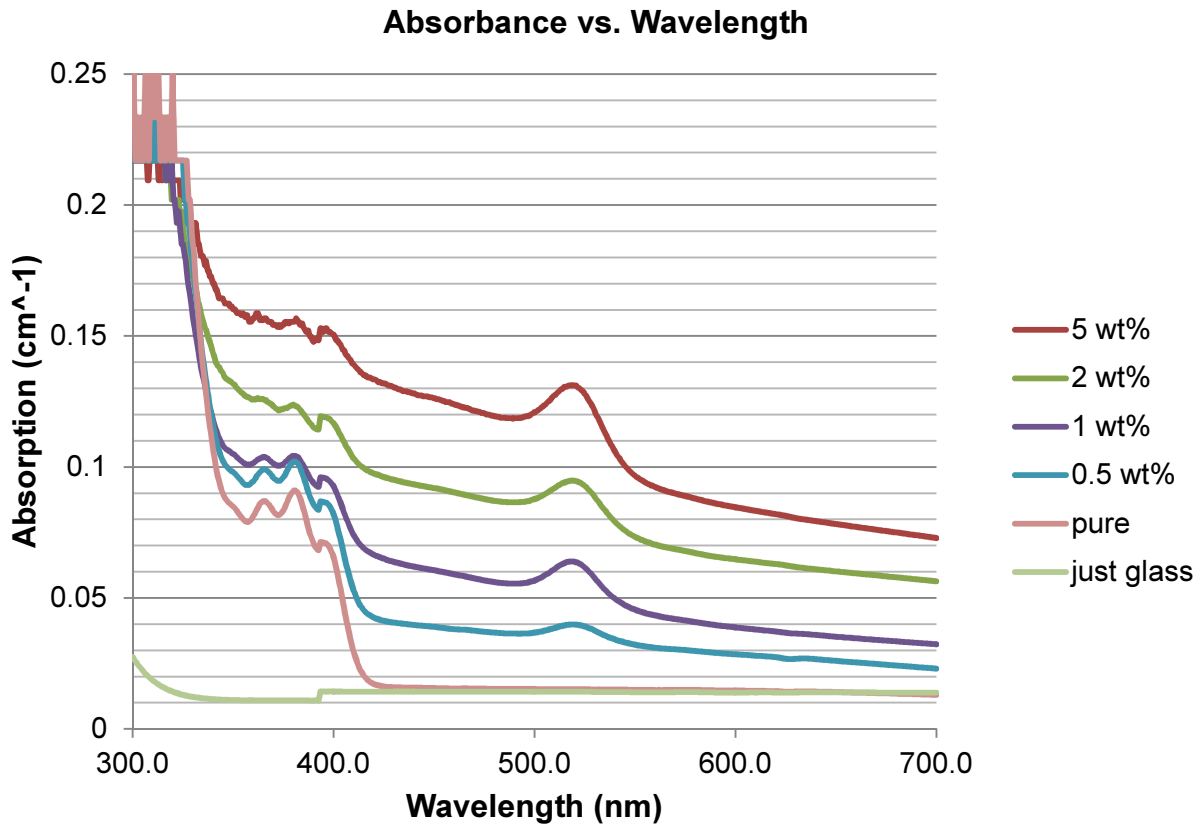

Figure 5-3: Spectrophotometer Data. Absorption of QD photopolymer suspensions verses wavelength of light.

The following conclusions can be drawn from the data in Figure 5-3:

- The absorption over all wavelengths increases with the increase in QD concentration.
- The two peaks around 365 nm and 520 nm represent the absorption peaks of the photopolymer and the QDs, respectively. This absorption peak for the QDs at 520 nm verifies that the QDs are between 2.4 and 2.6 nm in diameter [8].
- The asymptotic increase in absorption below the 350 nm wavelength mark is the absorption of the PolyJet photopolymer, which confirms that the polymer aggressively cures in the 300-350 nm wavelength range in addition to 365 nm.
- The predominantly linear profile of the absorption curves suggests that the dominant scattering mechanism is Mie scattering. Since Mie scattering occurs for particles that are large in diameter in comparison to the wavelength of light, the data suggests that the QDs have agglomerated. Further analysis by SEM was needed to determine the average agglomerate size (detailed in the following subsection).

Due to this proof of nanoparticle agglomeration, the Primary Research Hypothesis must be revised to incorporate Mie scattering rather than Rayleigh scattering. A revision of the Primary Research Hypothesis from to these results is discussed in Section 5.2.2.

A lot of the scattering efficiency of the QD-loaded particles (from 0.5 wt% to 5 wt%) at 365 nm wavelength of light (the wavelength at which PolyJet photopolymer cures) against the natural logarithm of the weight percent is shown in Figure 5-4. A linear relationship can be seen between the absorption and the natural logarithm of QD concentration. This aligns with the Primary Research Hypothesis, which states that the depth of penetration is inversely proportional to the product of the QD scattering efficiency and the QD loading.

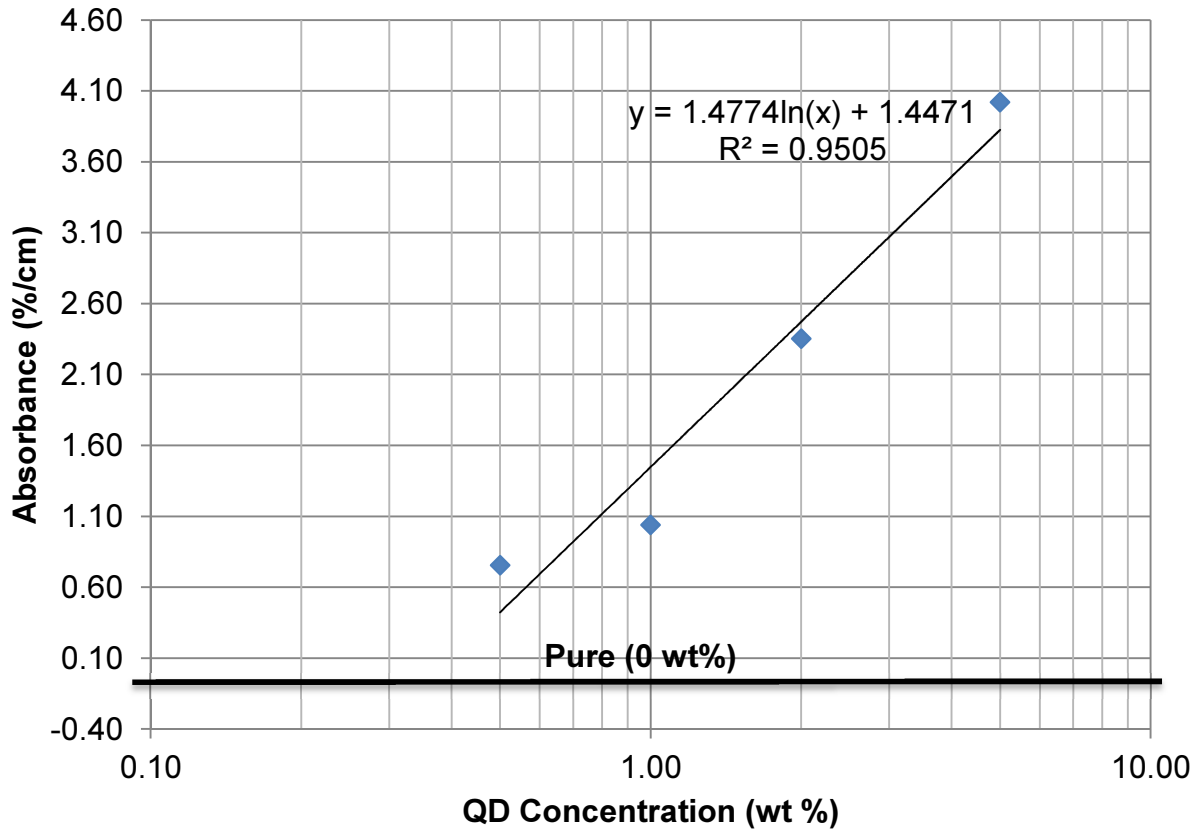

Figure 5-4: QD Absorbance at 365 nm vs. QD Loading

Scanning Electron Microscopy (SEM)

To further investigate the agglomeration of the QD nanoparticles in the photopolymer resin, SEM was conducted on cured samples. A SEM image of a cross section of a PolyJet photopolymer film created via μSLA is provided in Figure 5-5.

To obtain this image, the cured thin film was first frozen in nitrogen and then fractured to reveal the QD dispersion along the depth of the sample. The rough, mountain-like surface on the left side of the image is the bottom of the cure depth sample, and the smoother, flaky surface in the center of the image is the cross section.

It can be seen in Figure 5-5 that the majority of the QD agglomerates remain on the upper and lower surfaces of the film during curing via μSLA. This reveals that the QDs do not readily become part of the polymer matrix, despite functionalization (doping the QD surface with polymer ligands) (Section 2.3.2). Also, it appears that the majority of the larger agglomerates are pushed downward during curing. This is most likely due to the inability of the polymer networks to accommodate the large masses.

To obtain a particle-size distribution from the SEM images, images of the top surface of the photopolymer film were analyzed (See Figure 5-6). The top surface was chosen as the most appropriate point of reference for obtaining particle size distribution since the photo-curing light passes this surface before reaching the remaining photopolymer. Analyzing the SEM images revealed that the QD agglomerates ranged from 1- 50 microns in diameter and had an average diameter of 20 microns. Since 20 microns is significantly larger that the wavelength the curing light (365 nm), a 20 micron average agglomerate diameter further verifies that Mie scattering is the dominant scattering mechanism within the QD-doped polymer.

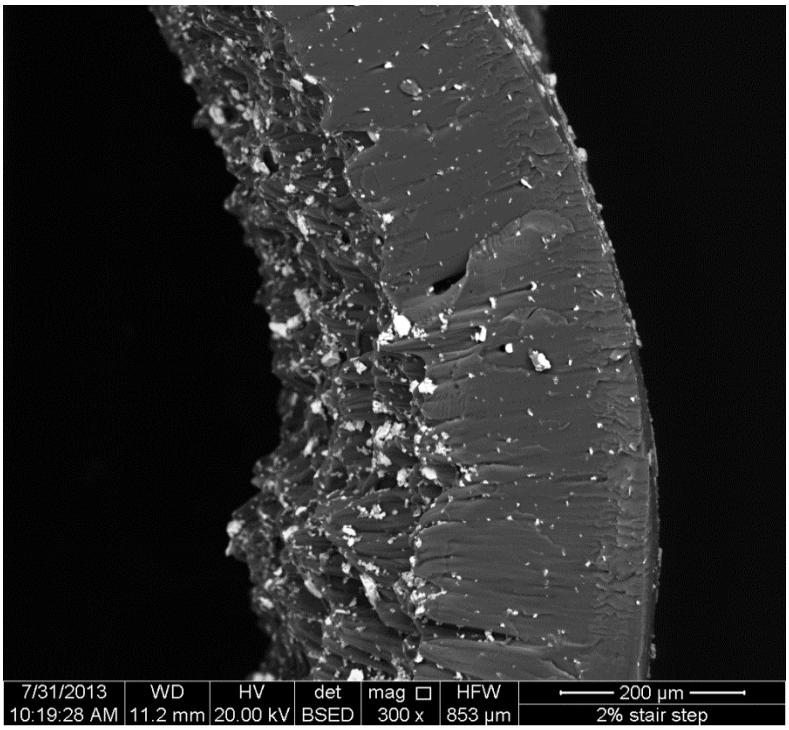

Figure 5-5: SEM image of QD-doped photopolymer film cross section

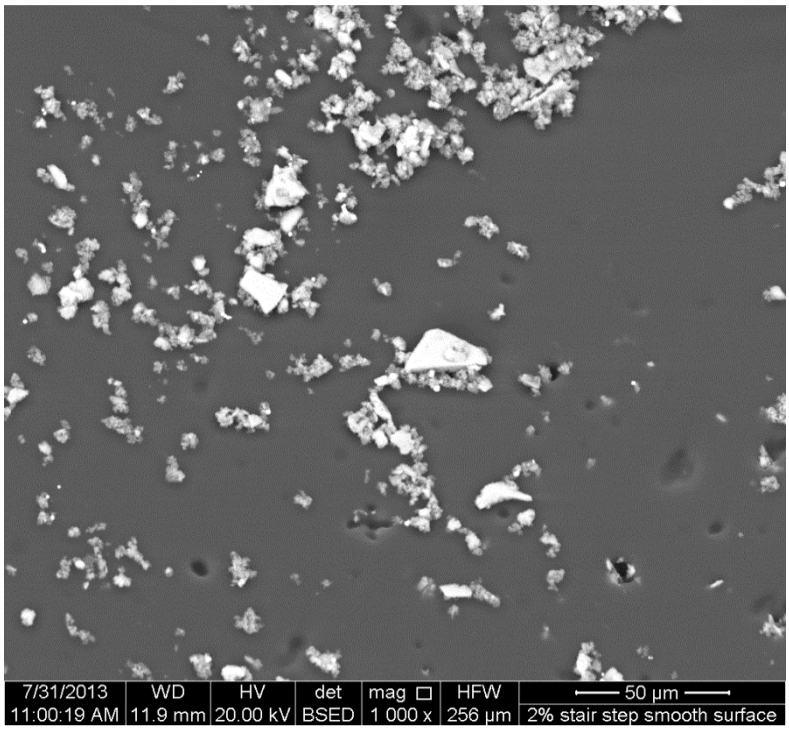

Figure 5-6: SEM image of the top surface of QD-doped photopolymer film

Refractive Index

Despite many attempts to measure the refractive index via UV refractometery, the value could not be assessed due to the aforementioned agglomeration of the QDs within the polymer. For a proper measurement, the solution must be homogenous and thickness of the film should be constant. The presence of agglomerates causes mounds along the film surface and non-homogeneity within the film. Thus, a value for the refractive index of CdSe at 365 nm wavelength was obtained from the literature [3]. To compensate for the uncertainty of the actual refractive index value of the QDs, an exploration of the sensitivity of the Primary Research Hypothesis to a change in the index of refraction term is presented in Section 5.3.

5.2.2 Primary Research Hypothesis Revision 1

The original Primary Research Hypothesis, which centered on the use of Rayleigh scattering as the dominant scattering mechanism, was based on the assumption that the QDs were dispersed in mostly nanoparticle sizes. However, the results from the spectrophotometer measurements and SEM imaging reveal that the QDs are agglomerated and have an average 20 microns in diameter. These large agglomerates suggest that Mie scattering dominates. Thus, the Primary Research Hypothesis must be revised to accommodate Mie scattering instead of Rayleigh scattering. The simplified Mie coefficient of scattering efficiency is shown in Equation 5-1 [7]:

$$Q_{Mie} = 2x^2m^2 = 2\left(\frac{2\pi d}{\lambda_o}\right)^2 \Delta n^2 \qquad (5\text{-}1)$$

The revised version of the Primary Research Hypothesis is stated in Equation 5-2 and 5-3.

Primary Research Hypothesis (Revision 1): The effect of QDs on the depth of penetration term for photopolymers can be predicted by Mie light scattering theory.

$$D_p = \frac{2\rho_{media}}{3d\rho_{particles}Qwt\%}; \quad Q = Q_{Mie} = 2\left(\frac{2\pi d}{\lambda_o}\right)^2 \Delta n^2 \qquad \text{(5-2), (5-1)}$$

The photocuring characterization results are discussed in the next section. The results of these experiments further clarify the role of QD on photopolymerization and help to further revise the Primary Research Hypothesis.

5.2.3 Photocuring Characterization

Films samples were created by exposing varying concentrations of QD-doped PolyJet photopolymer to varying amounts of UV light via the μSLA apparatus (Figure 5-1). The sample thicknesses were measured to produce working curves for each of the QD concentrations. From these working curves, trends in the depth of penetration and critical exposures values for increasing concentrations of QDs can be identified. This section reviews the experimental results related to characterizing the curing behavior of QD-photopolymer mixtures.

Micro Stereolithography

The thicknesses of the stair-step samples created by the μSLA were measured via a digital microscope. As shown in Figure 5-7, the edge thickness of the samples can

be readily measured, resulting in five different thicknesses or “steps.” The glass slide was measured with micrometers and used to calibrate the microscope.

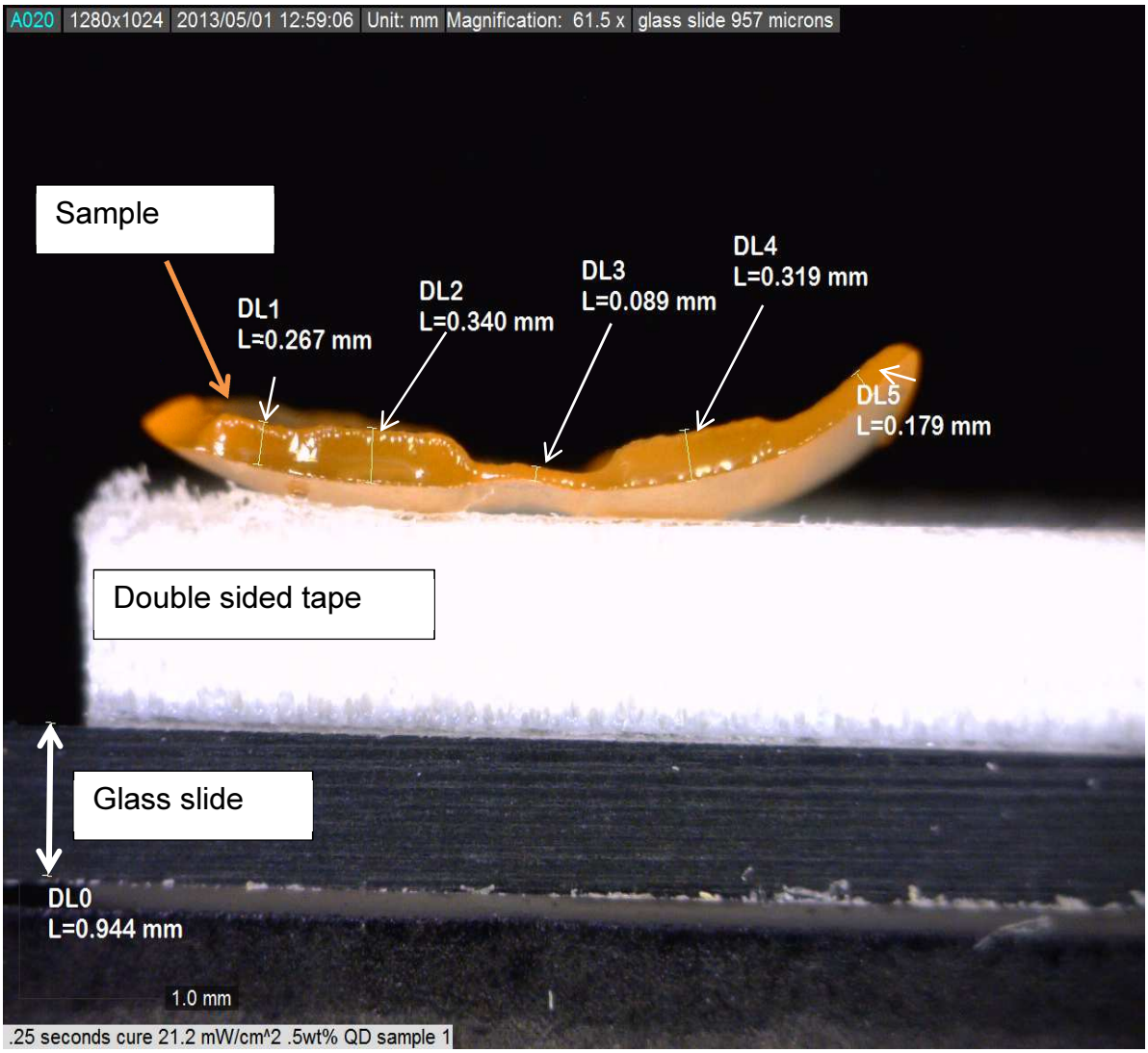

Figure 5-7: Stairstep sample created by uSLA.

Data from the stair step samples was compiled into working curves, which is a plot of the cure depth verses the exposure. Figure 5-8 contains the working curves for each QD concentration: Pure (0 wt%), 0.50 wt%, 1.0 wt%, 2.0 wt%, and 5.0 wt%. For each concentration, five stair step samples were created and analyzed. The working curves were formed by plotting the sample thicknesses verses the exposure dosage,

and each working curve represents the five different thicknesses of the stair step samples. The exposure doses were slightly altered to keep the film thicknesses somewhat consistent since thicker samples tended to curl excessively after a certain point during polymerization and thinner samples were too delicate to handle.

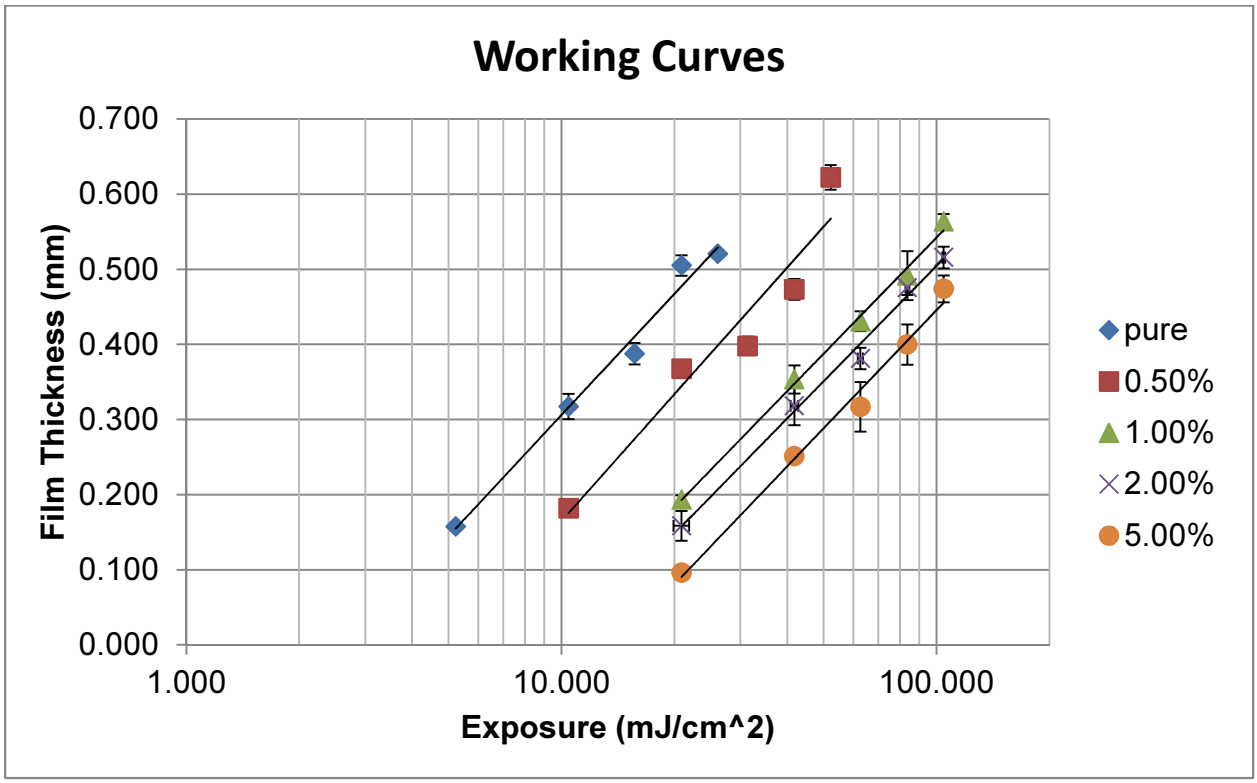

Figure 5-8: Working Curves for Varying Concentrations of QDs in PolyJet Photopolymer

From Figure 5-8 it can be seen that the slopes of the working curves bhave minimal change with increased QD concentration. From the definition of the Jacobs Equation (Equation 4-15), the slope of the working curves in Figure 5-8 constitute the depth of penetration (D_p) of QD-doped polymer at an intensity of 20 mW/cm^2. Figure 5-9 is a plot of these values verses the QD concentration with the range for pure polymer depth of penetration values in grey. It can be seen from the data that no discernable trend in depth of penetration occurs for increasing concentrations of QDs, and the error

bars overlap. For this reason it can be concluded that depth of penetration of the photopolymer is not affected by QD concentration above 1 wt%.

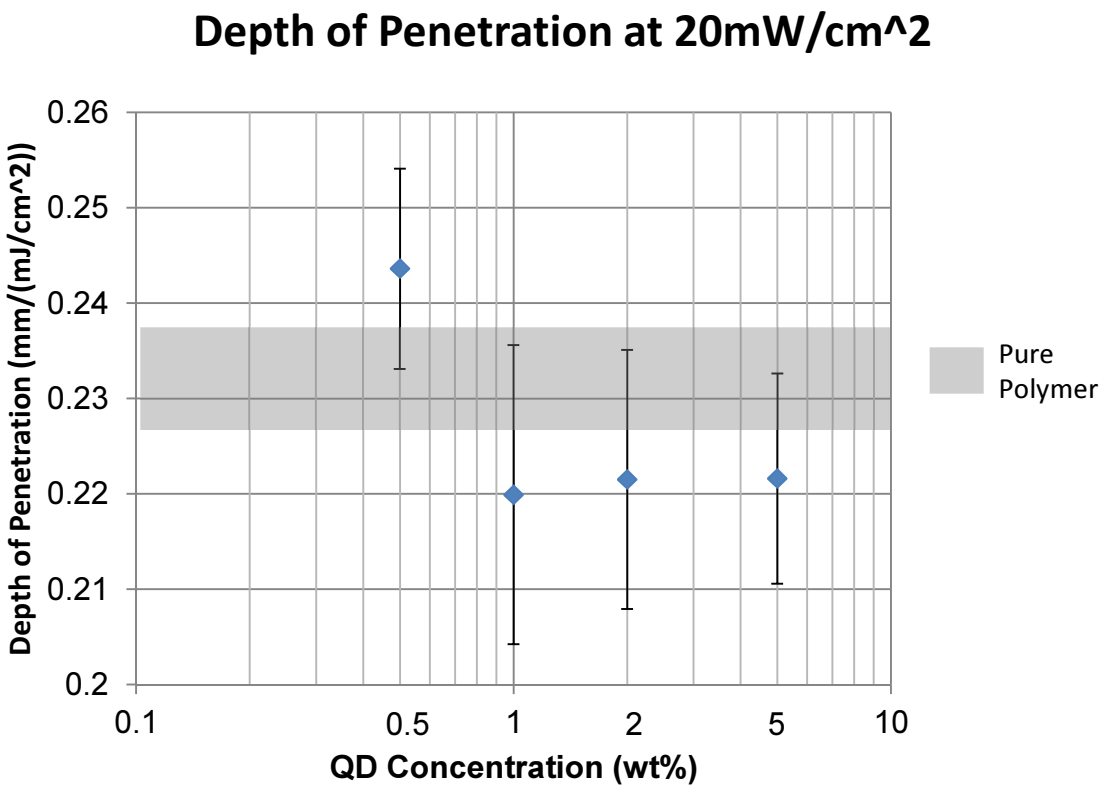

Figure 5-9: Depth of penetration values from working curves in Figure 5-10

In contrast to the trend in the depth of penetration data, a discernable trend can be seen in a plot of critical exposure verses QD concentration. The working curves in Figure 5-9 shift in a positive direction on the y axis, which corresponds to an increased critical exposure of the QD-photopolymer mixture. Plotting the critical exposures from Figure 5-8 verses the QD concentrations results in a linear trend, shown in Figure 5-10.

It is hypothesized that the increase in critical exposure with increased QD loading can be explained by the light scattering of the QDs. The more QDs present in the resins, the more light that gets scattered and becomes unavailable for polymerization.

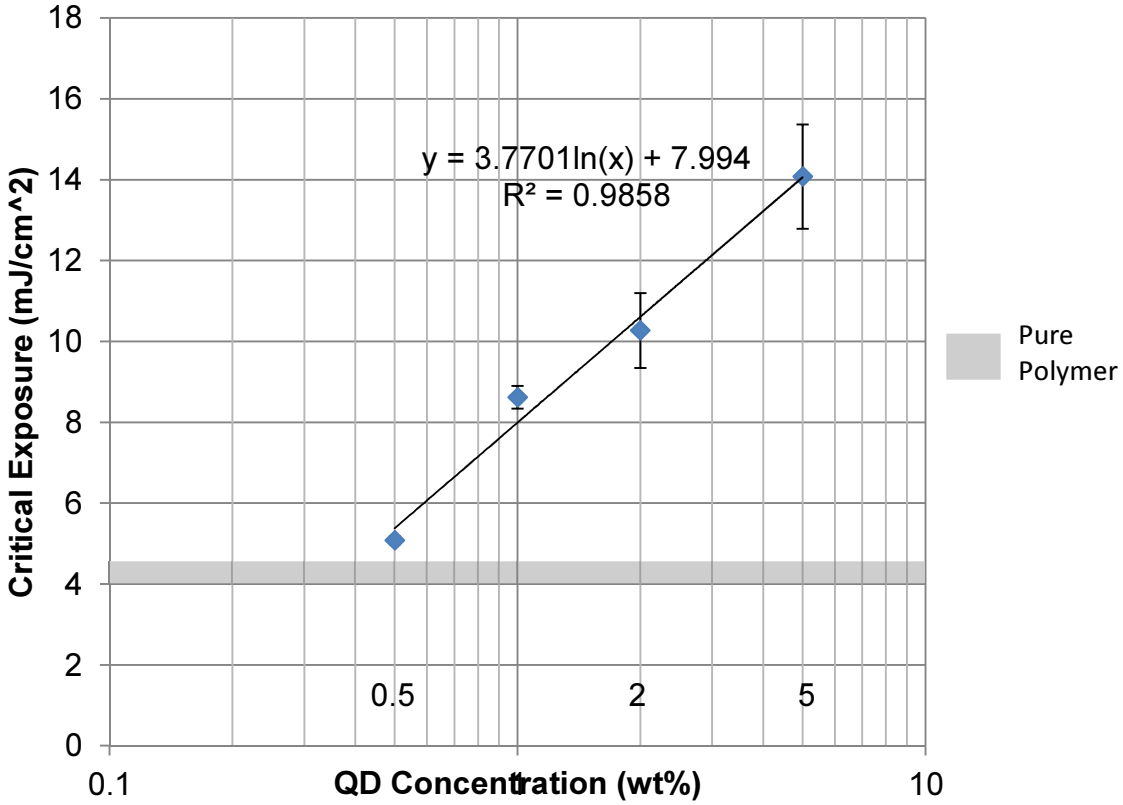

Figure 5-10: Critical Exposure values from working curves in Figure 5-8

Furthermore, it is hypothesized that the constancy of the depth of penetration verses loading and the increasing trend in critical exposure with loading is due to the formulation of the PolyJet photopolymer. Stereolithography resins, such as those used by Griffith's exploration of particle scattering [10], are tailored for a range of values for depth of penetration depending on the exposure intensity. This allows the operator to increase or decrease the depth of penetration with an adjustment of exposure intensity. PolyJet photopolymer, on the other hand, does not need to be responsive to a change in intensity since the layer heights are controlled by the height of the build platform roller and not the exposure intensity. PolyJet photopolymer simply must cure under enough UV exposure and not transmit excess UV light to the layers below. Thus, PolyJet photopolymer most likely contains an amount of photoinhibtors that provide a consistent

depth of penetration. In other words, the depth of penetration of PolyJet photopolymer is likely tailored by its chemistry such that the addition of QDs (at least up to 5 wt%) does not significantly affect the depth of penetration.

Since a trend in depth of penetration with increased QD loading is not seen in the experimental data, the original Primary Research Hypothesis is disproven. Furthermore, the trend in critical exposure with increased QD concentration suggests the need for a new hypothesis based on the prediction of critical exposure. Thus, a new hypothesis is presented in the next section.

5.2.4 Primary Research Hypothesis Revision 2

From the observed trend in critical exposure (Figure 5-10), it is hypothesized that the linear relationship between the critical exposure and the natural logarithm of the QD concentration is a result of the light scattering by the QDs. Since the Primary Research Hypothesis states that depth of penetration should decrease with increased loading, and the results show otherwise, the Primary Research Hypothesis must be revisited. Thus, taking into account the trend in Figure 5-10, a revised Primary Research Hypothesis is formed.

Primary Research Hypothesis (Revision 2): The critical exposure of PolyJet photopolymer increases linearly with an increase in the natural logarithm of weight fraction loading of QDs.

$$E_c \propto \ln(wt) \tag{5-3}$$

An important note about this new revision is that the QD loading should be incorporated as a “weight fraction” and not “weight percent” due to the natural logarithm

producing values less than one for percentages reported in decimal form. Revision 2 of the Primary Research Hypothesis (Equation 5-3) is validated by the critical exposure data in Figure 5-10, which shows linear relationship between critical exposure and the natural logarithm of weight fraction of loading.

To enhance the hypothesis to a point where critical exposure can be predicted, light scattering and photopolymerization theoretical models are enlisted. Specifically, the Mie scattering term Q_{mie} is added to the equation. Mie scattering occurs when the average particle diameter is larger than the incident wavelength of light. Experimental data from spectrophotometry (Section 5.2.1) revealed Mie scattering as the dominant scattering mechanism and SEM imaging revealed that the QDs had agglomerated to an average of 20 microns in diameter. Thus, the Mie scattering term is incorporated into the Primary Research Hypothesis and is repeated here for convenience [7]:

$$Q_{mie} = 2\left(\frac{2\pi d}{\lambda}\right)^2 \Delta n^2 \tag{5-1}$$

Where Q_{mie} is the Mie scattering term, *d* is the average agglomerate diameter, λ is the wavelength of incident light, and Δn is the difference in index of refraction of the QDs and the photopolymer.

In addition to incorporating a Mie scattering term, an empirical term *i* is introduced as an exponent to the particle diameter to wavelength ration for the purpose of given the model flexibility. This empirical exponent was first introduced by Griffith in modelling the effect of ceramic particles on the depth of penetration of SL resins [10]. Adding the empirical term to the Mie scattering coefficients results in Equation 5-4.

$$Q_{mie} = 2\left(\frac{2\pi d}{\lambda}\right)^i \Delta n^2 \tag{5-4}$$

In addition to the Mie scattering term and an empirical exponent, the critical exposure of pure polymer, $E_{c,o}$ is incorporated since the baseline sensitivity to exposure theoretically impacts the critical exposure of the QD-doped polymers. Furthermore, the particle cross section term from the original Primary Research Hypothesis is included and is isolated in Equation 5-5.

$$Particle\ Cross\ Section = \frac{2\rho_{media}}{3d\rho_{particles}Qwt\%} \tag{5-5}$$

Thus, the final form of the Primary Research Hypothesis incorporates the critical exposure of pure polymer, the QD cross section, Mie scattering theory, and empirical term, and the linear relationship between the natural logarithm of weight fraction and critical exposure. The final version of the Primary Research Hypothesis is stated as follows:

Primary Research Hypothesis (Final Version): The critical exposure of PolyJet photopolymer increases linearly with an increase in the natural logarithm of weight percent loading of QDs. The scattering efficiency can be modeling using a Mie scattering term, and empirical constant.

$$E_c = E_{c,0}\frac{4\rho_{media}}{3d\rho_{particles}}\left(\frac{2\pi d}{\lambda_o}\right)^i \Delta n^2 \ln(wt) \tag{5-6}$$

The remainder of this chapter contains analysis of this revised Primary Research Hypothesis with regard to experimental data and sensitivity of the critical exposure to each of the terms in the theoretical model.

5.3 Analysis of Primary Research Hypothesis

In review, modeling the effect of QDs on the photopolymerization of PolyJet photopolymer incorporates elements from the light scattering theory, photopolymerization modeling, and results discussed in this chapter. Current AM photopolymer theory predicts the cure depth of the photopolymer based on the Jacobs Equation (Equation 4-15), which incorporates a depth of penetration term (D_p) and a critical exposure term (E_c). For pure AM photopolymers, these properties are measured by creating a working curve from thin films created by varied UV light exposure (Figure 5-8). With depth of penetration and critical exposure values, the cure depth can then be predicted for a range of exposures. To predict the depth of penetration term based on particle loading, Griffith incorporated light scattering theory to produce an empirical equation (Equation 4-19). In this dissertation, an equation to predict the effects of QD nanoparticles on photopolymerization is developed based on this prior work. A progression of the theoretical models is provided in Table 5-3.

Based on the SEM results found in Section 5.2.1, the average particle size is large in comparison to the wavelength of light, meaning Mie scattering is dominant. Furthermore, analysis in a spectrophotometer confirms that Mie scattering is the dominant scattering mechanism for QD-loaded photopolymers. Finally, in the results it can be seen that there is a linear relationship between the scattering efficiency and the natural logarithm of the weight percent loading of QDs. By applying Griffith's empirical term *i* to the relationship, the critical exposure can be predicted for PolyJet photopolymers with varied loadings of QDs (Equation 5-6).

Table 5-3: Progression of Current Theory Toward Final Hypothesis

1. General Form Scattering Efficiency	Equation No.
$\gamma = \int_0^\infty \pi r^2 Q_{ext}(r) N(r) dr$	(4-3)
2. Take Average Radius	
$\gamma = \pi r^2 Q_{ext} n$	
3. Convert to Particle Density to Weight (wt)	
$\gamma = \frac{3 d \rho_{particls} wt\% \, Q_{ext}}{4 \rho_{media}}$	(4-6)
4. Mie Scattering Dominates (Chapter 5)	
$Q_{ext} = Q_{sca} + \cancel{Q_{abs}}$	(4-7)
5. Mie Scattering Coefficient, Q, from *x* and *Δn* boundary conditions	(5-1)
$Q_{mie} = 2\left(\frac{2\pi d}{\lambda}\right)^2 \Delta n^2$	
7. Griffith Model with Empirical Exponent, *i*	
$C_d = \frac{2d}{3Q\emptyset} \ln\left(\frac{E_o}{E_c}\right), \qquad Q = \left(\frac{2\pi d}{\lambda_o}\right)^i \Delta n^2$	(4-18) (4-19)
8. Final Version of the Primary Research Hypothesis	
$E_c = E_{c,0}\gamma, \qquad \gamma = \frac{3}{2d\rho} Q, \quad Q = 2\left(\frac{2\pi d}{\lambda_o}\right)^i \Delta n^2$	(5-7, 5-8, 5-9)
$Ec = E_{c,0} \frac{4\rho_{media}}{3 d \rho_{particles}} \left(\frac{2\pi d}{\lambda_o}\right)^i \Delta n^2 \ln(wt)$	(5-6)

Primary Research Hypothesis (Final Version): The critical exposure of PolyJet photopolymer increases linearly with an increase in the natural logarithm of weight percent loading of QDs. The scattering efficiency can be modeling using a Mie scattering term, and empirical constant.

$$E_c = E_{c,0}\gamma \ln(wt\%)\,, \qquad \gamma = \frac{4\rho_{media}}{3d\rho_{particles}}Q, \qquad Q = \; 2\left(\frac{2\pi d}{\lambda_o}\right)^i \Delta n^2 \qquad \text{(5-7, 5-8, 5-9)}$$

$$E_c \propto \; E_{c,0}\frac{4\rho_{media}}{3d\rho_{particles}}\left(\frac{2\pi d}{\lambda_o}\right)^i \Delta n^2 \ln(wt) \qquad \text{(5-6)}$$

Where E_c is the critical exposure, E_c is the critical exposure for pure polymer, d is the average particle diameter, λ_o is the wavelength of incident light, Δn is the difference in refractive indices of the QDs and the media, *i* is an empirical term, and wt is the weight fraction of QDs. Weight fraction is used instead of volume percent since the experimental quantities of the QDs were measured in weight percents (e.g., 1 wt%, 2 wt%, 5 wt%, etc.). A summary of the evolution of the Primary Research Hypothesis is provided in Table 5-4.

The proposed model integrates light scattering by particles theory (Mie theory for large particles) and current particle-doped AM photopolymer theory (Griffith's model) and constitutes the first attempt to predict critical exposure of a photopolymer based on particle loading.

Table 5-4: Evolution of the Primary Research Hypothesis

Primary Research Hypotheses		Background
Original (4-20, 4-21) (Rayleigh Scattering)	$D_p = \frac{2\rho_{media}}{3d\rho_{particles}Qwt\%}$; $Q = Q_{rayliegh} = \left(\frac{2\pi d}{\lambda_o}\right)^2 \Delta n^2$	This model incorporates a Rayleigh scattering term to predict an increase in Depth of Penetration (D_p) with an increase in particle loading.
Revision 1 (4-20, 5-9) (Mie scattering)	$D_p = \frac{2\rho_{media}}{3d\rho_{particles}Qwt\%}$; $Q = Q_{Mie} = 2\left(\frac{2\pi d}{\lambda_o}\right)^2 \Delta n^2$	Due to SEM and Spectrophotometry data, a Mie scattering term is used to predict D_p.
Revision 2 (5-3) (Predicts Critical Exposure)	$E_c \propto \ln(wt\%)$	Cure depth film data reveal no trend in D_p and a linear relationship between E_c and the natural logarithm of QD loading.
Final Version (5-6)	$E_c \propto E_{c,0}\frac{4\rho_{media}}{3d\rho_{particles}}\left(\frac{2\pi d}{\lambda_o}\right)^i \Delta n^2 \ln(wt)$	Mie scattering, Griffith's empirical term *i*, and natural log of weight fraction, not weight percent (wt not wt%)

Thus, the scientific contribution of this work can be stated as follows:

Scientific Contribution:

Answering the Primary Research Question in the form of mathematical characterization will contribute new knowledge to the area of QD-loaded photopolymers. Developing a mathematical model to predict the effects of QDs on photopolymerization will serve applications involving sensing, displays, and composites in addition to creating PUFs via PolyJet.

5.3.1 Comparison of Model and Experiment

The data in Figure 5-11 constitutes the premise of the final version of the Primary Research Hypothesis. The equations are repeated here for convenience:

$$E_c = E_{c,0}\gamma \ln(wt\%), \qquad \gamma = \frac{4\rho_{media}}{3d\rho_{particles}}Q, \qquad Q = 2\left(\frac{2\pi d}{\lambda_o}\right)^i \Delta n^2 \qquad \text{(5-7, 5-8, 5-9)}$$

$$E_c = E_{c,0}\frac{4\rho_{media}}{3d\rho_{particles}}\left(\frac{2\pi d}{\lambda_o}\right)^i \Delta n^2 \ln(wt) \qquad \text{(5-6)}$$

The values of the variables used in Equation 5-6 are listed in Table 5-5. Since the value for the index of refraction of the QDs was undetermined, a value for *Δn* was approximated based on values found in the literature. As previously stated, the RI of

Table 5-5: Values used in Primary Research Hypothesis Validation

Critical Exposure of Pure Polymer	2.69 mW/cm^2 (Section 5.2.3)
Average Particle Diameter, *d*	20 micron (20,000 nm)
Density of Particles, $\rho_{particles}$	5.82 g/cm^2 [2]
Density of Polymer, ρ_{media}	1.08 g/cm^2 (measured)
Wavelength of Incident Light, λ_o	365 nm (Objet Lamp)
Difference in Refractive Index of polymer (approximated as one) and QDs (2.65, [3]), *Δn*	1.65 [3]
$E_c = E_{c,0}\frac{4\rho_{media}}{3d\rho_{particles}}\left(\frac{2\pi d}{\lambda_o}\right)^i \Delta n^2 \ln(wt)$ (5-6) $= 2.69\frac{4(1.08\frac{g}{cm^3})}{3(20000\ nm)(5.86\frac{g}{cm^3})}\left(\frac{2\pi(20000\ nm)}{365\ nm}\right)^{1.821}(1.65)^2\ln(wt) = \mathbf{3.77}\ln(wt)$	

CdSe at 365 nm wavelength was found in the literature to be 2.65 [3]. Issues with spincoating and curing of PolyJet resin prevented the measurement of the RI of PolyJet resin, however, an alternative *Δn* states that the fluid RI can be approximated to one in most cases [7]. Thus, *Δn* = 1.65. The rest of the values are from literature or experimental data in this work.

The empirical term *i* was solved for *i = 1.821.* As shown at the bottom of Table 5-5, inputting values for each term in Equation 5-6 results in a coefficient of 3.77 for the ln(wt) term. This calculation of $E_c = \mathbf{3.77}\ln(wt)$ corresponds to the experimental findings in Figure 5-10, which has a logarithmic curve fit function of y = 3.7701ln(x) + 7.994 where y is critical exposure (E_c) and x is weight fraction (*wt*). Of course, the tailoring of the empirical term *i* allows this calculation in Table 5-5 to be changed to match these experimental findings. The sensitivity of critical exposure to the various terms in the Primary Research Hypothesis is discussed in Section 5.2.3.

5.3.2 Sensitivity Discussion

In addition to showing that the Primary Research Hypothesis being validated by the experimental data, the sensitivity of the Critical Exposure to each term in Primary Research Hypothesis is presented in Table 5-6. The sensitivity is calculated by taking the partial derivative of Equation 5-6 with respect to each variable in the equation and setting the rest of the variables to their respective nominal values. The rest of the equation is treated like constants, and the value for the partial derivative is calculated. A higher number yielded in this calculation means that the critical exposure is more sensitive to a change in this variable while a lower number corresponds to a low sensitivity.

The level of sensitivity simply shows which variables are most significant in the final calculation. For the variables in Equation 5-6 that can be derived out of the theoretical model, a value for sensitivity is calculated and reported in Table 5-6. For the other variables whose partial derivatives do not eliminate them from the equation, a plot of a reasonable range of their values verses the resulting critical exposure value is provided in Figures 5-11 through 5-15.

From the values calculated in Table 5-6, it can be seen that the *Δn* term has the highest sensitivity (3.17). To compare the sensitivity of *Δn* with terms not calculated in Table 5-6 (the ones which do not derive out of Equation 5-6), graphs of each term are presented for a range reasonable values verses the resulting critical exposure values.

Table 5-6: Sensitivity values for terms in Primary Research Hypothesis

Critical Exposure of Pure Polymer	$\frac{\partial E_c}{\partial E_{c,0}} = 0.97$
Scattering Term, Q	$\frac{\partial E_c}{\partial d} = 2.3 * 10\text{^} - 5$
Density of Polymer, ρ_{media}	$\frac{\partial E_c}{\partial \rho_{media}} = 2.422$
Difference in Refractive Index of polymer and QDs, *Δn*	$\frac{\partial E_c}{\partial \Delta n} = 3.17 \ (Figure\ 5-14)$
Average Particle Diameter, *d*	$\frac{\partial E_c}{\partial d} = Figure\ 5-13$
Density of Particles, $\rho_{particles}$	$\frac{\partial E_c}{\partial \rho_{particles}} = Figure\ 5-16$
Wavelength of Incident Light, λ_o	$\frac{\partial E_c}{\partial \lambda_o} = Figure\ 5-15$
Emperical Term, *i*	$\frac{\partial E_c}{\partial i} = Figure\ 5-12$

From Table 5-6 and Figures 5-11 through 5-15, it can be seen that the empirical term *i* has the largest impact on the value of critical exposure, with the next greatest being the particle diameter. Thus, incorporating the empirical term (first proposed by Griffith, [10]) is an effective solution to fitting the Primary Research Hypothesis model to the curing properties of a particle loaded photopolymer.

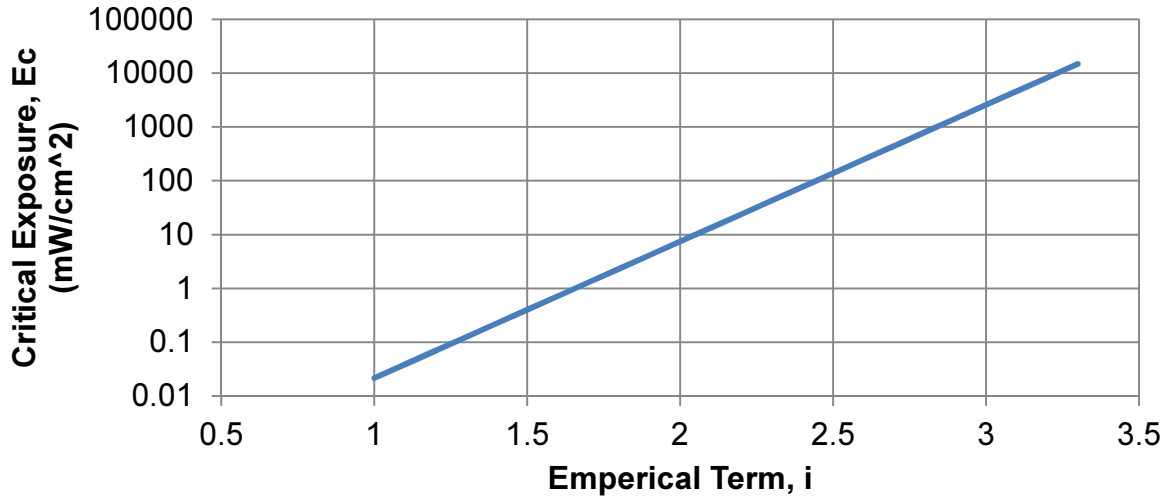

Figure 5-11: Sensitivity of Critical Exposure Emperical Term, *i*

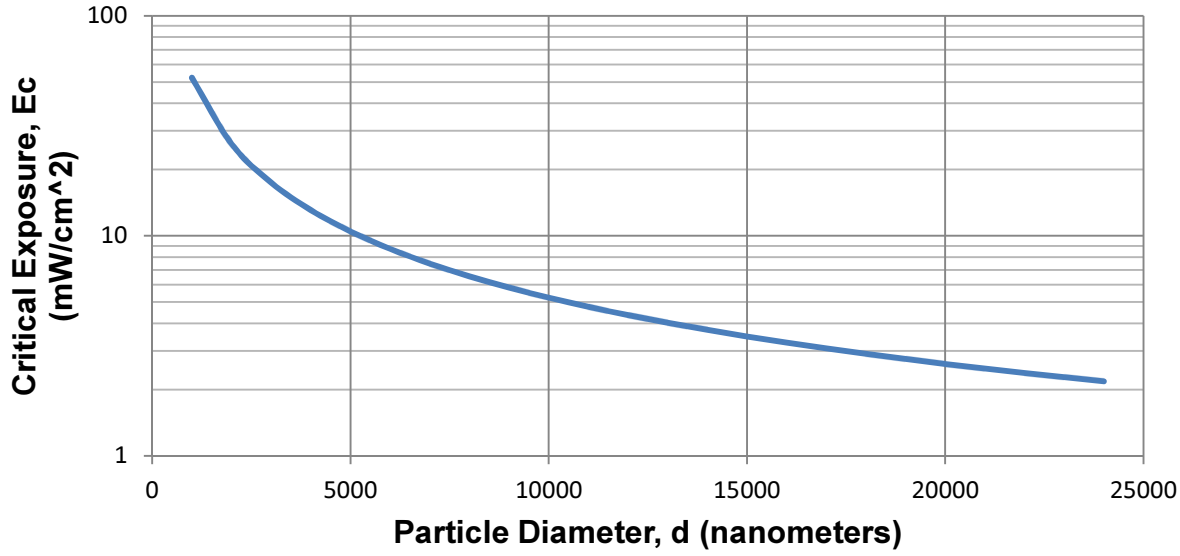

Figure 5-12: Sensitivity of Critical Exposure particle diameter, d

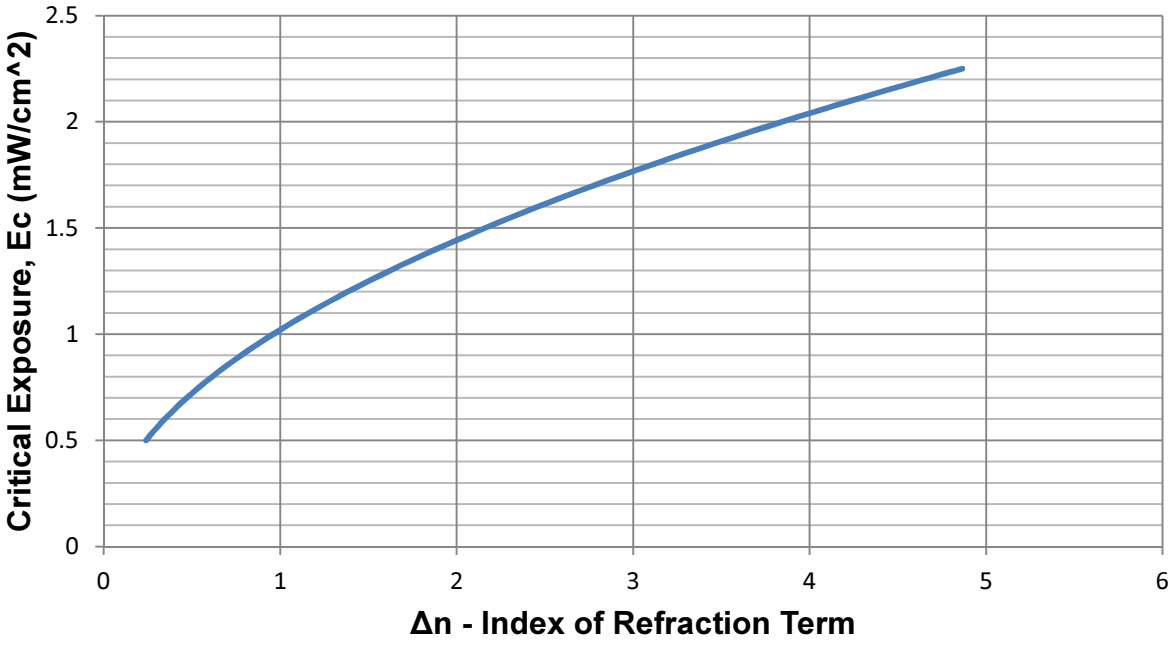

Figure 5-13: Sensitivity of Critical Exposure to Index of refraction term, *Δn*

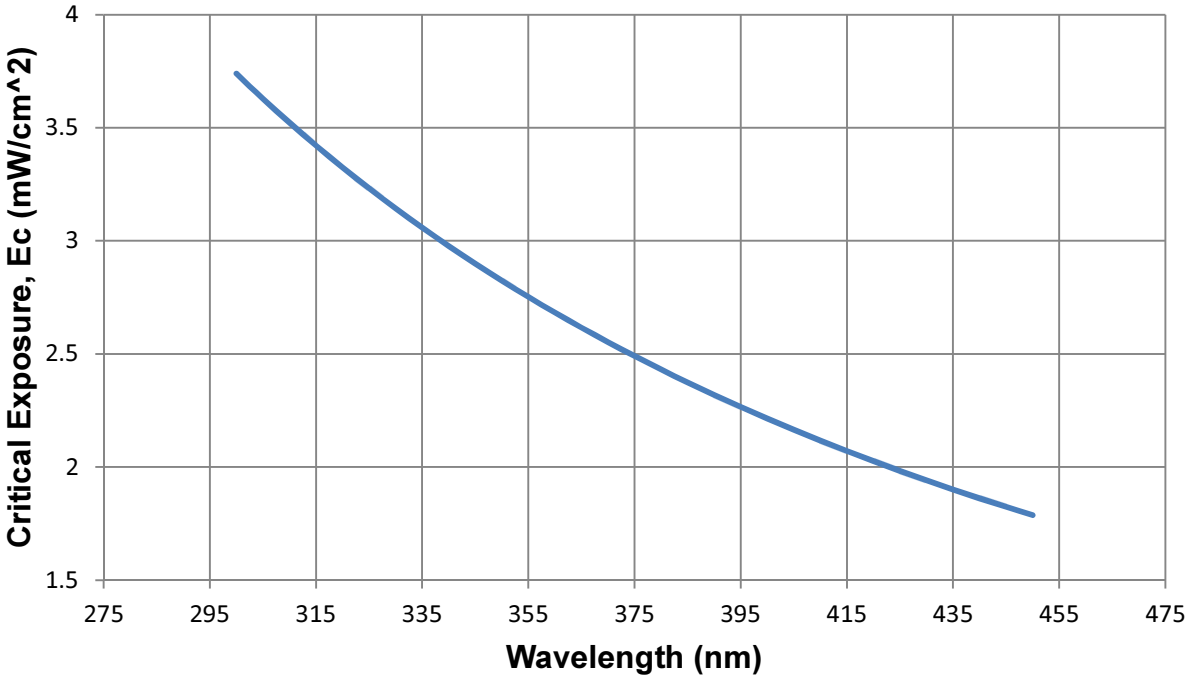

Figure 5-14: Sensitivity of Critical Exposure to changes in wavelength, λ_o

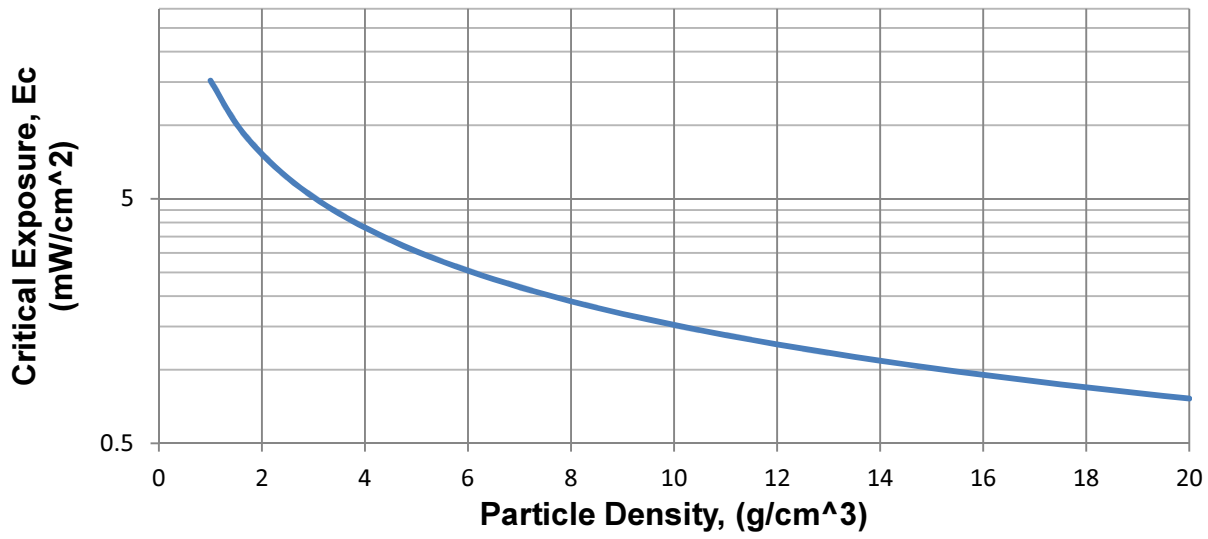

Figure 5-15: Sensitivity of Critical Exposure particle density, $\rho_{particle}$

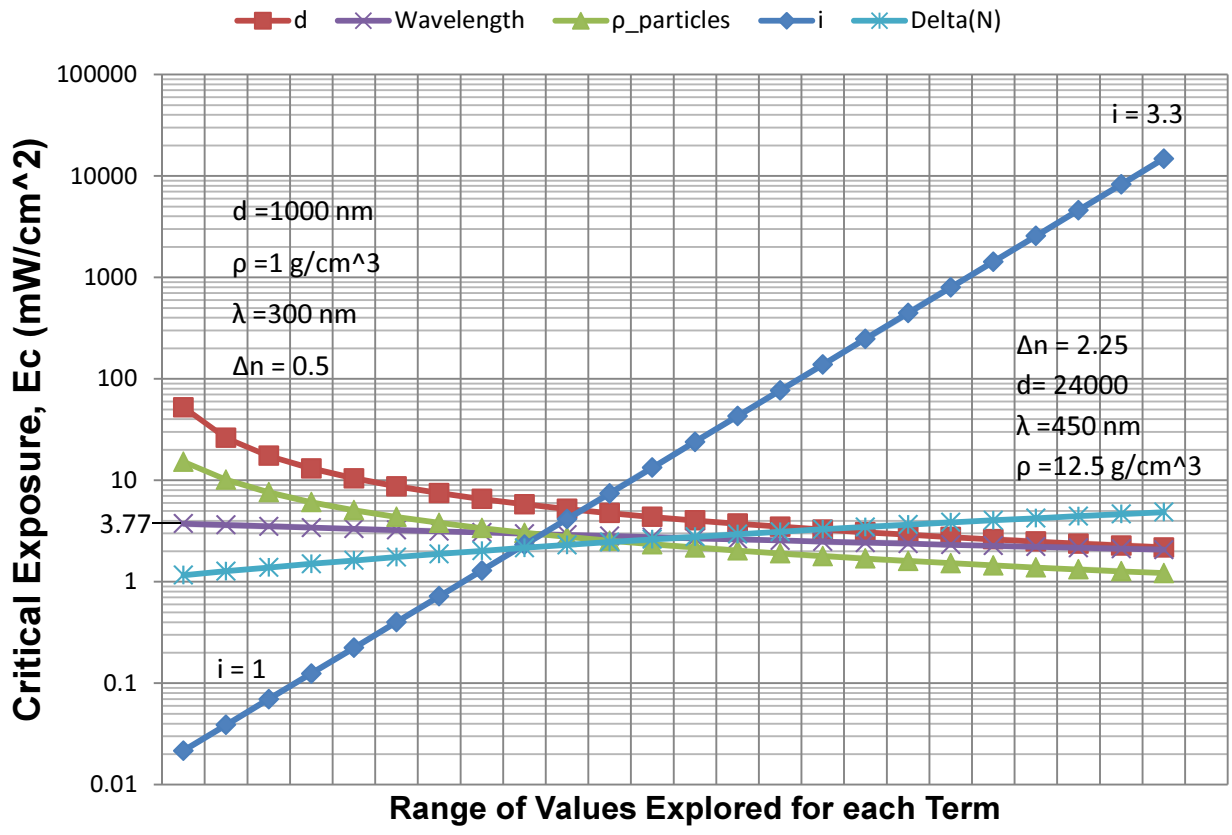

Figure 5-16: A range of values explored for Terms in Equation 5-6 to compare sensitivity

Overall, the sensitivity of the Primary Research Hypothesis to each of the equation variables can be discerned by the sensitivity values presented in Table 5-6 and Figure 5-16.

5.4 Roadmap

Thus far in the dissertation, the experiments to determine the feasibility of utilizing QDs in the PolyJet to create PUFs have been described and their results presented. Visibility and jetting results show that QDs in concentrations sufficient to produce PUFs are both visible and ink-jettable, meaning the overall project goal is feasible. The major contribution of this work is the modeling and characterization of the photopolymerization of QD-doped PolyJet photopolymer. The literature review for photopolymerization modeling was presented in Chapter 4, and the experimental methods and results toward characterizing photopolymerization with QDs are presented in Chapter 5. Chapter 6 deals with experimental results that did not contribute to the validation of the Primary Research Hypothesis but revealed evidence of the role of intensity on critical exposure. Chapter 7 will present the major conclusions of this work, limitations, and suggestions for future work. A roadmap of the dissertation is provided in Table 5-7.

Table 5-7: Roadmap

	Research Phase	Chapter	Goals
Introduction	Problem Identification Solution Proposal	**Chapter 1** Introduction, Motivation, and Project Outline	**Describe the problem** **Describe a solution** to the problem and the process for implementing that solution **Identify the qualifying and research questions** related to the proposed solution
Background & Feasibility Analysis	Information Gathering Preliminary Experimentation	**Chapter 2** Visibility of Quantum Dots within PolyJet Media (QQ1) **Chapter 3** Inkjetting with Quantum Dots in PolyJet Media (QQ2)	**Synthesize literature** related to the Qualifying Questions **Perform Experiments** to address Qualifying Questions 1 and 2 **Draw Conclusions** to address Qualifying Questions
Research Methods	Hypothesis Formulation Experimental Methods Hypothesis Validation	**Chapter 4** Literature Review of Photopolymer-ization Theory, Proposed Theoretical Model **Chapter 5** Experimental Techniques, Results and Critique and Modification of Theoretical Model **Chapter 6** Effects of Intensity on Critical Exposure	**Synthesize literature** related to the Primary Research Question **Identify gaps** in existing literature that prevent answering the research question **Form hypotheses** based on existing literature **Establish Methods** for validating the hypothesis **Perform Experimentation** to validate hypothesis
Summary	Conclusions Outlining Future Work	**Chapter 7** Project Summary and Future Work	**Draw Conclusions** based on experiment results **Identify significant contributions** **Summarize accomplishments** related to answering each of the research questions **Propose future work**

CHAPTER 6 THE EFFECTS OF INTENSITY ON CRITICAL EXPOSURE

As experiments were conducted to validate the Primary Research Hypothesis, it was discovered that the intensity of the light source altered the results of the experiment. Specifically, the critical exposure of the photopolymer increased with an increase in intensity. This is in contrast to traditional beliefs that critical exposure is a characteristic of the photopolymer and is independent of intensity [1-2]. Previous work in this area revealed some relationship between the critical exposure of the photopolymer and the intensity of the incident light; however, the specific relationship was not described [3]. Further investigation into this phenomena lead to a second research question:

Secondary Research Question:

How does intensity affect the critical exposure of photopolymers?

This chapter contains the experimental methods and results completed toward answering the Secondary Research Question.

6.1 Methods

To explore the effects of intensity on critical exposure, two different curing strategies were utilized. First, a lamp and shutter mechanism was used to cure QD-doped polymer samples in different thicknesses to develop a working curve for the polymer at the UV lamp intensity, which is 1.6 mW/cm^2. From the working curve, the critical exposure was extrapolated (Section 5.1.2) and compared with the critical exposure of the photopolymer under standard PolyJet lamp intensity (20 mW/cm^2). Furthermore, photorheometry was performed for various QD loadings under two

different intensities. The specifics of the methods and results toward the investigation of the Secondary Research Question are presented in this section.

6.1.1 Lamp and Shutter Apparatus

A simple way to create film samples and measure their thickness is to expose a well of polymer to a known amount of UV light, remove the cured polymer film from the top of the well, and measure the thickness with micrometers. Typically photopolymer film samples are created with a UV conveyor system, which uses a conveyor to pass the sample under the lamp for a controlled amount of time. The speed of the conveyor controls the light dosage received by the sample. Unfortunately, the intensity of this type of lamp system is significantly higher than the intensity needed to cure PolyJet photopolymer, which is on the order of 20-50 mJ/cm^2. Therefore, a new method to generate controlled exposure to the photopolymer was devised in the form of a lamp and shutter mechanism.

The UV lamp and shutter setup consists of a lamp, shutter mechanism, and fixtures. An 8 Watt UV lamp with a peak wavelength of 365nm is used, and a locator bracket is attached to the lamp at its center to ensure that each sample is placed in the same location under the lamp as every other sample. A small petri dish (30mm in diameter) is filled with 2 mL of polymer sample and set within the Sample Shroud. The Sample Shroud ensures that the pool of polymer is only exposed to UV light from the top and not from the sides. The “shutter” is a slab of black plastic that separates the polymer sample from the UV lamp above. The shutter is attached to a servo motor, which is controlled by a microcontroller. Once the sample is ready for exposure, the microcontroller receives input from the user and sends a signal to the servo motor to

rotate around 180 degrees. This moves the shutter from blocking the UV light above the sample and allows the sample to receive UV dosage. At the specified time, the microcontroller then returns the servo to the initial position, which brings the shutter back to the position in which the UV light is blocked from the sample again. After the film is cured, it is removed and patted dry with Chem wipes and then measured in the center with micrometers. The setup used in this work is depicted in Figure 6-1.

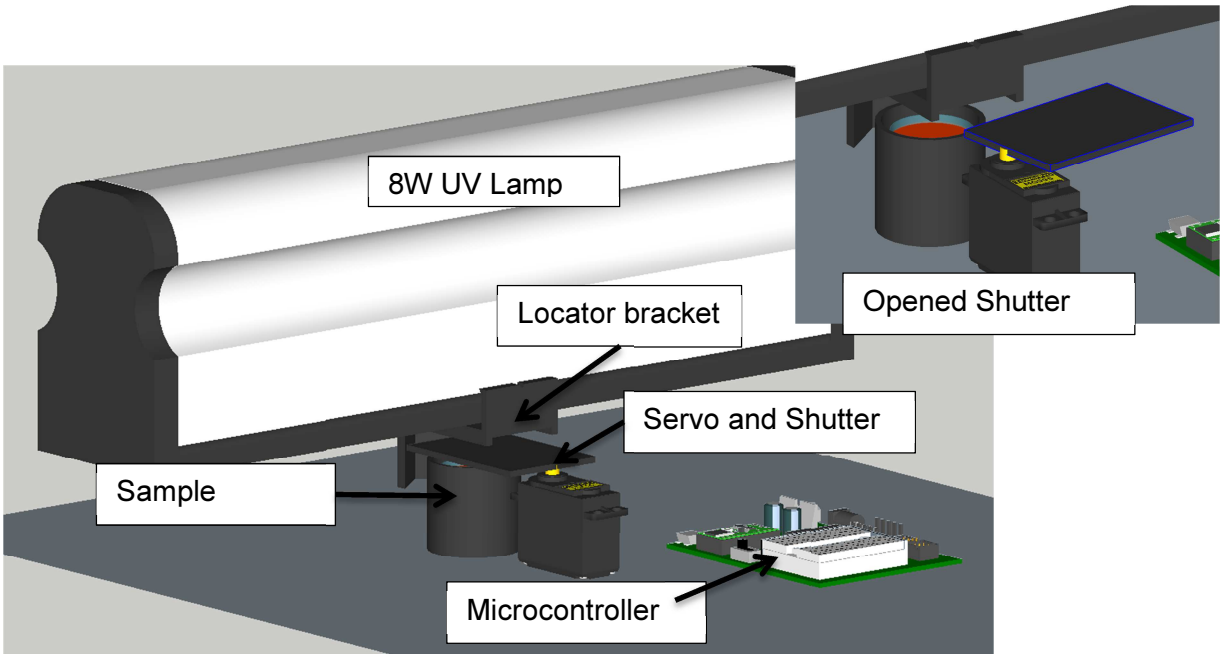

Figure 6-1: UV lamp and shutter setup used to create thin films

Once the films are created, they are removed from the petri dish, rinsed in isopropyl alcohol, dried overnight, and measured with micrometers. The cost-effectiveness and simplicity with regard to equipment setup is the main advantage of this system. Preliminary results were obtained using this method to determine the appropriate dosage and concentrations to produce films that were measurably different in thickness.

6.1.2 Photorheometery

A Discovery Hybrid Rheometer (TA Instruments; New Castle, Delaware) with a photo accessory was used to measure the critical exposure of the VeroClear photopolymer. The combination of the photo accessory and the rheometer is called a photorheometer. A photorheometer utilizes flow-resistance (viscosity) measurement to identify the amount of cure of a photopolymer. The sample is placed between the upper and lower plate of the machine, the upper being made of steel or aluminum and the lower being made of acrylic or quartz (Figure 6-2). An oscillation is induced on the upper plate, and equilibrium is achieved for a certain period of time. Once the equilibrium time has passed, the UV light source is activated and shines through the bottom plate onto the sample. A diagram of a photorheometer is shown in Figure 6-2.

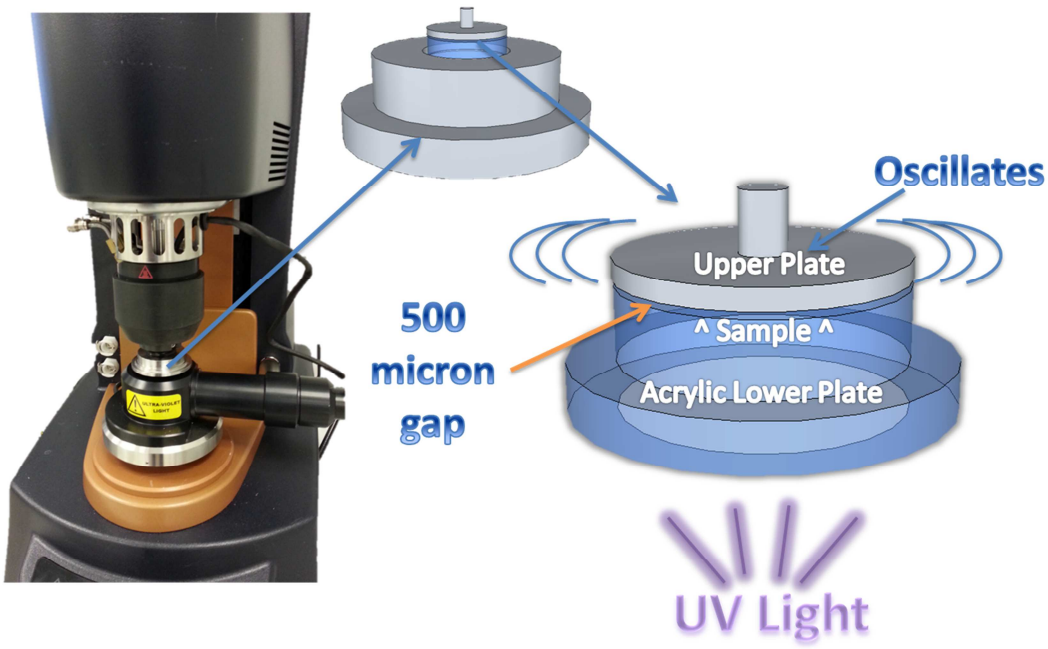

Figure 6-2: Photorheometer Components

The instrument then measures characteristics of the polymer, including storage modulus (G') and loss modulus (G"). The critical exposure can be identified by identifying the time between the light activation and the first sign of storage modulus increase and then multiplying that time by the intensity of the light source. The advantage of this method is that it is a direct method of measuring critical exposure.

For rheometry in fluids that convert to solids, the resistance to flow is measured as the storage modulus of the material. The data shown in Figure 6-3 below is a representative example of data obtained from a photorheological experiment in which the amount of exposure required to initiate curing (i.e., critical exposure) is identified. The sample was given a small, sinusoidal oscillation via the upper plate for the first 30 seconds of the experiment to remove static effects. At the 30 second mark, the UV light source was activated and the sample was illuminated. The oscillation from the upper plate continued while the resistance to the oscillation was measured. Two intensities were targeted: 20 mW/cm^2 and 0.1 mW/cm^2. These intensities were chose to provide enough contrast to illustrate the effects of intensity on the critical exposure of the photopolymer.

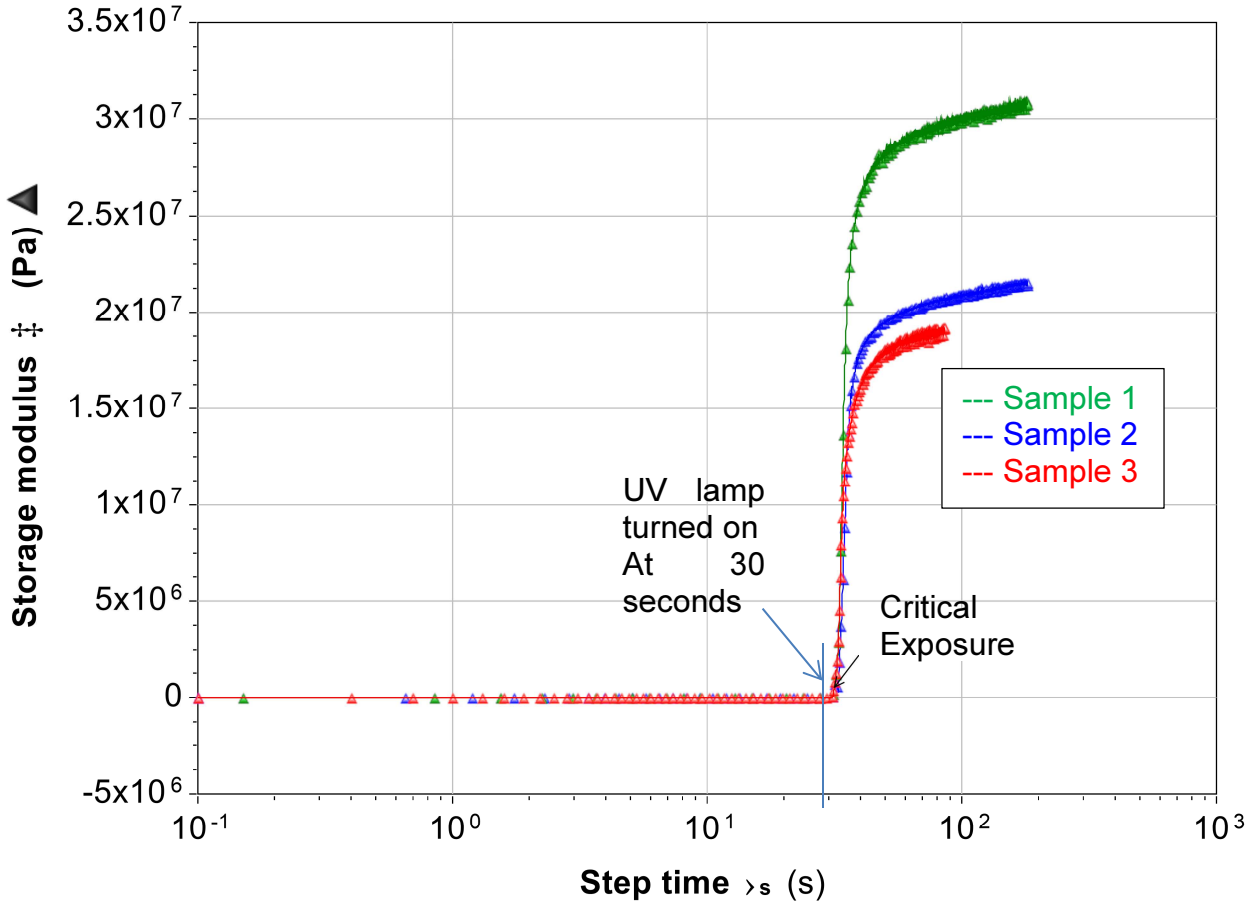

Figure 6-3: Storage Modulus of pure VeroClear photopolymer (three samples) versus step time

6.2 Experimental Results

6.2.1 Lamp and Shutter Apparatus

Figures 6-4 and 6-5 contain plots of the film thickness verses the QD concentration for the lamp and shutter assembly and the μSLA machine, respectively. Eight different QD concentrations (from pure polymer to 0.5 wt% QDs) were evaluated on both experimental setups. The intensity of the lamp and shutter assembly is

approximately 1.6 mW/cm^2, while the intensity of the μSLA machine is approximately 20 mW/cm^2 (same as the PolyJet curing lamp).

Comparing the two plots, it can be seen that the data is much less sporadic for the lamp and shutter assembly than for the μSLA. This is most likely due to the ability to measure the lamp and shutter film samples with micrometers rather than with a microscope as was used on the μSLA samples (which was required due to the small sample size).

Data from the shutter and lamp assembly demonstrated the effects of intensity on cure depth. It can be seen that films of approximately the same thicknesses required less exposure on the lamp and shutter assembly than that of the μSLA machine. For example, the 10 mJ/cm^2 sample (state cure depth here) in Figure 6-4 shows a greater cure depth than the 10.6 mJ/cm^2 sample (state cure depth here), as seen in Figure 6-5. This is due to the difference in intensities between the two setups, as previously mentioned. The effect of intensity on critical exposure will be discussed in further detail in the next section.

6.2.2 Photorheometer

For rheometry in fluids that convert to solids, the resistance to flow is measured as the storage modulus of the material. The critical exposure is determined by identifying the first peak in the storage modulus, which indicates the photopolymer has begun crosslinking. A major drawback of the photorheometer in identifying critical exposure is that the crosslinking begins very quickly - usually within the first few seconds of UV exposure.

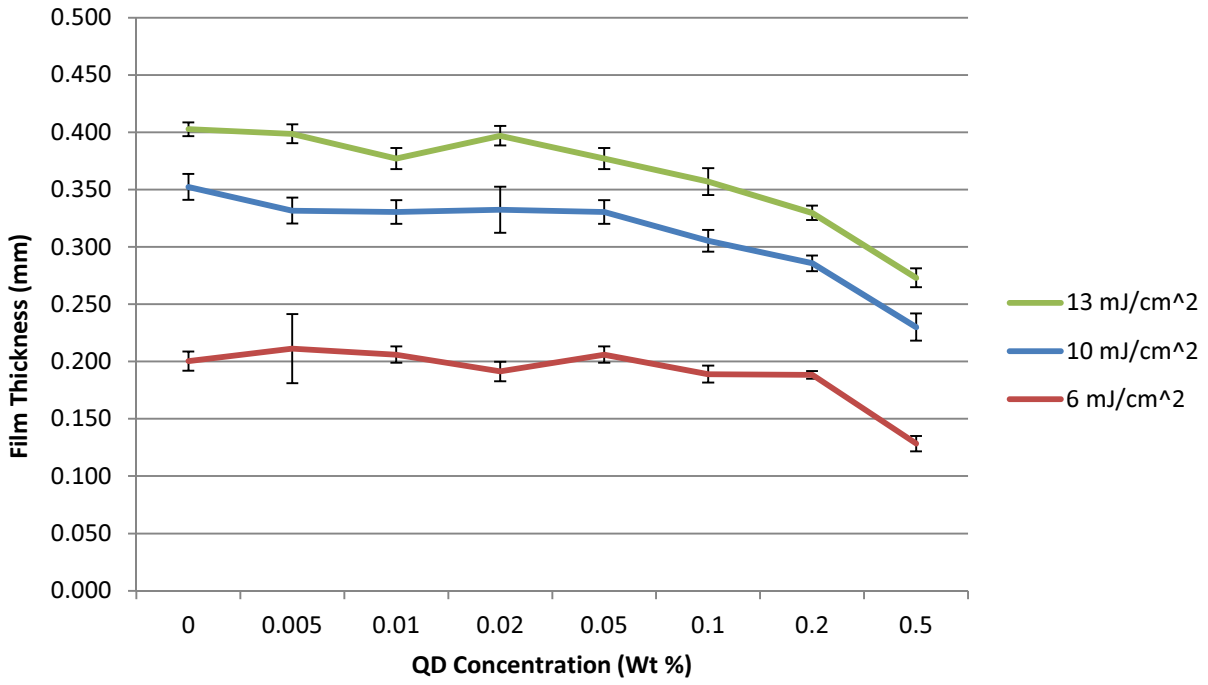

Figure 6-4: Film thicknesses vs. concentration for shutter and lamp apparatus, 1.6 mW/cm^2 intensity

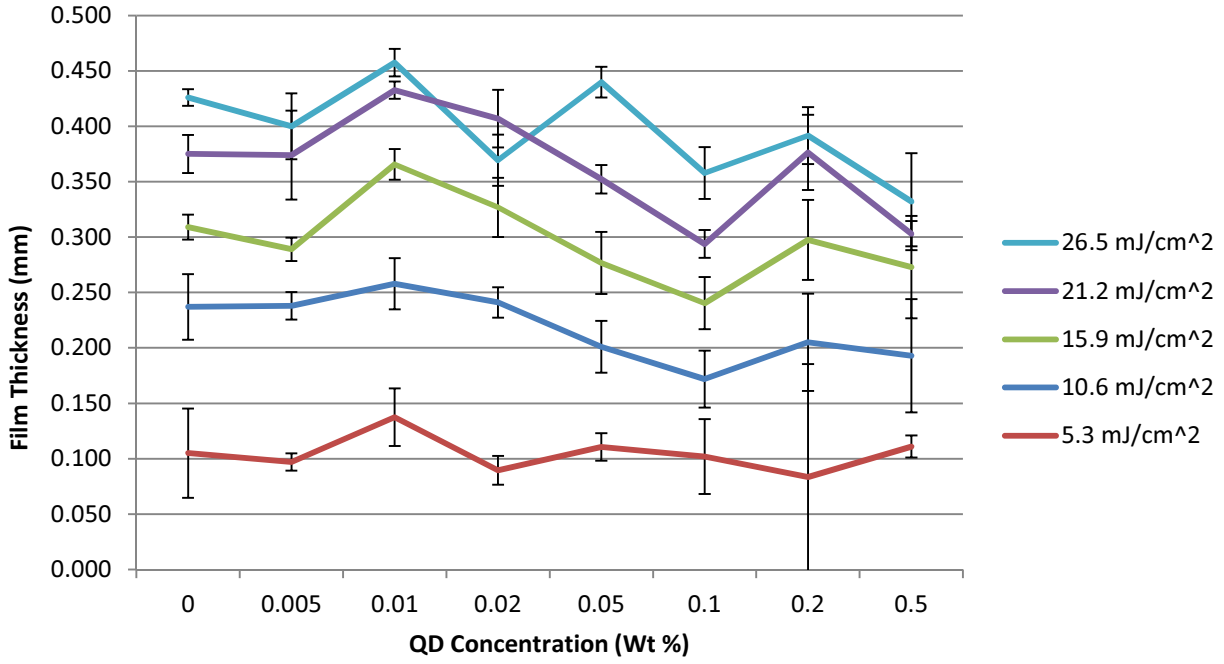

Figure 6-5: Film thicknesses vs. concentration for µSLA, 20 mW/cm^2 intensity

This quick reaction, in combination with the resolution of the data logging software, makes it difficult to identify the critical exposure with an accuracy of more than a 1-2 mJ/cm^2 at an intensity of 20 mW/cm^2. Furthermore, for higher concentrations (Figures 6-6 and 6-7), the storage modulus increases very gradually with exposure and lacks a distinct peak, which makes identifying the critical exposure difficult for high QD concentrations.

Measurements were taken via photorheometry on photopolymer-QD mixtures in multiple concentrations. It was found that the critical exposure increased with increasing concentration of QDs (in accordance with data presented in Figure 5-11). Samples with concentrations of 1, 2, and 5 weight percent were exposed to UV light at intensities of 20 mW/cm^2 and 0.1 mW/cm^2, and the dose required to initiate photocuring was noted. As shown in Figures 6-6 and 6-7, samples with the same QD concentrations have lower critical exposures with less intensity than with higher intensities. In other words, the less intense the exposure power, the less total energy is require to initiate the cure.

To our knowledge, the work in Section 6.2.2 constitutes the first use of a Photorheometer to characterize AM photopolymers. It is noted that critical exposure data from the photorheometer does not match the μSLA data due to the high and low pass filters used on the light source of the photorheometer and not on the μSLA. The high pass filters block wavelengths of light greater than around 450nm, while the low pass filters block light wavelengths below 350 nm.

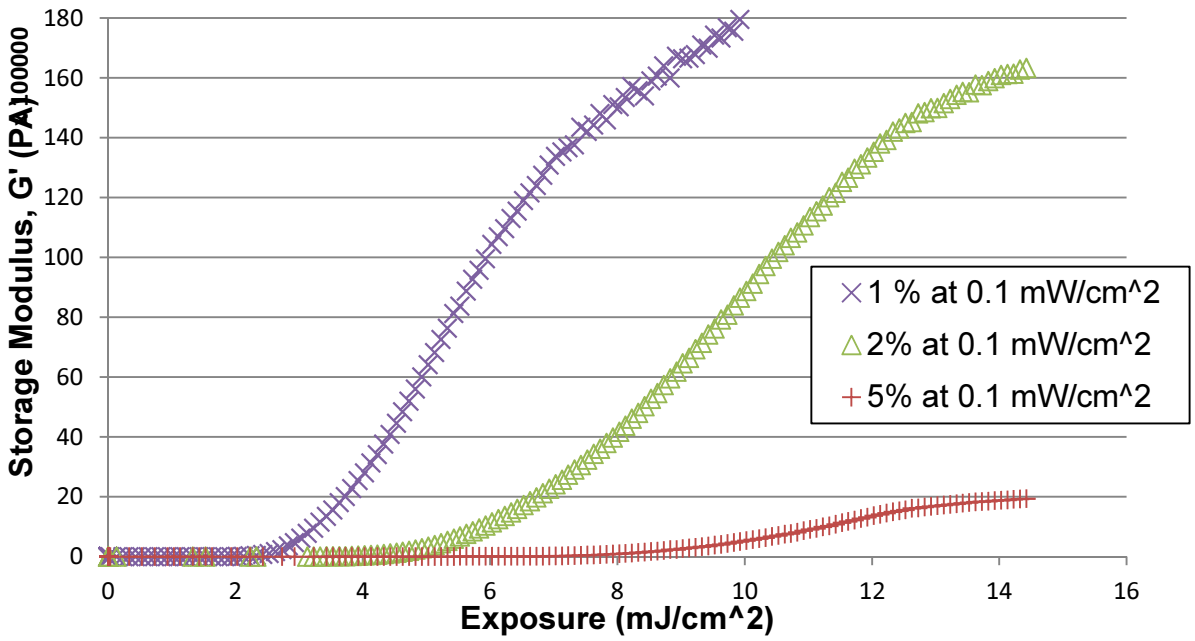

Figure 6-6: Storage Modulus of the QD-dope photopolymer verses the exposure dosage for 0.1 mw/cm^2 intensity.

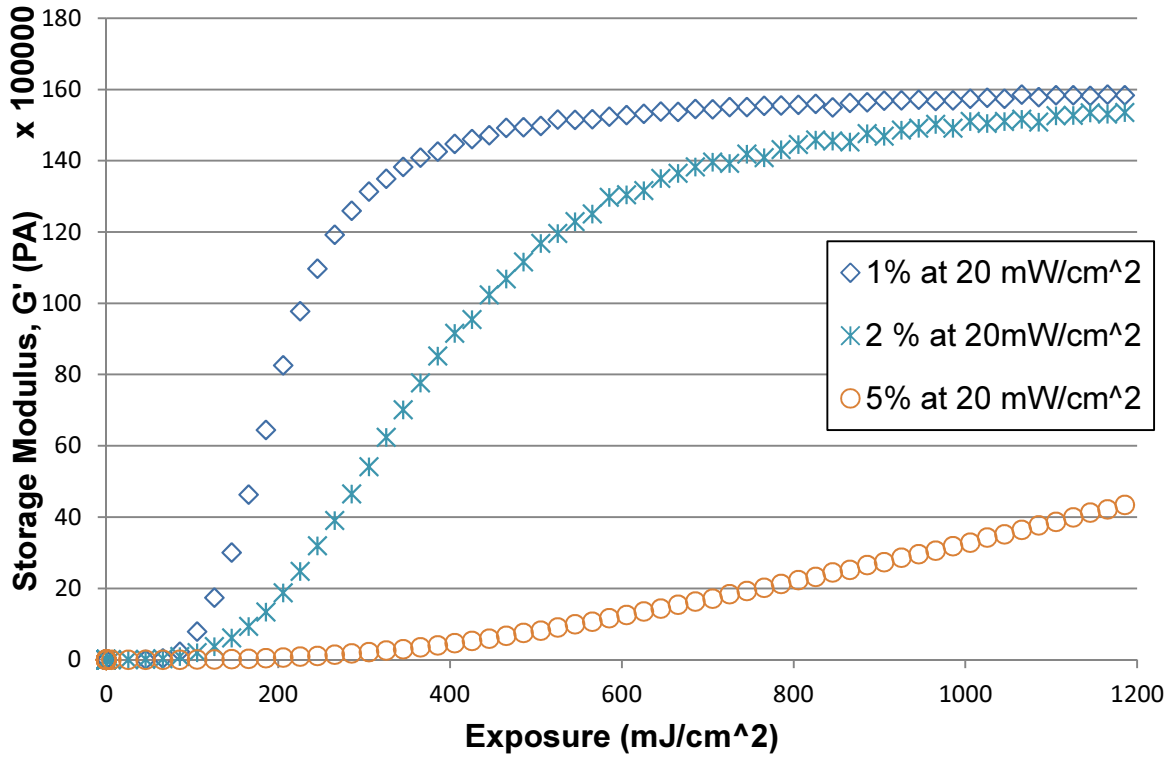

Figure 6-7: Storage Modulus of the QD-dope photopolymer verses the exposure dosage for 20 mw/cm^2 intensity.

The spectrophotometer data presented in Figure 5-4 reveals that the absorbance of the photopolymer peaks around 365nm wavelength but also absorbs significantly at wavelengths below 350 nm. Since the UV lamp used in the PolyJet system represents a broader spectrum of light, the values of critical exposure obtained from the photorheometer data are not relatable to actual PolyJet process curing. Thus, results from the photorheometer data were not used toward validating the Primary Research Hypothesis.

6.3 Discussion and Roadmap

Historically, it has been cited that that the critical exposure and depth of penetration terms in the Jacob's equation are purely a function of polymer resin properties and can be used universally for any energy intensity [2, 3]. However, a recent publication proves experimentally that critical exposure (E_c) is not independent of intensity [6]. The experimental setup consisted of a device for measuring the change in refractive index of the photopolymer as it cures, and the depth to which the refractive index is measured (thus measuring the cure depth). Upon varying the intensity of exposure from 20 $\mu W/cm^2$ to 200 $\mu W/cm^2$, but maintaining the same overall dose of 800 $\mu J/cm^2$, it was found that the critical exposure decreased with increasing intensity. However, it was not specified whether the actual critical exposure energy decreased or increase. Therefore, the results in Figures 6-6 and 6-7 constitute the first evidence that critical exposure of AM photopolymer increases with increased exposure intensity.

Table 6-1: Roadmap

	Research Phase	Chapter	Goals
Introduction	Problem Identification Solution Proposal	**Chapter 1** Introduction, Motivation, and Project Outline	**Describe the problem** **Describe a solution** to the problem and the process for implementing that solution **Identify the qualifying and research questions** related to the proposed solution
Background & Feasibility Analysis	Information Gathering Preliminary Experimentation	**Chapter 2** Visibility of Quantum Dots within PolyJet Media (QQ1) **Chapter 3** Inkjetting with Quantum Dots in PolyJet Media (QQ2)	**Synthesize literature** related to the Qualifying Questions **Perform Experiments** to address Qualifying Questions 1 and 2 **Draw Conclusions** to address Qualifying Questions
Research Methods	Hypothesis Formulation Experimental Methods Hypothesis Validation	**Chapter 4** Literature Review of Photopolymer-ization Theory, Proposed Theoretical Model **Chapter 5** Experimental Techniques, Results and Critique and Modification of Theoretical Model **Chapter 6** Effects of Intensity on Critical Exposure	**Synthesize literature** related to the Primary Research Question **Identify gaps** in existing literature that prevent answering the research question **Form hypotheses** based on existing literature **Establish Methods** for validating the hypothesis **Perform Experimentation** to validate hypothesis
Summary	Conclusions Outlining Future Work	**Chapter 7** Project Summary and Future Work	**Draw Conclusions** based on experiment results **Identify significant contributions** **Summarize accomplishments** related to answering each of the research questions **Propose future work**

CHAPTER 7 CONCLUSIONS AND FUTURE WORK

7.1 Summary of Research

The overall motivation for this work is to develop a method for incorporating Physical Unclonable Functions (PUFs) into Additive Manufacturing (AM) parts. PUFs were chosen as the type of security features due to their unclonable nature. Optical PUFs take advantage of the stochastic nature of randomly dispersed particles in creating an unclonable pattern of material. Quantum Dots (QDs) were chosen as the optical PUF particle because of their ability to emit light at a different wavelength than it is received. This ability to produce a "response" that is distinguishable from the "challenge" is a critical component of security features. Thus, to develop a process to create security features within AM builds, QDs were chosen to be dispersed in AM media (Section 1.3).

In order for the QD signal to be retrievable (optically visible), the QDs must be dispersed in a transparent media. The PolyJet AM process was chosen because of its ability to process transparent materials as well as process multiple materials in one build layer. PolyJet uses inkjet technology to deposit liquid photopolymer in a layer on a build surface. In Polyjet, a UV lamp passes over the layer after it is deposited to cure the photopolymer into a solid. Just as a document inkjet printer can process multiple colors, PolyJet can process multiple materials in a single build. This multiple-material capability set PolyJet apart from other AM technologies and also provides the opportunity to embed the QD PUFs within a part to avoid making the entire part from the QD PUF material. Furthermore, incorporating QDs in the PolyJet media provides an opportunity to embed PUFs without the need for a separate embedding process; the QD

PUFs can be created as part of the AM build. Thus, the Overall Project Goal can be stated as follows:

> **Overall Project Goal:** Create Physical Unclonable Functions via PolyJet 3D Printing of Quantum Dots

To reach this goal, the effects of QDs on the PolyJet process must be understood. Subsequently, the Overall Research Question encompasses this need:

> **Overall Research Question:** How Do Quantum Dots Affect the PolyJet Process?

Qualifying Questions are formed to guide feasibility analysis of incorporating QDs in the PolyJet process, which are discussed in the next section. A Primary Research Question is also formed to guide understanding of how QDs affect the PolyJet process, which is discussed in Section 7.1.2.

7.1.1 Qualifying Questions

Before investigating the effects of QDs on the PolyJet process, it was necessary to determine the viability of PUF creation via PolyJet. Specifically, it was necessary to validate that QDs are visible within cured PolyJet photopolymer. Considering this constraint, Qualifying Question 1 was formed (Section 2.2):

> **Qualifying Question 1 (QQ1):** What concentration of QDs within PolyJet media is necessary to provide readily visible fluorescence to the naked eye?

The key feature of an optical PUF is a pattern of discrete objects or light signatures that can be readily recognized with some type of optical imaging. For QDs in PolyJet Photopolymer, this means that the QDs must be recognizable via fluorescent (FL) microscopy. FL microscopy uses specific wavelengths of light to excite an object and uses filters for certain wavelengths of light to filter around the emitted signal. With FL microscopy, the QDs can be excited with UV light and their emission in the visible light spectrum can be detected. To answer QQ1, QDs were dispersed in PolyJet photopolymer, ink-jetted onto a substrate, cured into a solid, and imaged via DSLR camera and FL microscopy. In the FL images the QDs can be readily seen in distinguishable patterns within the inkjet droplets (Section 2.4, repeated in Figure 6-1 below for convenience).

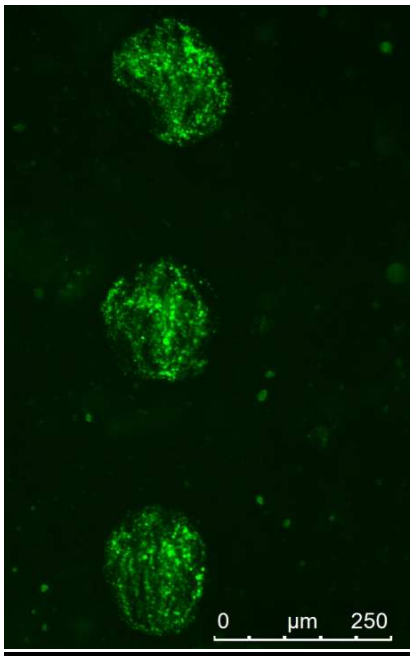

Figure 6-1: Drops of QD-doped photopolymer deposited onto a substrate shown under UV light (also used in Chapter 6)

Techniques to improve the visibility of the QDs below the surface of the cured photopolymer were investigated by embedding the QDs within PolyJet prints and treating the sample surfaces (Section 2.3). These experimental methods provided the answer to QQ1: adding QDs to PolyJet media was a feasible means of creating PUFs within an AM process.

Since PolyJet utilizes inkjet technology to deposit the build material, it was critical that the addition of QDs in the media did not affect the jettability of the media. Therefore, Qualify Question 2 was proposed (Section 3.1):

Qualifying Question 2 (QQ2): Can the Quantum Dots be added to the PolyJet media and successfully ink-jetted without a significant change in jetting behavior?

To answer QQ2, QDs were added to PolyJet photopolymer in varying concentrations (up to 5 wt%) and characterized rheologically. The values for surface tension and viscosity of the QD-doped media were compared to that of the pure photopolymer, and it was found that the addition of QDs in up to 5 wt% did not theoretically affect the jettability of the photopolymer (Figure 3-6). A single nozzle inkjet test stand was used to create inkjet droplets from the QD-doped media and image the droplet shape as the droplets traveled out of the nozzle. Experimentation with an inkjet test stand proved that the QD-doped polymer's jetting characteristics were not significantly different from the jetting characteristics of the pure polymer. Thus, the feasibility of processing the QDs within the inkjet step of the PolyJet process was established toward answering QQ2. These results were published in the peer-reviewed journal, *Advanced Engineering Materials* [5].

7.1.2 Primary Research Question, Hypothesis, and Validation

Beyond the visibility and jettability of the QDs within the PolyJet photopolymer lays the final step of the PolyJet process, which is curing of the photopolymer media. For this process it becomes necessary to understand the interaction of the QD nanoparticles and the photopolymer components during photopolymerization. Thus, the Primary Research Question was formed:

Primary Research Question (PRQ): How do QDs affect the photopolymerization of PolyJet resin?

To answer the Primary Research Question, a literature review was performed to identify potential mechanisms by which the QDs could affect photopolymerization (Chapter 4). It was found that either Rayleigh or Mie scattering would most likely be the dominate effect on photopolymerization energy. Determining which mechanism was dominant required characterization of the QDs within the photopolymer. Characterization of the QDs was performed in the form of spectrophotometry and SEM imaging of QD doped films (Section 5.2). It was found in the spectrophotometry data that the dominant scattering mechanism was Mie scattering, which is caused by particles much larger than the wavelength of incident light. This result was corroborated by the SEM imaging (Figure 5-6) that revealed QD agglomerates with an approximate average diameter of 20 microns.

It was hypothesized that employing the theoretical scattering efficiency of the QDs could predict the amount of exposure light being scattering and thus predict critical exposure of the QD-doped photopolymer based on QD loading. A theoretical model was

created to describe the scattering efficiency of the QDs in their agglomerated form (Section 5.2.4):

Primary Research Hypothesis (Final Version): The critical exposure of PolyJet photopolymer increases linearly with an increase in the natural logarithm of weight percent loading of QDs. The scattering efficiency can be modeling using a Mie scattering term and empirical constant.

$$E_c = E_{c,0}\gamma \ln(wt\%), \qquad \gamma = \frac{4\rho_{media}}{3d\rho_{particles}} Q_{Mie}, \qquad Q_{Mie} = 2\left(\frac{2\pi d}{\lambda_o}\right)^i \Delta n^2 \quad (5\text{-}7,\ 5\text{-}8,\ 5\text{-}9)$$

$$E_c \propto E_{c,0} \frac{4\rho_{media}}{3d\rho_{particles}} \left(\frac{2\pi d}{\lambda_o}\right)^i \Delta n^2 \ln(wt) \quad (5\text{-}6)$$

where E_c is the theoretical critical exposure, $E_{c,o}$ is the critical exposure of pure photopolymer, $\boldsymbol{\gamma}$ is the overall scattering efficiency, $\boldsymbol{Q}$ is the scattering coefficient, d is the average QD particle diameter, $\rho_{particles}$ is the QD density, ρ_{media} is the photopolymer density, $\boldsymbol{\lambda_o}$ is the wavelength of incident light, Δn is the value of refractive index of the QDs minus one, and wt is the concentration of QDs in weight fraction.

To verify the proposed curing model, curing characterization was performed by exposing QD-doped polymer in varying concentrations to varying doses of UV light. By plotting the cure depth against the exposure level, the working curves for the various QD concentrations were obtained. From the working curves, the values for depth of penetration and critical exposure of the QD-doped photopolymer can be obtained and were investigated for trends. Historically, the depth of penetration term has been the focus of scattering models for AM particle-doped photopolymers because photopolymers are typically used in Stereolithography. However, plotting the critical

exposures of the photopolymers with varying QD concentrations revealed a linear relationship between the critical exposure and the natural logarithm of the QD concentration (Figure 5-10). As shown in Figure 5-10, curing characterization via micro-stereolithography revealed a linear relationship between the critical exposure of the photopolymer and the weight loading of QDs (Section 5.2.3). This increase in critical exposure can be explained by scattering properties of the QDs.

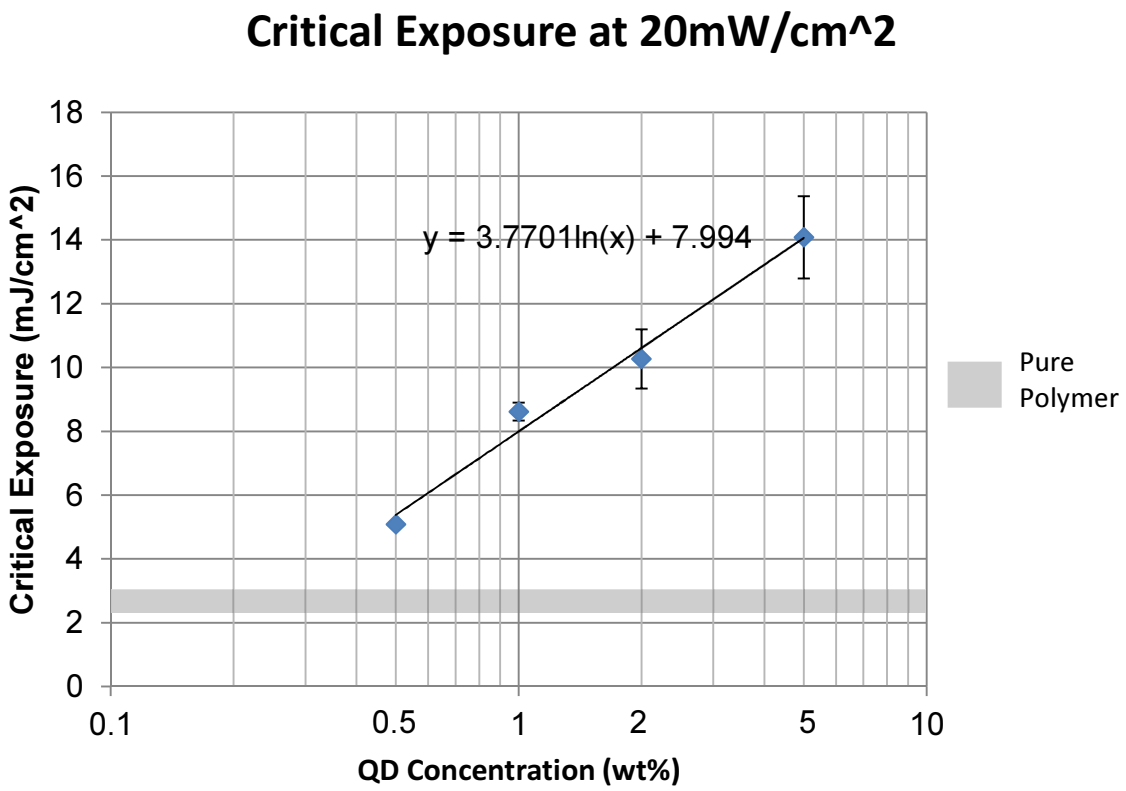

Figure 5-10: Critical Exposure values from working curves in Figure 5-8 (also used in Chapter 5)

To validate the Primary Research Hypothesis, a calculation was performed with nominal values for each of the variables (Table 5-5).

Table 5-5: Values Used in Primary Research Hypothesis Validation (also used in Chapter 5)

Critical Exposure of Pure Polymer	2.69 mW/cm^2 (Section 5.2.3)
Average Particle Diameter, *d*	20 micron (20,000 nm)
Density of Particles, $\rho_{particles}$	5.82 g/cm^2 [1]
Density of Polymer, ρ_{media}	1.08 g/cm^2 (measured)
Wavelength of Incident Light, λ_o	365 nm (Objet Lamp)
Difference in Refractive Index of polymer and QDs, *Δn*	1.65 [2]
Empirical Term, *i*	1.821

$$E_c = E_{c,0}\frac{4\rho_{media}}{3d\rho_{particles}}\left(\frac{2\pi d}{\lambda_o}\right)^i \Delta n^2 \ln(wt) \quad \text{5-6)}$$

$$= 2.69\frac{4(1.08\frac{g}{cm^3})}{3(20000\ nm)(5.86\frac{g}{cm^3})}\left(\frac{2\pi(20000\ nm)}{365\ nm}\right)^{1.821}(1.65)^2\ln(wt) = \mathbf{3.77}\ln(wt)$$

Table 5-5 shows that the ln(wt) coefficient equals 3.77, which is the same value found in the logarithmic curve fit equation in Figure 6-2. Thus, using an appropriate value for the empirical term *i*, the critical exposure of particle doped PolyJet polymer can be approximated.

In addition to the curing data, a sensitivity analysis was performed to explore the impact of deviations in each variable in the Primary Research Hypothesis. It was found that the empirical term *i* had the highest sensitivity by far, with the particle diameter being the second highest in sensitivity. A comparison of the sensitivity of each variable is providing in Section 5.3.2.

7.1.3 Secondary Hypothesis: The Effects of Intensity

Chapter 6 contains a discussion of findings related to the effect of intensity on the critical exposure of PolyJet photopolymer. Traditional knowledge holds that the critical exposure of a photopolymer is independent of intensity. However, photorheometer data presented in Section 5.4 shows that critical exposure increases as intensity increases. In other words, for higher exposure intensities, the critical exposure energy is higher. Thus, this discovery contributes to understanding of the role of intensity of PolyJet photopolymers.

7.2 Research Contributions

7.2.1 First Work to Integrate Nanoparticles in PolyJet Resin

The work in this dissertation constitutes the first reported attempt to integrate nanoparticles in PolyJet resin and characterize the effects on visibility, rheology, inkjetting, and photopolymerization. QDs incorporated within the PolyJet polymer showed evidence of agglomeration and settling, and functionalization of the QDs was shown to decrease agglomeration. The results from this work pave the way for future efforts to incorporate particles into PolyJet Direct 3D printing.

7.2.2 Validation of QD visibility within PolyJet Resin

In answering QQ1, it was proven that QDs can be seen within clear PolyJet resin on a macroscopic level:

Qualifying Question 1 (QQ1): What concentration of QDs within PolyJet media is necessary to provide readily visible fluorescence to the naked eye?

Furthermore, fluorescent microscope images reveal that discrete QD agglomerates are readily detectable in patterns characteristic of PUFs (Section 2.3.5). Finally, processing techniques were explored for their effects on the visibility of the QDs within the PolyJet polymer, and it was found that factors such as print settings, post-processing techniques, QD concentration, PUF geometry, and functionalization affected the visibility of the QD PUF patterns as well as the appearance of the PUFs under UV light to the naked eye. This visibility analyses is a step toward establishing process settings for creating PUFs via PolyJet of QD-doped photopolymers. The results from this work can also be generalized for improving visibility of PolyJet clear resins through appropriate post-processing.

7.2.3 Validation of Jettability of QDs in Polyjet Resin

The work described in Chapter 3 constitutes the first attempt to inkjet QD-doped PolyJet resin. This work is framed by QQ2:

> **Qualifying Question 2 (QQ2):** Can the Quantum Dots be added to the PolyJet media and successfully inkjetted without a significant change in jetting behavior?

Rheological measurements were taken to verify that the addition of QDs to PolyJet resin did not significantly change the jettability of the resin (Sections 3.4.1 and 3.4.2). Calculations for jettability based on the rheological measurement revealed no significant change in jettability (Section 3.4.3). Ultimately, QQ2 was validated by the successful jetting of QDs in up to 0.5 wt% (Section 3.4.3). This work was published in a peer-reviewed journal, *Advanced Engineering Materials* [3].

7.2.4 Model for Critical Exposure

The Primary Research Hypothesis (Equation 5-6) constitutes the first attempt to predict the critical exposure of a photopolymer based on particle loading for PolyJet photopolymers.

Primary Research Hypothesis (Final Version): The critical exposure of PolyJet photopolymer increases linearly with an increase in the natural logarithm of weight percent loading of QDs. The scattering efficiency can be modeling using a Mie scattering term and empirical constant.

$$E_c \propto E_{c,0} \frac{4\rho_{media}}{3d\rho_{particles}} \left(\frac{2\pi d}{\lambda_o}\right)^i \Delta n^2 \ln(wt) \quad (5\text{-}6)$$

The model incorporates light scattering theory, light scattering characterization of the QDs within the photopolymer, curing characterization of the QDs within the polymer, and AM photopolymer curing theory. The theoretical model and characterization methods for the effects of QDs on AM photopolymer curing constitute new knowledge in the area of curing of particle-doped photopolymers. Such a theoretical model provides the necessary information for the PolyJet process parameters (e.g., exposure) to be set to process QDs to fabricate AM PUFs. In addition, the model also benefits applications including QDs and photopolymers, such as printed electronics. Furthermore, the model proposed in this work serves as a stepping stone for future work in the area of particle-doped PolyJet materials.

7.2.5 Evidence of the Effect of Intensity on Critical Exposure

In addition to the Primary Research Hypothesis, data from the cure depth samples show that the critical exposure changes for varying intensities of incident light (Chapter 6). It was found that photopolymer cured at an intensity of 20 mw/cm^2 had a critical exposure of around 100 mJ/cm^2 while the same polymer cured at an intensity of 0.1 mW/cm^2 had a critical exposure of around 2.5 mJ/cm^2. This discovery conflicts with traditional understanding which holds that critical exposure is a characteristic of the photopolymer independent of intensity [4-5]. Furthermore, to our knowledge this is the first use of a photorheometer to characterize the curing properties of AM photopolymers. Thus, the scientific contribution of this work is the understanding that critical exposure is affected by the intensity of the incident exposure light.

7.3 Limitations and Future Work

The limitations of this work are discussed in this section along with the corresponding future work needed to reduce those limitations. The limitations include creating a stable dispersion of QDs within the polymer, modelling the *x*-intercept found in the curve fit of the critical exposure (Figure 6-2), measuring the index of refraction of the QDs and the photopolymer, completing a similar curing characterization with more materials, printing QDs with PolyJet equipment, and finally, creating a system to identify, store, and retrieve PUF patterns created by QDs dispersed in photopolymer.

7.3.1 Stabilize QDs within the Polymer

Functionalization was performed on the QDs in effort to decrease the amount of agglomeration and improve the stability of the QDs within the polymer. However, QD agglomerates with diameters of several microns were seen in the SEM imaging.

Fortunately, filters on the polymer feed lines to the printhead remove such large objects. Settling, however, is still an issue since the QDs settle out of the polymer within 5 days (Appendix). Therefore, a strategy to stabilize the QDs within the polymer is needed. Strategies for accomplishing stability include formulating a polymer with a density that is comparable to QD density or including a dispersant in the polymer that does not significantly affect curing or jetting properties.

7.3.2 X-intercept of Theoretical Model

In fitting a logarithmic function to the curing data in Figure 5-10, a constant is formed that describes the x-intercept of the function (Equation 6-1).

$$y = 3.7701 * \ln(wt) + \mathbf{7.994} \quad (6\text{-}1)$$

The model proposed in the Primary Research Hypothesis is limited in that this X-intercept term is not modeled. Theoretically, the x-intercept of the model is where critical exposure equals zero for a certain QD loading, which is not achievable. Using the rules of natural logarithms, the constant can be incorporated into natural logarithm term. Equation 6-2 states the product rule for natural logarithms and Equations 6-3 and 6-4 are the original and modified versions of the Figure 5-6 curve fit, respectively.

$$y = \ln(a * b) = \ln(a) + \ln(b) \quad (6\text{-}2)$$

$$y = 3.7701 * \ln(wt) + \mathbf{7.994} \quad (6\text{-}3)$$

$$y = 3.7701 * \ln(\mathbf{8.33} * wt) \quad (6\text{-}4)$$

Thus, future work should include the investigation and modeling of this x-intercept term.

7.3.3 Refractive Index Measurement

The difference in refractive index (Δn) between the particles and the photopolymer ($\Delta n = n_{particles} - n_{polymer}$) plays a role in the scattering efficiency of the particles. Experiments were attempted in this work to measure the index of refraction of QD-doped photopolymer in varying concentrations via a thin film, broad spectrum refractometer to ultimately extrapolate the index of refraction for 100% QDs. However, measurements failed due to the agglomeration of the QDs within the polymer and the resistance of the pure photopolymer to be cured into a thin film without significant peeling. The agglomeration caused inhomogeneity within the sample to a point that accurate measurements were not achievable. As a result, a value from the literature was used for the refractive index of QDs, and an *n-1* term was used in the model instead of $n_{particles} - n_{polymer}$.

To increase the accuracy of the Primary Research Hypothesis, the refractive index of the particles and the polymer should be measured. This should be accomplished with a UV refractometer that accepts liquid samples and can measure with low intensity (to avoid curing the photopolymer during the measurement). The QDs should be measured in pure, powdered form or dispersed (without agglomeration) in liquid in varying concentrations.

7.3.4 Measurements with Additional Materials

Curing measurements were taken on QD-doped samples with 0.5, 1, 2, and 5 weight percent loadings of QDs. Do to the expense of the QDs material, additional concentrations were not examined. To further validate the Primary Research Hypothesis, additional concentrations such as 10 and 20 wt% should be explored for

scattering and curing properties. Furthermore, additional materials should be explored to determine whether the linear trend between critical exposure and natural logarithm of QD loading (Figure 6-2) is due to the presence of QDs or if the same trend would occur with another type of material such as ceramic particle. In addition, the curing experiments should be performed using stereolithography resin instead of the PolyJet resin to determine whether the photopolymer composition is the driving factor behind the change in critical exposure with particle loading and not depth of penetration.

7.3.5 Investigate Chemistry between Polymer and QDs

In investigations to determine the role of QDs in photopolymerization, Barichard and authors determined that QDs can trap co-initiators on their surfaces [7]. Furthermore, it was found that QDs can serve as photoinitiators when in the presence of certain types of polymer compounds. In addition to light scattering, these effects could also contribute to the decrease in critical exposure with increasing QD concentration. To develop a more robust model to predict the effects of QDs on photopolymerzation, taking the chemical role of QDs in photopolymerization is necessary.

7.3.6 3D Print QDs for the Creation of PUFs

The work in this dissertation serves as a starting point for creating PUFs in AM builds. The conclusions reveal the feasibility of such an endeavor as well as a model to predict the amount of energy required for curing (critical exposure). It has been shown in this work that concentrations of QDs sufficient to produce PUF patterns are inkjettable. Furthermore, the energy needed to cure the QD-doped polymer has been modeled. To reach the final goal of this work, future work includes creating PUFs by

incorporating QDs into PolyJet media for the creation of embedded PUFs. The process for incorporating QDs into existing PolyJet equipment is outlined in Chapter 1.

7.3.7 Create systems to recognize, record, and store PUF information

As detailed in Chapter 1, security functions require an excitation signal and an output signal as well as components to emit and receive those signals. A method such as fluorescent microscopy will be needed to excite the QDs and detect their individual light signatures. Once the QDs are detectable, a computer algorithm will be needed to analyze the images and encode the spatial arrangement of the QDs into a storable form. Finally, a method of retrieving the stored security information will be needed. Other work includes developing systems to identify, track, and store AM PUF patterns as well as geometric design and place of the PUFs within AM build geometries.

WORKS CITED

Chapter 1

[1] L. J. Stiltner, A. M. Elliott, C. B. Williams, “A method for creating actuated joints via fiber embedding in a polyjet 3D printing process,” International Solid Freeform Fabrication Symposium, 2011, Austin, TX.

[2] S. Bradshaw, A. Bowyer, and P. Haufe, “The intellectual property implications of low-cost 3D printing,” *ScriptEd*, vol. 7, no. 1, 2010.

[3] C. Mota, “The rise of personal fabrication,” *Proceedings of the 8th ACM Conference on Creativity and Cognition - C&C ’11*, p. 279, 2011.

[4] M. Weinberg, “It will be awesome if they don’t screw it up: 3D printing, intellectual property, and the fight over the next great disruptive technology,” November, 2010. Retreived from http://www.publicknowledge.org/it-will-be-awesome-if-they-dont-screw-it-up. [Accessed 20-Feb-2013].

[5] H. Fountain, “Tools of modern gunmaking : plastic and a 3-D printer,” *New York Times*, 29-Jan-2013. Available: http://www.nytimes.com/2013/01/30/science/surprising-tools-of-modern-gunmaking-plastic-and-a-3-d-printer.html?pagewanted=2&_r=0. [Accessed: 20-Feb-2013].

[6] R. S. Pappu, “III. Physical one-way functions,” *Cryptobytes*, vol. 21, 2003.

[7] S. Stanzione, D. Puntin, G. Iannaccone, and S. Member, “CMOS silicon physical unclonable functions based on intrinsic process variability,” *IEEE Journal of Solid-State Circuits*, vol. 46, no. 6, pp. 1456–1463, 2011.

[8] Ruhrmair, U.R., F. Sehnke, J. Solter, G. Dror, S. Devadas, “Modeling attacks on physical unclonable functions,” in *17th ACM Conference on Computer and Communications Security*, 2010.

[9] B. L. P. Gassend, “Physical random functions,” Masters Thesis. Dept. Elect. Eng. and Comp. Sci., Massachussetts Institute of Technology, Boston, MA, 2001.

10] O. S. Ivanova, A. M. Elliott, T. A. Campbell, and C. B. Williams, “Additive manufacturing with quantum dot nano-inks,” *Nanotech*, vol. 2, pp. 275–278, 2012.

[11] H. M. Haverinen, R. A. Myllyla, and G. E. Jabbour, “Inkjet printing of light emitting quantum dots,” *Applied Physics Letters*, vol. 94, p. 073108, 2009.

[12] C. Paquet and E. Kumacheva, “Patterning semiconductor nanocrystals in polymer films,” *Advanced Functional Materials*, vol. 17, no. 16, pp. 3105–3110, Nov. 2007.

[13] V. Wood, M. J. Panzer, J. Chen, M. S. Bradley, J. E. Halpert, M. G. Bawendi, and V. Bulovic, “Inkjet-printed quantum dot–polymer composites for full-color AC-driven displays,” *Advanced Materials*, vol. 21, pp. 2151–2155, 2009.

[14] S. Jun, E. Jang, J. Park, and J. Kim, “Photopatterned semiconductor nanocrystals and their electroluminescence from hybrid light-emitting devices.,” *Langmuir : the ACS journal of surfaces and colloids*, vol. 22, no. 6, pp. 2407–10, Mar. 2006.

[15] H. Jorkaala and H. Stennenen, “Nonlinear optical properties of ZnSe nanocrystals incorporated within polyvinyl alcohol photopolymer matrices,” *Journal of Optics A: Pure and Applied Optics*, vol. 4, pp. 366–369, 2002.

[16] X. Li, C. Bullen, J. W. M. Chon, R. a. Evans, and M. Gu, “Two-photon-induced three-dimensional optical data storage in CdS quantum-dot doped photopolymer,” *Applied Physics Letters*, vol. 90, no. 16, 2007.

[17] E. Tekin, E. Holder, D. Kozodaev, and U. S. Schubert, “Controlled pattern formation of poly[2-methoxy-5-(2′-ethylhexyloxyl)–1,4-phenylenevinylene] (MEH–PPV) by ink-jet printing,” *Advanced Functional Materials*, vol. 17, no. 2, pp. 277–284, Jan. 2007.

[18] S. B. Fuller, E. J. Wilhelm, and J. M. Jacobson, “Ink-jet printed nanoparticle microelectromechanical systems,” *Journal of Microelectromechanical Systems*, vol. 11, no. 1, pp. 54–60, 2002.

[19] A. Hancock and L. Lin, “Challenges of UV curable ink-jet printing inks – a formulator’s perspective,” *Pigment & Resin Technology*, vol. 33, no. 5, pp. 280–286, 2004.

[20] X. Liu, Y. Tomita, J. Oshima, K. Chikama, K. Matsubara, T. Nakashima, and T. Kawai, “Holographic assembly of semiconductor CdSe quantum dots in polymer for volume Bragg grating structures with diffraction efficiency near 100%,” *Applied Physics Letters*, vol. 95, no. 26, p. 261109, 2009.

[21] A. M. Elliott, O. S. Ivanova, C. B. Williams, and T. C. Campbell, “An investigation of the effects of quantum dot nanoparticles on photopolymer resin for use in polyjet direct 3D printing,” International Solid Freeform Fabrication Symposium, 2012, Austin, TX.

Chapter 2

[1] Olga S. Ivanova, Kristen A. Zimmermann, James R. Tuggle, Thomas A. Campbell, (2013) “Synthesis of non-spherical CdSe nanocrystals,” Journal of Nanoparticle Research, 15, 1382-1390, http://10.1007/s11051-012-1382-7.

[2] Objet Geometries, “Objet VeroClear – Printing Tips,” 2011.

[3] Objet Geometries, “Creating clear or translucent models,” 2007.

[4] L. J. Stiltner, A. M. Elliott, C. B. Williams, “A method for creating actuated joints via fiber embedding in a polyjet 3D printing process,” International Solid Freeform Fabrication Symposium, 2011, Austin, TX.

Chapter 3

[1] A. Hancock and L. Lin, “Challenges of UV curable ink-jet printing inks – a formulator’s perspective,” *Pigment & Resin Technology*, vol. 33, no. 5, pp. 280–286, 2004.

[2] A. Kamyshny, M. Ben-Moshe, S. Aviezer, and S. Magdassi, “Ink-Jet printing of metallic nanoparticles and microemulsions,” *Macromolecular Rapid Communications*, vol. 26, no. 4, pp. 281–288, Feb. 2005.

[3] B. J. de Gans, P. C. Duineveld, and U. S. Schubert, “Inkjet printing of polymers: state of the art and future developments,” *Advanced Materials*, vol. 16, no. 3, pp. 203–213, Feb. 2004.

[4] S. Vafaei, A. Purkayastha, A. Jain, G. Ramanath, and T. Borca-Tasciuc, “The effect of nanoparticles on the liquid-gas surface tension of Bi2Te3 nanofluids,” *Nanotechnology*, vol. 20, no. 18, p. 185702, May 2009.

[5] S. Vafaei, A. Purkayastha, A. Jain, G. Ramanath, and T. Borca-Tasciuc, “The effect of nanoparticles on the liquid-gas surface tension of Bi2Te3 nanofluids.,” *Nanotechnology*, vol. 20, no. 18, p. 185702, May 2009.

[6] B. Derby, “Inkjet printing of functional and structural materials: fluid property requirements, feature stability, and resolution,” *Annual Review of Materials Research*, vol. 40, no. 1, pp. 395–414, Jun. 2010.

[7] M. E. Mackay, T. T. Dao, A. Tuteja, D. L. Ho, B. van Horn, H.-C. Kim, and C. J. Hawker, “Nanoscale effects leading to non-Einstein-like decrease in viscosity,” *Nature materials*, vol. 2, no. 11, pp. 762–6, Nov. 2003.

[8] V. Wood, M. J. Panzer, J. Chen, M. S. Bradley, J. E. Halpert, M. G. Bawendi, and V. Bulovic, “Inkjet-printed quantum dot–polymer composites for full-color ac-driven displays,” *Advanced Materials*, vol. 21, pp. 2151–2155, 2009.

[9] E. Tekin, E. Holder, D. Kozodaev, and U. S. Schubert, “Controlled pattern formation of poly[2-methoxy-5-(2′-ethylhexyloxyl)–1,4-phenylenevinylene] (MEH–

PPV) by ink-jet printing," *Advanced Functional Materials*, vol. 17, no. 2, pp. 277–284, Jan. 2007.

[10] H. M. Haverinen, R. A. Myllyla, and G. E. Jabbour, "Inkjet printing of light emitting quantum dots," *Applied Physics Letters*, vol. 94, p. 073108, 2009.

[11] V. Wood, M. J. Panzer, J. Chen, M. S. Bradley, J. E. Halpert, M. G. Bawendi, and V. Bulovic, "Inkjet-printed quantum dot–polymer composites for full-color ac-driven displays," *Advanced Materials*, vol. 21, pp. 2151–2155, 2009.

[12] E. Tekin, E. Holder, D. Kozodaev, and U. S. Schubert, "Controlled pattern formation of poly[2-methoxy-5-(2′-ethylhexyloxyl)–1,4-phenylenevinylene] (MEH–PPV) by ink-jet printing," *Advanced Functional Materials*, vol. 17, no. 2, pp. 277–284, Jan. 2007.

[13] E. Tekin, P. J. Smith, S. Hoeppener, A. M. J. van den Berg, A. S. Susha, A. L. Rogach, J. Feldmann, and U. S. Schubert, "Inkjet printing of luminescent cdte nanocrystal–polymer composites," *Advanced Functional Materials*, vol. 17, pp. 23–28, 2007.

[14] A. Kamyshny, M. Ben-Moshe, S. Aviezer, and S. Magdassi, "Ink-jet printing of metallic nanoparticles and microemulsions," *Macromolecular Rapid Communications*, vol. 26, no. 4, pp. 281–288, Feb. 2005.

[15] Z.-B Sun, X.-Z. Dong, W.Q. Chen, S. Nakanishi, X.-M. Duan, & S. Kawata, "Multicolor Polymer Nanocomposites: In Situ Synthesis and Fabrication of 3D

Microstructures," *Advanced Materials*, *20*(5), 914–919, 2008. doi:10.1002/adma.200702035

[16] S. B. Fuller, E. J. Wilhelm, and J. M. Jacobson, "Ink-jet printed nanoparticle microelectromechanical systems," *Journal of Microelectromechanical Systems*, vol. 11, no. 1, pp. 54–60, 2002.

[17] A. Kamyshny, M. Ben-Moshe, S. Aviezer, and S. Magdassi, "Ink-jet printing of metallic nanoparticles and microemulsions," *Macromolecular Rapid Communications*, vol. 26, no. 4, pp. 281–288, Feb. 2005.

[18] B. J. de Gans, P. C. Duineveld, and U. S. Schubert, "Inkjet printing of polymers: state of the art and future developments," *Advanced Materials*, vol. 16, no. 3, pp. 203–213, Feb. 2004.

[19] E. Tekin, P. J. Smith, S. Hoeppener, A. M. J. van den Berg, A. S. Susha, A. L. Rogach, J. Feldmann, and U. S. Schubert, "Inkjet printing of luminescent cdte nanocrystal–polymer composites," *Advanced Functional Materials*, vol. 17, pp. 23–28, 2007.

[20] N. Reis, C. Ainsley, and B. Derby, "Ink-jet delivery of particle suspensions by piezoelectric droplet ejectors," *Journal of Applied Physics*, vol. 97, no. 9, p. 094903, 2005.

[21] J. Wang, M. M. Mohebi, and J. R. G. Evans, “Two methods to generate multiple compositions in combinatorial ink-jet printing of ceramics,” *Macromolecular Rapid Communications*, vol. 26, no. 4, pp. 304–309, Feb. 2005.

[22] V. Fakhfouri, G. Mermoud, J. Kim, A. Martinoli, and J. Brugger, “Drop-On-Demand Inkjet Printing of SU-8 Polymer,” *Micro and Nanosystemse*, vol. 1, no. 1, pp. 63–67, Mar. 2009.

[23] K. A. M. Seerden, N. Reis, J. R. G. Evans, P. S. Grant, J. W. Halloran, and B. Derby, “Ink-jet printing of wax-based alumina suspensions,” *Journal of the American Ceramic Society*, vol. 84, no. 11, pp. 2514–2520, 2001.

[24] A. M. Elliott, O. S. Ivanova, C. B. Williams, and T. A. Campbell, “Inkjet printing of quantum dots in photopolymer for use in additive manufacturing of nanocomposites,” *Advanced Engineering Materials*, Volume 15, Issue 10, pages 903–907, October 2013. doi:10.1002/adem.201300020

Chapter 4

[1] D. Day, M. Gu, and A. Smallridge, “Use of two-photon excitation for erasable-rewritable three-dimensional bit optical data storage in a photorefractive polymer.” *Optics Letters*, vol. 24, no. 14, pp. 948–50, Jul. 1999.

[2] H. Jorkaala and H. Stennenen, “Nonlinear optical properties of ZnSe nanocrystals incorporated within polyvinyl alcohol photopolymer matrices.” *Journal of Optics A: Pure and Applied Optics*, vol. 4, pp. 366–369, 2002.

[3] J. J. Park, P. Prabhakaran, K. K. Jang, Y. Lee, J. Lee, K. Lee, J. Hur, J. M. Kim, N. Cho, Y. Son, D. Y. Yang, and K. S. Lee, “Photopatternable quantum dots forming quasi-ordered arrays.” *Nano letters*, vol. 10, no. 7, pp. 2310–7, Jul. 2010.

[4] X. Liu, Y. Tomita, J. Oshima, K. Chikama, K. Matsubara, T. Nakashima, and T. Kawai, “Holographic assembly of semiconductor CdSe quantum dots in polymer for volume Bragg grating structures with diffraction efficiency near 100%,” *Applied Physics Letters*, vol. 95, no. 26, p. 261109, 2009.

[5] M. J. Panzer, K. E. Aidala, and V. Bulović, “Contact printing of colloidal nanocrystal thin films for hybrid organic/quantum dot optoelectronic devices,” *Nano reviews*, vol. 3, pp. 1–8, Jan. 2012.

[6] C. Paquet and E. Kumacheva, “Patterning semiconductor nanocrystals in polymer films,” *Advanced Functional Materials*, vol. 17, no. 16, pp. 3105–3110, Nov. 2007.

[7] O. V Sakhno, L. M. Goldenberg, J. Stumpe, and T. N. Smirnova, “Effective volume holographic structures based on organic–inorganic photopolymer nanocomposites,” *Journal of Optics A: Pure and Applied Optics*, vol. 11, no. 2, p. 024013, Feb. 2009.

[8] Y. Tomita, N. Suzuki, and K. Chikama, “Holographic manipulation of nanoparticle distribution morphology in nanoparticle-dispersed photopolymers,” *Optics letters*, vol. 30, no. 8, pp. 839–41, Apr. 2005.

[9] X. Li, C. Bullen, J. W. M. Chon, R. A. Evans, and M. Gu, “Two-photon-induced three-dimensional optical data storage in CdS quantum-dot doped photopolymer,” *Applied Physics Letters*, vol. 90, no. 16, 2007.

[10] Z. B. Sun, X. Z. Dong, W. Q. Chen, S. Nakanishi, X.-M. Duan, and S. Kawata, “Multicolor polymer nanocomposites: in situ synthesis and fabrication of 3D microstructures,” *Advanced Materials*, vol. 20, no. 5, pp. 914–919, Mar. 2008.

[11] Z. B. Sun, X. Z. Dong, S. Nakanishi, W. Q. Chen, X. M. Duan, and S. Kawata, “Log-pile photonic crystal of CdS-polymer nanocomposites fabricated by combination of two-photon polymerization and in situ synthesis,” *Applied Physics A*, no. 86, pp. 427–431, 2007.

[12] C. Ingrosso, V. Fakhfouri, M. Striccoli, A. Agostiano, A. Voigt, G. Gruetzner, M. L. Curri, and J. Brugger, “An epoxy photoresist modified by luminescent nanocrystals for the fabrication of 3d high-aspect-ratio microstructures,” *Advanced Functional Materials*, vol. 17, no. 13, pp. 2009–2017, Sep. 2007.

[13] A. Barichard, T. Galstian, and Y. Israëli, “Influence of CdSe/ZnS quantum dots in the polymerization process and in the grating recording in acrylate materials,” *The Journal of Physical Chemistry. B*, vol. 114, no. 46, pp. 14807–14, Nov. 2010.

[14] A. Barichard, T. Galstian, and Y. Israëli, “Physico-chemical role of CdSe/ZnS quantum dots in the photo-polymerization process of acrylate composite materials,” *Physical Chemistry Chemical Physics : PCCP*, vol. 14, no. 22, pp. 8208–16, Jun. 2012.

[15] K. C. Wu, K. F. Seefeldt, M. J. Solomon, and J. W. Halloran, “Prediction of ceramic stereolithography resin sensitivity from theory and measurement of diffusive photon transport,” *Journal of Applied Physics*, vol. 98, no. 2, p. 024902, 2005.

[16] C. Hinczewski, S. Corbel, and T. Chartier, “Stereolithography for the fabrication of ceramic three-dimensional parts,” *Rapid Prototyping Journal*, vol. 4, no. 3, pp. 104–111, 1998.

[17] M. L. Griffith and J. W. Halloran, “Freeform fabrication of ceramics via stereolithography,” *Journal of the American Ceramic Society*, vol. 79, no. 10, pp. 2601–608, 1996.

[18] G. Brady and J. Halloran, “Stereolithography of ceramic suspensions,” *Rapid Prototyping Journal*, July, pp. 1–3, 1997.

[19] E. Hanamura, “Rapid radiative decay and enhanced optical nonlinearity of excitons in a quantum well,” *Physical Review B*, vol. 38, no. 2, 1988.

[20] S. Schmitt-Rink, D. A. Miller, and D. S. Chemla, “Theory of the linear and nonlinear optical properties of semiconductor microcrystallites,” *Physical Review B*, vol. 35, no. 15, pp. 8113–8125, 1987.

[21] T. Brocke, “Electronic raman spectroscopy on semiconductor quantum dots dissertation,” Ph.D. dissertation. Dept. of Physics, Univ. of Hamburg, Hamburg, Germany, 2007.

[22] M. Fisher, “Optical sensing with cdse quantum dots in condensed phase media,” Ph.D. dissertation. Dept. of Chem. and Biochem., Florida State Univ., Tallahassee, FL, 2009.

[23] C. F. Bohren and D. R. Huffman, *Absorption and scattering of light by small particles*. New York, New York, USA: Wiley, 1983.

[24] A. Balandin, K. L. Wang, N. Kouklin, and S. Bandyopadhyay, “Raman spectroscopy of electrochemically self-assembled CdS quantum dots,” *Applied Physics Letters*, vol. 76, no. 2, p. 137, 2000.

[25] A. Ekimov and A. Onushchenko, “Quantum size effect in three-dimensional microscopic semiconductor crystals,” *ZhETF Pis ma Redaktsiiu*, 1981.

[26] A. Khare, A. W. Wills, L. M. Ammerman, D. J. Norris, and E. S. Aydil, “Size control and quantum confinement in Cu2ZnSnS4 nanocrystals,” *Chemical Communications*, vol. 47, pp. 11721–11723, 2011.

[27] C. Woelfle and R. O. Claus, “Transparent and flexible quantum dot–polymer composites using an ionic liquid as compatible polymerization medium,” *Nanotechnology*, vol. 18, no. 2, 2007.

[28] T. Tokizaki, H. Akiyama, M. Takaya, and A. Nakamura, “Linear and nonlinear optical properties of CdSe microcrystallites in glasses,” *Journal of Crystal Growth*, vol. 117, no. 1–4, pp. 603–607, Feb. 1992.

[29] K. Y. Narsingi, M. O. Manasreh, and B. D. Weaver, “Proton irradiation effect on cdse-zns core-shell nanocrystals embedded in ultra violet curable resin,” in *IEEE Region 5 Technical Conference*, 2007, pp. 436–440.

[30] D. Segets, J. M. Lucas, R. N. K. Taylor, M. Scheele, H. Zheng, P. Alivisatos, and W. Peukert, “Determination of the quantum dot band gap dependence on particle size from optical absorbance and measurements,” no. 10, pp. 9021–9032, 2012.

[31] C. A. Mack, “Absorption and exposure in positive photoresist,” *Applied Optics*, vol. 27, no. 23, pp. 4913–9, Dec. 1988.

[32] J. W. Halloran, V. Tomeckova, S. Gentry, S. Das, P. Cilino, D. Yuan, R. Guo, A. Rudraraju, P. Shao, T. Wu, T. R. Alabi, W. Baker, D. Legdzina, D. Wolski, W. R. Zimbeck, and D. Long, “Photopolymerization of powder suspensions for shaping ceramics,” *Journal of the European Ceramic Society*, vol. 31, no. 14, pp. 2613–2619, Nov. 2011.

[33] H.C. van de Hulst. *Light Scattering By Small Particles*, New York: John Wiley & Sons, 1957.

[34] R. Singh, “C. V. Raman and the discovery of the Raman Effect,” *Physics in Perspective (PIP)*, vol. 4, no. 4, pp. 399–420, Dec. 2002.

[35] Y. Rakovich, S. Filonovich, and M. Gomes, “A. Eychmüller anti-Stokes photoluminescence in ii-vi colloidal nanocrystals,” *Phys. Stat. Sol.(b)*, vol. 229, no. 1, pp. 449–452, 2002.

[36] M. Fujii, S. Hayashi, and K. Yamamoto, “Raman scattering from quantum dots of Ge embedded in SiO2 thin films,” *Applied Physics Letters*, vol. 57, no. 25, p. 2692, 1990.

[37] A. F. Bin Omar and M. Z. Bin Matjafri, “Turbidimeter design and analysis: a review on optical fiber sensors for the measurement of water turbidity,” *Sensors (Basel, Switzerland)*, vol. 9, no. 10, pp. 8311–35, Jan. 2009.

[38] M. L. Griffith, “Stereolithography of ceramics,” Ph.D. dissertation, Dept. of Matls. Sci. and Eng., University of Michigan, Ann Arbor, MI, 1995.

[39] F. Jacobs, *Rapid Prototyping & Manufacturing: Fundamentals of StereoLithography*, 1st ed. Society of Manufacturing Engineers, 1992.

[40] I. Gibson, D. W. Rosen, and B. Stucker, *Additive Manufacturing Technologies*. Boston, MA: Springer US, 2010.

[41] A. J. Cox, A. J. DeWeerd, and J. Linden, “An experiment to measure Mie and Rayleigh total scattering cross sections,” *American Journal of Physics*, vol. 70, no. 6, p. 620, 2002.

[42] R. J. Hunter, *Introduction to Modern Colloidal Science*, 1st ed. Oxford: Oxford University Press, 1993.

[43] T. Allen, *Particle Size Measurement*, Fourth. London: Chapman and Hall, 1990.

[44] E. D. Palik, Ed., *Handbook of optical properties of solids*. Orlando: Academic Press Hanbook Series, 1985.

[45] M. L. Griffith and J. W. Halloran, “Stereolithography of Ceramics,” in *The Sixth International Conference on Rapid Prototyping*, 1995.

Chapter 5

[1] F. Jacobs, *Rapid Prototyping & Manufacturing: Fundamentals of StereoLithography*, 1st ed. Society of Manufacturing Engineers, 1992.

[2] Henini, M. (2004). *Semiconductors: Data Handbook*. Microelectronics Journal. doi:10.1016/j.mejo.2004.04.001

[3] Piller, H. “Handbook of Optical Constants of Solids,” Academic Press. ISBN 0-12-544422-2, page 570, 1991.

[4] A. F. Bin Omar and M. Z. Bin Matjafri, “Turbidimeter design and analysis: a review on optical fiber sensors for the measurement of water turbidity,” *Sensors (Basel, Switzerland)*, vol. 9, no. 10, pp. 8311–35, Jan. 2009.

[5] X. W. Cheng, "Spectral characteristics of cdse quantum dots," *Infrared Millimeter Waves and 14th International Conference on Teraherz Electronics, 2006. IRMMW-THz 2006*, pp.494,494, 18-22 Sept. 2006. doi 10.1109/ICIMW.2006.368702

[6] A. Jariwala, F. Ding, X. Zhao, D. W. Rosen, "A film fabrication process on transparent substrate using mask projection micro-stereolithography,"

Proceedings of the 19th Solid Freeform Fabrication Symposium, Austin, Texas, 2008, pp. 216-229.

[7] H.C. van de Hulst. *Light Scattering By Small Particles*, New York: John Wiley & Sons, 1957.

[8] D. Segets, J. M. Lucas, Taylor, R. N. K, Scheele, M, Zheng, H, Alivisatos, P, & W. Peukert, "Determination of the Quantum Dot Band Gap Dependence on Particle Size from Optical Absorbance and Measurements," ACS Nano *6*, (10), 9021–9032, 2012.

[9] I. Gibson, D. W. Rosen, and B. Stucker, *Additive Manufacturing Technologies*. Boston, MA: Springer US, 2010.

[10] M. L. Griffith and J. W. Halloran, "Freeform Fabrication of Ceramics via Stereolithography," *Journal of the American Ceramic Society*, vol. 79, no. 10, pp. 2601–608, 1996.

Chapter 6

[1] F. Jacobs, *Rapid Prototyping & Manufacturing: Fundamentals of StereoLithography*, 1st ed. Society of Manufacturing Engineers, 1992.

[2] I. Gibson, D. W. Rosen, and B. Stucker, *Additive Manufacturing Technologies*. Boston, MA: Springer US, 2010.

[3] A. S. Jariwala, F. Ding, X. Zhao, and D. W. Rosen, “A Film Fabrication Process on Transparent Substrate using Mask Projection Micro-Stereolithography,” Solid Freeform Fabrication Symposium, Austin, TX, 216–229, 2008.

Chapter 7

[1] Henini, M., “Semiconductors: Data Handbook,” *Microelectronics Journal* 35(8), 685, 2004. doi:10.1016/j.mejo.2004.04.001

[2] Palik, E. D. *Handbook of Optical Constants of Solids,* Academic Press, page 570, 1991. ISBN 0-12-544422-2

[3] A. M. Elliott, O. S. Ivanova, C. B. Williams, and T. A. Campbell, “Inkjet printing of quantum dots in photopolymer for use in additive manufacturing of nanocomposites,” *Advanced Engineering Materials*, Volume 15, Issue 10, pages 903–907, October 2013. doi:10.1002/adem.201300020

[4] F. Jacobs, *Rapid Prototyping & Manufacturing: Fundamentals of StereoLithography*, 1st ed. Society of Manufacturing Engineers, 1992.

[5] I. Gibson, D. W. Rosen, and B. Stucker, *Additive Manufacturing Technologies*. Boston, MA: Springer US, 2010.

[6] A. Barichard, T. Galstian, and Y. Israëli, “Physico-chemical role of CdSe/ZnS quantum dots in the photo-polymerization process of acrylate composite materials.” *Physical Chemistry Chemical Physics : PCCP*, vol. 14, no. 22, pp. 8208–16, Jun. 2012.

APPENDIX A

Working Curves: uSLA Data

The data presented in section are the working curves formed from the cure depth samples created by the uSLA machine. These working curves were averaged and their critical exposures were calculated and plotted in Figure 5-10.

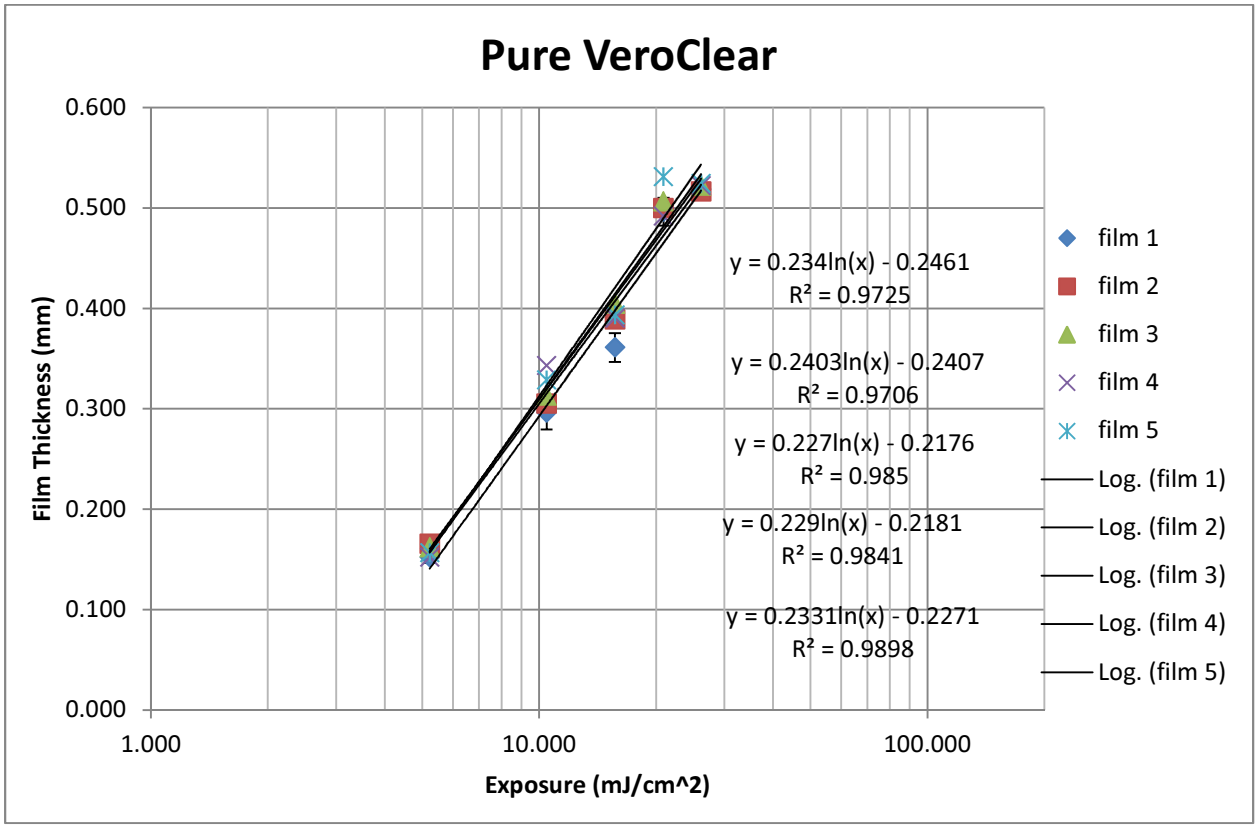

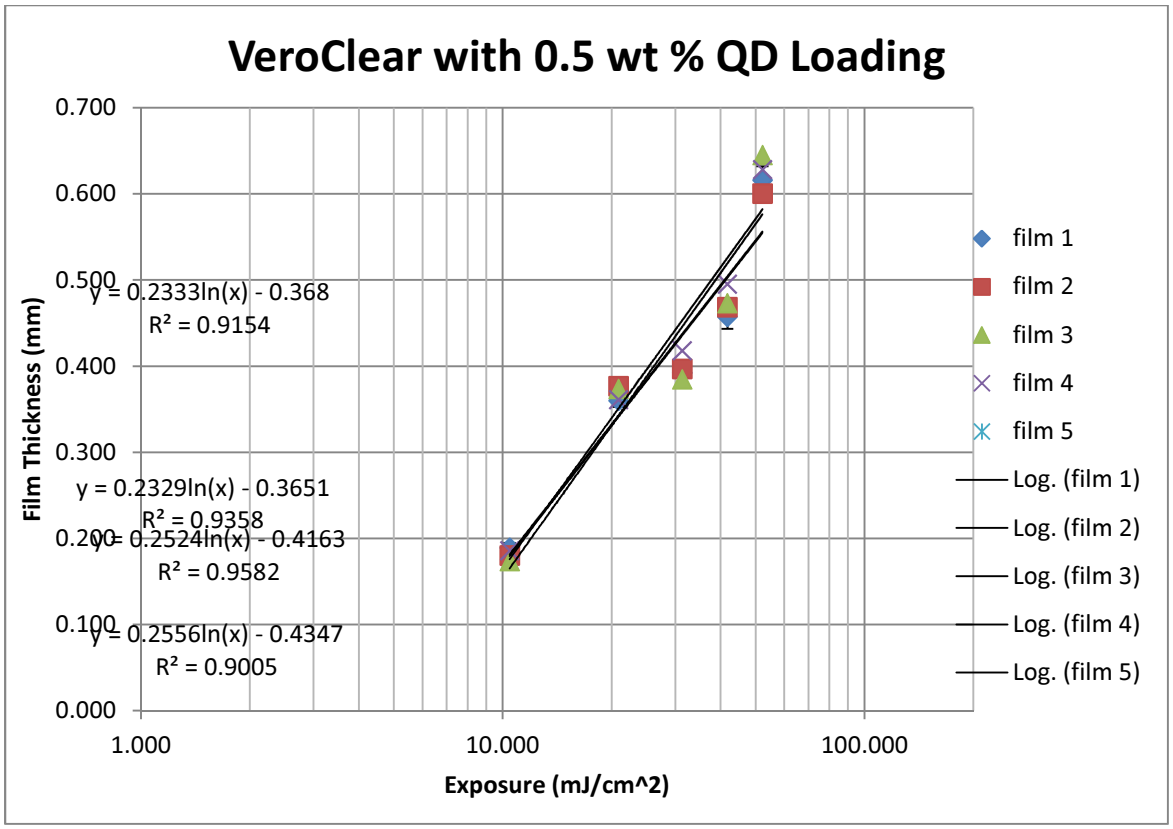
VeroClear with 0.5 wt % QD Loading
Film Thickness (mm)
0.700
0.600
0.500
0.400
0.300
0.200
0.100
0.000
1.000
10.000
100.000
Exposure (mJ/cm^2)
y = 0.2333ln(x) - 0.368
R² = 0.9154
y = 0.2329ln(x) - 0.3651
R² = 0.9358
y = 0.2524ln(x) - 0.4163
R² = 0.9582
y = 0.2556ln(x) - 0.4347
R² = 0.9005
film 1
film 2
film 3
film 4
film 5
Log. (film 1)
Log. (film 2)
Log. (film 3)
Log. (film 4)
Log. (film 5)

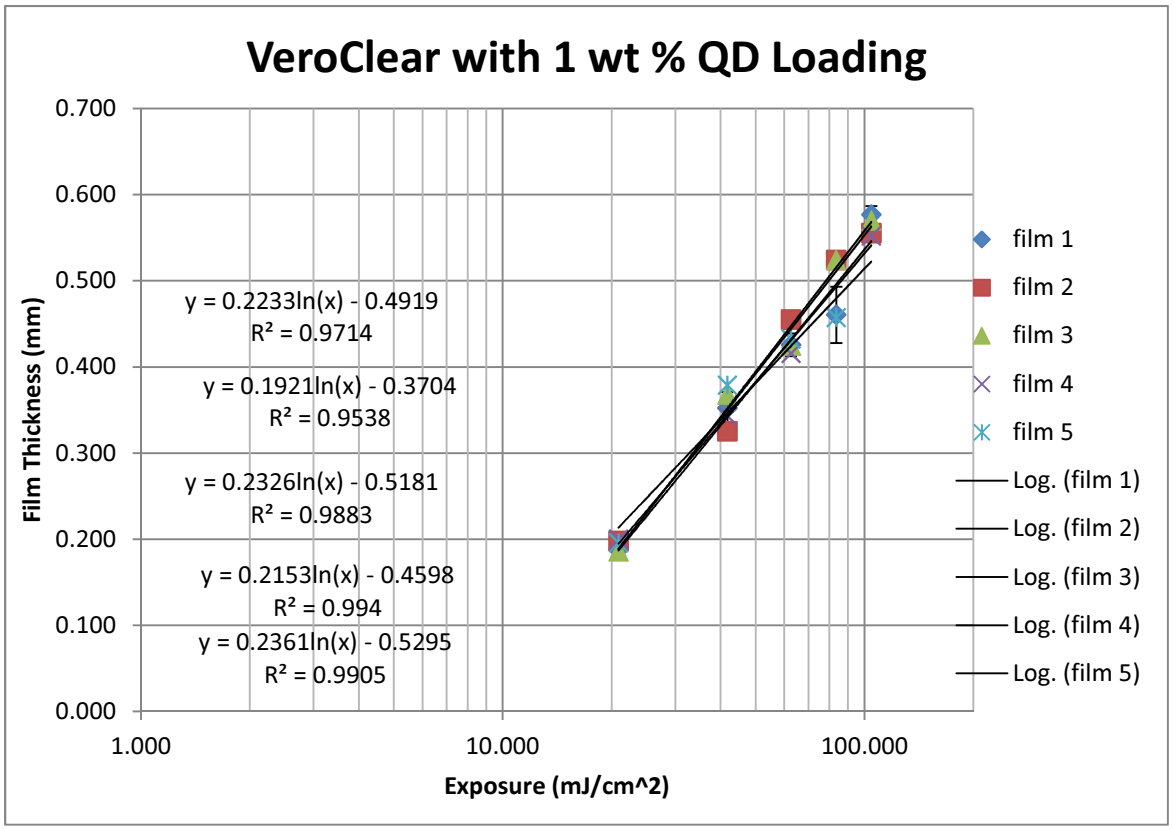
VeroClear with 1 wt % QD Loading
Film Thickness (mm)
0.700
0.600
0.500
0.400
0.300
0.200
0.100
0.000
1.000
10.000
100.000
Exposure (mJ/cm^2)
y = 0.2233ln(x) - 0.4919
R² = 0.9714
y = 0.1921ln(x) - 0.3704
R² = 0.9538
y = 0.2326ln(x) - 0.5181
R² = 0.9883
y = 0.2153ln(x) - 0.4598
R² = 0.994
y = 0.2361ln(x) - 0.5295
R² = 0.9905
film 1
film 2
film 3
film 4
film 5
Log. (film 1)
Log. (film 2)
Log. (film 3)
Log. (film 4)
Log. (film 5)

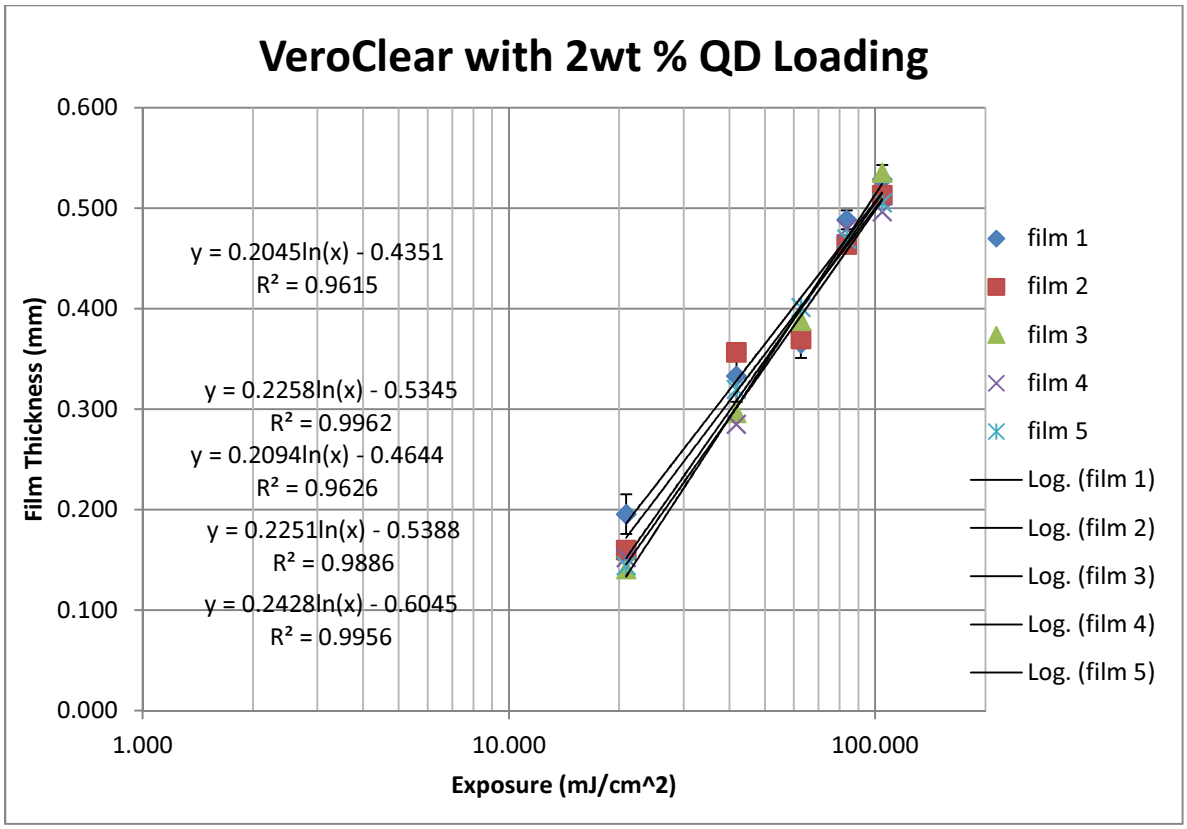
VeroClear with 2wt % QD Loading
Film Thickness (mm)
0.600
0.500
0.400
0.300
0.200
0.100
0.000
1.000
10.000
100.000
Exposure (mJ/cm^2)
y = 0.2045ln(x) - 0.4351
R² = 0.9615
y = 0.2258ln(x) - 0.5345
R² = 0.9962
y = 0.2094ln(x) - 0.4644
R² = 0.9626
y = 0.2251ln(x) - 0.5388
R² = 0.9886
y = 0.2428ln(x) - 0.6045
R² = 0.9956
film 1
film 2
film 3
film 4
film 5
Log. (film 1)
Log. (film 2)
Log. (film 3)
Log. (film 4)
Log. (film 5)

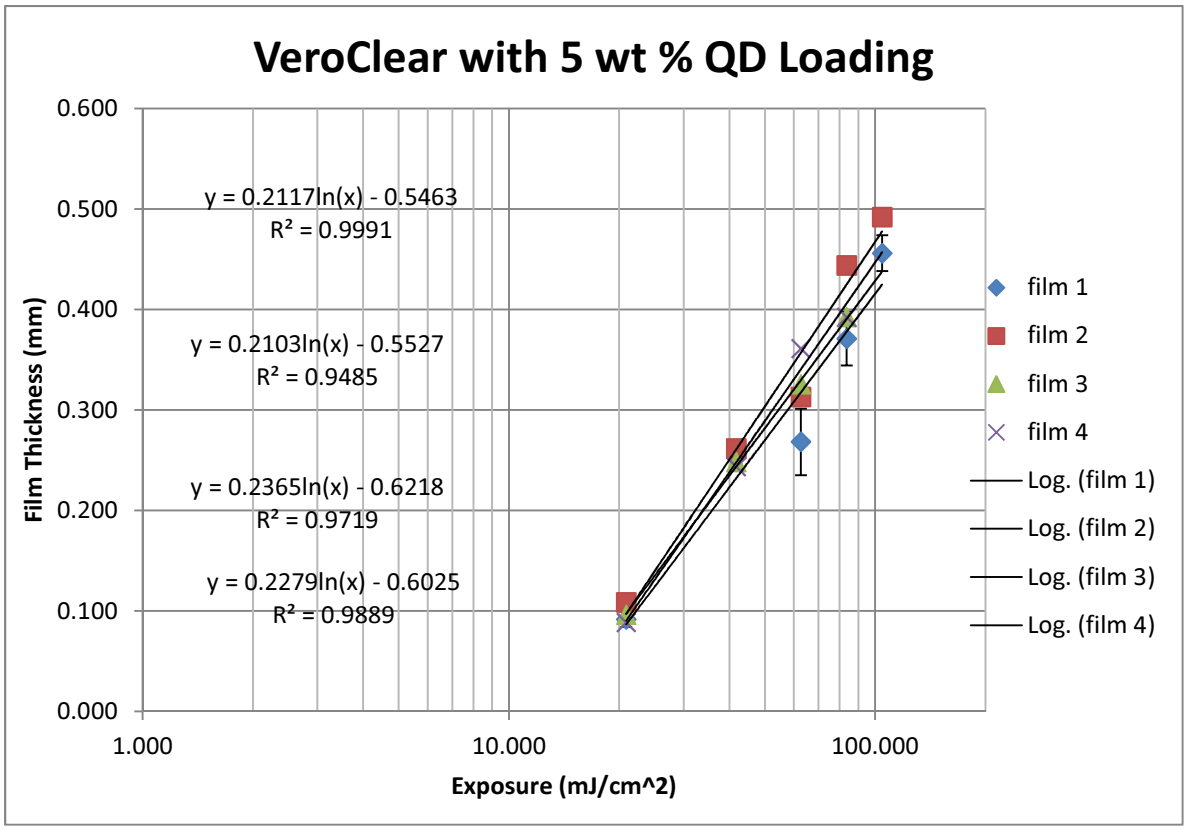
VeroClear with 5 wt % QD Loading
Film Thickness (mm)
0.600
0.500
0.400
0.300
0.200
0.100
0.000
1.000
10.000
100.000
Exposure (mJ/cm^2)
y = 0.2117ln(x) - 0.5463
R² = 0.9991
y = 0.2103ln(x) - 0.5527
R² = 0.9485
y = 0.2365ln(x) - 0.6218
R² = 0.9719
y = 0.2279ln(x) - 0.6025
R² = 0.9889
film 1
film 2
film 3
film 4
Log. (film 1)
Log. (film 2)
Log. (film 3)
Log. (film 4)